



HAL
open science

Hydrochar derived from municipal sludge through hydrothermal processing: A critical review on its formation, characterization, and valorization

Huan Liu, Ibrahim Alper Basar, Ange Nzihou, Cigdem Eskicioglu

► To cite this version:

Huan Liu, Ibrahim Alper Basar, Ange Nzihou, Cigdem Eskicioglu. Hydrochar derived from municipal sludge through hydrothermal processing: A critical review on its formation, characterization, and valorization. *Water Research*, 2021, 199, pp.1-52/117186. 10.1016/j.watres.2021.117186 . hal-03211746

HAL Id: hal-03211746

<https://imt-mines-albi.hal.science/hal-03211746v1>

Submitted on 18 May 2021

HAL is a multi-disciplinary open access archive for the deposit and dissemination of scientific research documents, whether they are published or not. The documents may come from teaching and research institutions in France or abroad, or from public or private research centers.

L'archive ouverte pluridisciplinaire **HAL**, est destinée au dépôt et à la diffusion de documents scientifiques de niveau recherche, publiés ou non, émanant des établissements d'enseignement et de recherche français ou étrangers, des laboratoires publics ou privés.

Hydrochar derived from municipal sludge through hydrothermal processing: A critical review on its formation, characterization, and valorization

Huan Liu^a, Ibrahim Alper Basar^a, Ange Nzihou^b, Cigdem Eskicioglu^{a,*}

^a*UBC Bioreactor Technology Group, School of Engineering, The University of British Columbia, Okanagan Campus, 1137 Alumni Avenue, Kelowna, British Columbia V1V 1V7, Canada*

^b*Université de Toulouse, IMT Mines Albi, RAPSODEE CNRS UMR-5302, Campus Jarlard, Albi 81013 Cedex 09, France*

*Corresponding author.

E-mail addresses:

liu@alumni.ubc.ca (H. Liu); alperbasar@alumni.ubc.ca (I.A. Basar); ange.nzihou@mines-albi.fr (A. Nzihou); cigdem.eskicioglu@ubc.ca (C. Eskicioglu).

Abstract

Additional options for the sustainable treatment of municipal sludge are required due to the significant amounts of sludge, high levels of nutrients (e.g., C, N, and P), and trace constituents it contains.

Hydrothermal processing of municipal sludge has recently been recognized as a promising technology to efficiently reduce waste volume, recover bioenergy, destroy organic contaminants, and eliminate pathogens. However, a considerable amount of solid residue, called hydrochar, could remain after hydrothermal treatment. This hydrochar can contain abundant amounts of energy (with a higher heating value up to 24 MJ/kg, dry basis), nutrients, and trace elements, as well as surface functional groups. The valorization of sludge-derived hydrochar can facilitate the development and application of hydrothermal technologies. This review summarizes the formation pathways from municipal sludge to hydrochar, specifically, the impact of hydrothermal conditions on reaction mechanisms and product distribution. Moreover, this study comprehensively encapsulates the described characteristics of hydrochar produced under a wide range of conditions: Yield, energy density, physicochemical properties, elemental distribution, contaminants of concern, surface functionality, and morphology. More importantly, this review compares and evaluates the current state of applications of hydrochar: Energy production, agricultural application, adsorption, heterogeneous catalysis, and nutrient recovery. Ultimately, along with the identified challenges and prospects of valorization approaches for sludge-derived hydrochar, conceptual designs of sustainable municipal sludge management are proposed.

Keywords: Municipal sludge; hydrochar; hydrothermal conversion; pathway; contaminants; waste valorization

Abbreviations

2D-PCIS	two-dimensional perturbation correlation infrared spectroscopy
AAEMs	alkali and alkaline earth metals
AD	anaerobic digestion
AGS	anaerobic granular sludge
AP	apatite phosphorus
ASTM	American Society for Testing and Materials
BCR	Community Bureau of Reference
BOD	biochemical oxygen demand
Ca-P	calcium phosphates
CEC	cation exchange capacity
COD	chemical oxygen demand
CSTR	continuously stirred tank reactor
daf	dry ash free basis
db	dry basis
DS	digested sludge
DTG	derivative thermogravimetry
EBC	European Biochar Foundation
EDS	energy dispersive X-ray spectrometry
EPA	Environmental Protection Agency
ER	energy recovery
EU	European Union
f1	acid soluble fraction
F1	exchangeable fraction
F2	carbonate-bound fraction
f2	reducible fraction
F3	Fe-Mn oxides fraction
f3	oxidizable fraction
F4	organic matter/sulfide fraction
f4	residual fraction
F5	residual fraction

FC	fixed carbon
FS	fecal sludge
FTIR	Fourier-transform infrared spectroscopy
H/C	hydrogen to carbon atomic ratio
HHV	higher heating value
HTC	hydrothermal carbonization
HTG	hydrothermal gasification
HTL	hydrothermal liquefaction
HTP	hydrothermal processing
ID	inner diameter
IP	inorganic phosphorus
I-TEQ	international toxic equivalent
LHV	lower heating value
MPS	mixed primary and secondary sludge
MS	municipal sludge
NAIP	non-apatite inorganic phosphorus
NMR	Nuclear magnetic resonance
O/C	oxygen to carbon atomic ratio
OFG	oxygen-containing functional groups
OP	organic phosphorus
ortho-P	orthophosphate
PAHs	polycyclic aromatic hydrocarbons
PCBs	polychlorinated biphenyls
PCDD/Fs	polychlorinated dibenzo-dioxins/-furans
PF	plug-flow reactor
PFCs	perfluorinated compounds
POPs	persistent organic pollutants
PPCPs	pharmaceuticals, personal care products
PS	primary sludge
pyro-P	pyrophosphate
SEM	scanning electron microscopy
SEPs	sequential extraction procedures

SRT	solids retention time
SAC	sludge-based activated carbon
SS	secondary sludge
T	reaction temperature
t	residence time
TCLP	toxicity characteristic leaching procedure
TEM	transmission electron microscope
TEQ	toxic equivalent
TG	thermogravimetry
TOC	total organic carbon
TS	total solids
US	United States
VM	volatile matter
v/v	volume ratio
WAS	waste activated sludge
WHSV	weight hourly space velocity
wt%	percentage by weight
WWTP	wastewater treatment plant
XPS	X-ray photoelectron spectroscopy
XRD	X-ray diffractometry

Table of Contents

1. Introduction.....	9
2. Formation of municipal sludge-derived hydrochar.....	13
2.1. Characteristics of municipal sludge.....	13
2.2. Formation pathways to hydrochar.....	16
2.3. Process parameters governing hydrochar.....	17
2.3.1. Initial solids or moisture content.....	17
2.3.2. Temperature, pressure, and residence time (severity factor).....	18
2.3.3. Heating rate.....	20
2.3.4. Co-processing of municipal sludge.....	20
2.3.5. Catalyst.....	22
2.3.6. Solvent or co-solvent.....	25
3. Characterization of hydrochar.....	27
3.1. The proximate and ultimate analyses.....	27
3.2. Distribution of macronutrients in hydrochar.....	30
3.3. Contaminants of concern.....	31
3.3.1. Heavy metals.....	32
3.3.2. Persistent organic pollutants (POPs).....	35
3.4. Characterization of surface functionality and structure.....	39
3.4.1. Fourier-transform infrared spectroscopy (FTIR).....	39
3.4.2. Two-dimensional perturbation correlation infrared spectroscopy (2D-PCIS).....	40
3.4.3. X-ray photoelectron spectroscopy (XPS).....	40
3.4.4. Nuclear magnetic resonance (NMR) spectroscopy.....	42
3.4.5. X-ray diffractometry (XRD).....	43
3.5. Characteristics of morphology.....	44
4. Valorization of hydrochar.....	45
4.1. Energy production.....	46
4.1.1. Biofuel for combustion.....	46
4.1.2. Hydrochar for syngas production.....	49
4.2. Agricultural applications.....	50
4.3. Adsorption: Water remediation.....	52
4.4. Heterogeneous catalysis.....	56
4.5. Nutrient recovery.....	57
4.5.1. Wet-chemical extraction.....	57
4.5.2. Thermochemical process.....	60

4.5.3. Integrated biotechnology.....	61
4.6. Evaluation of valorization technologies for hydrochar	61
5. Prospects towards sustainable waste management	63
6. Conclusions.....	67
Acknowledgments.....	69
References.....	69

1. Introduction

Due to increasing population and rapid urbanization, a significant amount of wastewater solids, often called municipal sludge (MS), are generated at municipal wastewater treatment plants (WWTPs) worldwide (Kor-Bicakci and Eskicioglu, 2019). In China, the annual MS production doubled within five years and reached 5.7 million dry tonnes in 2013 (Yang et al., 2015). In the United States (US), the MS generation rate is nearly 12.7 million dry tonnes per year (2018) (Marrone et al., 2018). The world total production rate of MS was recorded at 45 million dry tonnes per year in 2017 (Gao et al., 2020).

Originating from households, food-processing, agricultural, and industrial wastewater and associated biological treatment, MS including primary sludge (PS), secondary sludge (SS), and digested sludge (DS) is a reservoir of organic materials, nitrogen (N), phosphorus (P), and other inorganic nutrients (Zhai et al., 2014a). MS has been identified as a complementary P sink in regions with limited phosphate rock resources (Shi et al., 2019). However, MS, especially non-stabilized sludge, may also contain various hazardous materials, including pathogens (Lopes et al., 2020), organic contaminants, such as polycyclic aromatic hydrocarbons (PAHs) and polychlorinated biphenyls (PCBs) (Brookman et al., 2018), inorganic pollutants (e.g., heavy metals) (Chen et al., 2020), and emerging contaminants or micropollutants (e.g., antibiotics, hormones, pharmaceuticals, and personal care products) (Taboada-Santos et al., 2019).

Considering the magnitude of sludge production and its potential nutrients and hazards, the search for alternative treatment options has been stimulated for decades.

Proper management of MS through conventional disposal methods, such as landfilling, composting, land application, and incineration, requires significant expenditures (Xu et al., 2018). It has been reported that managing MS could cost as much as 57% of the total operation cost in a WWTP (Ma et al., 2018). Even though anaerobic digestion (AD) treatment has been applied to break down the organic matters in MS and generate biogas (mainly methane), a considerable amount of sludge (approximately 40–50% of the input) remains and requires appropriate disposal (Zhen et al., 2017). The long solids retention time (SRT) (typically 15 – 20 days) requirement further limits the efficiency of conventional AD treatment.

Given the increasing sludge amount, conventional treatment methods for MS may not be sustainable in the future.

The high moisture content in sludge (almost 98 wt%) causes the biggest handling challenges: The massive volume and consequent high cost of treatment. An emerging technique, hydrothermal processing (HTP), also called hydrothermal conversion, is promising to address these challenges efficiently and economically (Huang et al., 2019). HTP can treat waste with high moisture content through a thermochemical process. This ability is a significant advantage compared to other techniques that require dry feedstocks (e.g., incineration and pyrolysis). It has been reported that the drying cost of MS is the majority energy input of pyrolysis treatment, occupying 65–75% of the total inputs (Kim and Parker, 2008). Conversely, without drying requirement, HTP could substantially reduce the energy input. HTP utilizes hot pressurized water as a reaction medium to break down large complex organic matters or macromolecules into smaller and simpler units at elevated temperature and pressure (Mathimani and Mallick, 2019). The reaction rate especially raises when the treatment conditions reach the critical point of water (374.3 °C and 22.1 MPa) (He et al., 2014a). Thus, HTP can efficiently decompose organic matters and reduce the volume of residual solids. The dewaterability of MS is also significantly enhanced after HTP treatment, even at low temperatures (e.g., 180 °C). Wang et al. (2014) reported that the moisture content of excess sludge was reduced to 27% after HTP at 180 °C for 1 h followed by mechanical dewatering, while over 65% of moisture was retained when only mechanical dewatering technologies were used. Ahmed et al. (2021) found that after HTP of DS at 190 °C for 1 h, the capillary suction time decreased by 91%. Moreover, the greatest benefit of HTP is its use to produce renewable biofuels (e.g., coal-like char, biocrude, and syngas) from sludge (Moreno and Espada, 2019). In summary, HTP is used to simultaneously recover energy, promote organic pollutants decomposition, enhance dewaterability and eliminate pathogens (via high-temperature sterilization).

In recent decades, many researchers have focused on sludge valorization using HTP treatment (Merzari et al., 2019). HTP for sludge-to-energy conversion is classified into three main categories based on the treatment temperature, pressure, and featured fuel products: Hydrothermal carbonization (HTC),

hydrothermal liquefaction (HTL), and hydrothermal gasification (HTG) (as shown in [Table 1](#)). Other hydrothermal technologies, such as thermal hydrolysis, wet oxidation, and supercritical water oxidation, do not aim for energy recovery and thus are not considered in this review. In this review, the carbonaceous char produced in the form of solid residue from HTP processes is defined as hydrochar. As can be seen in [Table 1](#), different fuel products or coproducts (i.e., hydrochar, biocrude, syngas, and aqueous phase) are generated in all hydrothermal conditions; however, their yields vary.

=====

Please Insert Table 1 Here

=====

[Fig. 1](#) presents the normal distribution of product yields based on data gathered from numerous HTP studies. As the treatment severity intensifies in the order of HTC, HTL, and HTG, there is a noticeable trend of decreasing yield of solid and aqueous phase products, while the gas yield increases. The biocrude yield tends to be maximized through the HTL of MS. It is noted that a considerable amount of hydrochar remains as a product or coproduct despite the hydrothermal conditions. As the figure shows, average yields of hydrochar are 60.2%, 44.7%, and 20.5%, dry basis (db), from HTC, HTL, and HTG treatment of MS, respectively ([Fig. 1](#)). However, it should be noted that the yield of hydrochar varies substantially depending on the reaction severity and processing conditions. For example, in a continuous plug-flow HTL system (276–358 °C for 18–30 min), the hydrochar yield from PS, SS, and DS were 9.5, 20.5, and 36.4%, db, respectively (Marrone et al., 2018).

=====

Please Insert Fig. 1 Here

=====

The reduced mass percent of hydrochar causes a high concentration of nutrients (particularly P) and contaminants, such as heavy metals, PAHs, and PCBs (Chanaka Udayanga et al., 2018). Yu et al. (2019)

reported that almost all P (> 90%) remained in the hydrochar after HTC treatment of PS. However, due to the accumulation of toxic contaminants (e.g., Cr and Ni), direct recycling of hydrochar as P fertilizer is restricted by many jurisdictions (Chanaka Udayanga et al., 2018). Direct burning of HTC hydrochar for heat generation would cause a wide distribution of P-rich ash and potential secondary pollution (Oliver-Tomas et al., 2019). Therefore, enrichment of the nutrients and pollutants in hydrochar seems to be a key bottleneck for HTP application to MS. Several studies for P recovery from MS-derived hydrochar and risk assessment of contaminants have been conducted in the past ten years (Li et al., 2012; Liu et al., 2018a; Ovsyannikova et al., 2019; vom Eyser et al., 2015). To date, few reviews have detailed the characteristics of MS-derived hydrochar produced under various HTP conditions or mentioned its application opportunities. Therefore, it is necessary to critically and comprehensively investigate current information and expose knowledge gaps of MS-derived hydrochar for its sustainable management.

This review aims to show current knowledge of the properties of MS and its corresponding hydrochar from HTP and to present and evaluate sustainable application processes for MS-derived hydrochar. Recent studies of HTP technique are application-oriented and often issued as technical reports. Consequently, this review involves an extensive search of all related peer-reviewed journal articles, conference proceedings, theses, books, as well as technical reports from bibliometric databases (e.g., Google Scholar, Science Direct, Scopus, and Web of Science). The following keywords have been searched in different combinations: Hydrochar, sludge, municipal sludge, sewage sludge, hydrothermal, hydrothermal conversion, HTC, HTL, HTG, HTP, and supercritical water gasification. The search period is concentrated in the last twenty years because more attention has been paid to HTP treatment of MS since 2000. After rejecting articles referring to industrial sludge or irrelevant hydrothermal processes (e.g., thermal hydrolysis and oxidation) based on title, abstract, and scanning, the remaining articles (in total 319 references) were analyzed thoroughly. Based on collected information from all selected papers, this review is divided into the following sections. Firstly, the formation of hydrochar from MS is comprehensively presented from the perspectives of mechanisms and hydrothermal conditions. Secondly, unique characteristics of MS-derived hydrochar and the associated contaminants of concern are

summarized to guide the application of hydrochar. Thirdly, this review evaluates current utilizations of MS-derived hydrochar for sustainable management. Lastly, special attention is given to the feasibilities and challenges of each technology for hydrochar valorization.

2. Formation of municipal sludge-derived hydrochar

The contents and distributions of hydrothermal products, as well as the reaction pathways, are dependent on the feedstock properties and process conditions, such as initial total solids (TS) of MS, reaction temperature and pressure, residence time, heating and cooling rates, co-feedstock, catalysts, and solvents. Hence, this section comprehensively reviews the formation of MS to hydrochar under the influence of various hydrothermal parameters.

2.1. Characteristics of municipal sludge

Generated through different wastewater treatment processes (i.e., primary sedimentation, aeration tank, and AD), MS can be categorized into PS, waste activated sludge (WAS) or SS, and DS. [Table 2](#) summarizes the properties of various types of MS that were studied for energy conversion using HTP technologies. To maintain consistency, the higher heating value (HHV) of MS (and corresponding hydrochar) is calculated by using the correlation formula ([Eq. 1](#)) developed by Channiwalaa and Parikh (Channiwala and Parikh, 2002).

$$\text{HHV (MJ/kg)} = 0.3491C + 1.1783H + 0.1005S - 0.1034O - 0.0151N - 0.0211\text{Ash} \quad (1)$$

where C, H, S, O, N, and ash are mass percentages of material on a dry basis.

=====

Please Insert Table 2 Here

=====

MS received from WWTP clarifiers or centrifuges normally contains around 2–12 wt% of TS (Kacprzak et al., 2017; Moran, 2018). To maximize the energy conversion rate of HTP, moisture content of MS is typically reduced to minimum levels while not limiting its pumpability using various dewatering

technologies (e.g., centrifuges and belt presses) (Elliott et al., 2015). As shown in Table 2, all different types of MS are complex heterogeneous mixtures of organic and inorganic matters. The high variety of MS is derived from its specific origin and unique processing conditions. The volatile matters (VM) vary with 37.7–76.6%, 33.6–79.3%, 25.1–70.0%, db, for PS, WAS, and DS, respectively. Due to the concentrated organic matter, MS has become an attractive source of energy with a higher heating value (HHV) up to 22.2 MJ/kg, db. Such energy content is comparable to low-rank coal, such as lignite (Syed-Hassan et al., 2017). However, it should be noted that high ash contents of MS and its derived hydrochar could constrain their applicability for direct combustion due to the slagging problems from ash melting.

Fig. 2 illustrates the elemental and other properties of MS reported in numerous HTP studies. Mean and 10th and 90th percentile data of each property are presented. Based on the percentile distribution analysis, MS has a large variety of ash from 19.7% to 56.6%, db, which could cause a high variation of ash content in hydrochar. Other than ash, MS is composed of 18.9–41.7% C, 3.1–6.5% H, 15.1–33.0% O, 2.1–6.8% N, 0.4–2.4% S, and 1.0–3.8% P on a dry basis. Most reported MS samples (80%) have fixed carbon (FC) and HHV of 1.0–12.2% and 9.7–19.9 MJ/kg, respectively. The average pH of MS reported in the previous studies is neutral (6.9), within a range of 5.7–8.0.

=====

Please Insert Fig. 2 Here

=====

Unlike other types of biomass that are dominated by a single organic compound, MS can be broadly balanced by carbohydrates (cellulose and hemicellulose), protein, lipids, lignin, and humic substances, with a dry weight percentage of 1.3–62.6, 0.1–26.0, 8.0–43.2, 1.1–35.0 and 3.8–23.9, respectively. Lignocellulosic biomass and macroalgae are mainly composed of carbohydrates (typically 40–50% and 55–60%, respectively), while microalgae primarily consist of protein (30–60%) or carbohydrates (20–40%) (Basar et al., 2021). The diverse compositions of MS could lead to complex reaction pathways in HTP and the MS-derived hydrochar with abundant functionalities. Moreover, MS also contains valuable

inorganic compounds, such as Na, K, Al, Ca, Fe, and Mg, along with pollutants and potential carcinogens, such as heavy metals, polychlorinated compounds, and PAHs, which tend to be recalcitrant to HTP and accumulated in hydrochar (Brookman et al., 2018; Chanaka Udayanga et al., 2018; Raheem et al., 2018). Therefore, properties of MS-derived hydrochar should be carefully reviewed prior to applications to avoid potential secondary contamination.

Fig. 3 shows the concentration distribution of metals present in MS samples that were used in HTP studies. These metals can be categorized as alkali metals (e.g., K and Na), alkaline earth metals (e.g., Ca and Mg), transition metals (e.g., Fe, As, Cd, Cr, Co, Cu, Hg, Mn, Mo, Ni, Pb, and Zn), and other metals (e.g., Al and Se). Among the studied samples, most (80%) MS contains abundant K (0.2–1.6%), Na (0.1–0.5%), Ca (0.3–4.1%), Mg (0.2–1.2%), Al (0.3–4.0%), Fe (0.5–6.3%), Cr (19–151 ppm), Co (1–2,700 ppm), Cu (127–1,175 ppm), Mn (59–812 ppm), Ni (16–600 ppm), Pb (15–151 ppm), and Zn (303–2,288 ppm) on a dry basis. Several studies have reported that most of these metal ions could have a significant effect, either catalytic or inhibitory, on the decomposition of carbohydrates during HTP treatment (Cao et al., 2015; Chen and Lee, 2020; Hoşgün, 2020; Kong et al., 2008; Kumar et al., 2018; Liu et al., 2017; Lu et al., 2016; Zahari et al., 2020; Shen et al., 2009). Shen et al. (2009) found that alkali and alkaline-earth metal ions could promote the hydrothermal conversion (at 300 °C) of glycerin to lactic acid or lactate salts, and the catalytic effectiveness varied on metal ions. Cao et al. (2015) demonstrated that transition metal ions, such as Cu(II) and Fe(III) could greatly stimulate the hydrolysis of cellulose into glucose, which was further decomposed into levulinic acid and formic acid under the HTP at 200 °C. Hoşgün (2020) also discovered that Al(III) had a catalytic effect on the yields of 5-hydroxymethylfurfural and furfural through HTP (at 200 °C) of poppy stalks. On the other hand, inhibitory effects on hydrothermal conversion could occur when transition metal ions exceeded certain concentrations. Kong et al. (2008) reported that with Cr(III) and Ni(II) ions increasing from 0 to 800 ppm, the yield of lactic acid converted from maize straw, rice husk, and sawdust initially improved, and then decreased under HTP at 300 °C, while Cr(III), Ni(II) and Zn(II) showed a negative impact on the conversion of wheat bran. However, the effects of existing metals on hydrothermal conversion of MS are still undiscovered. Considering the

significant load of metal ions in MS, their impacts on HTP should be exposed as they may become catalysts instead of burdens.

=====

Please Insert Fig. 3 Here

=====

2.2. Formation pathways to hydrochar

In the past decades, various feedstocks have been studied from HTP, from model compounds, such as cellulose (Sevilla and Fuertes, 2009), to any wet biomass (Wang et al., 2018). As one of the most complex substrates, the generation process of hydrochar from MS can be complicated. Fig. 4 summarizes possible pathways from numerous studies of how major compounds in MS are transferred to the products via HTP as a function of temperature. It is known that the organic components (i.e., carbohydrates, protein, lipids, lignin, and humic substances) in MS are depolymerized into their corresponding monomers, which form intermediates mainly via hydrolysis, decomposition, dehydration, decarboxylation, and deamination. It should be noted that the significant load of metal ions in MS may promote or inhibit the hydrolysis, decomposition, and dehydration of carbohydrates. The intermediates are eventually recombined in hydrochar through aromatization, condensation, and polymerization. However, it is suggested that these reaction pathways occur simultaneously during the HTP of MS. Detailed descriptions of each reaction mechanism can be found in our previous literature review (Basar et al., 2021) and elsewhere (He et al., 2014a; Wang et al., 2019a; Wang et al., 2018). Indeed, diverse products formed through different pathways can largely affect the properties of hydrochar. To broadly evaluate the characteristics and the sustainable applications of hydrochar, it is necessary to investigate how process parameters govern the mechanisms of hydrochar formation.

=====

Please Insert Fig. 4 Here

=====

2.3. Process parameters governing hydrochar

2.3.1. Initial solids or moisture content

As the reaction medium, water under HTP conditions principally contributes to the cleavage of hydrogen bonds, especially hydrolysis, due to ionic or free-radical reactions favored by dramatically enhanced water properties (Wang et al., 2019a). The amount of water in feedstock represents a key factor in affecting the reaction pathways and product distribution. Generally, MS with higher initial solid content in HTP exhibits higher hydrochar yield. Xu and Lancaster (2008) reported a higher hydrochar yield when the solid content of feedstock (secondary pulp/paper sludge) increased from 4.8 wt% to 16.7 wt% under HTL treatment (280 °C for 60 min). A decrease in biocrude and an increase in gas were also observed. They indicated that low moisture could restrict the solvolysis/hydration of lignocellulosic compounds and resulted in a higher yield of hydrochar. High solid content may also promote the dehydration reactions of the intermediates/products during HTP and thus enhance the yield of heavy oil fractions (Xu and Lancaster, 2008). Xu et al. (2012) suggested more carbon conversion into hydrochar with the decrease of MS moisture from 94.4 wt% to 76.2 wt% under supercritical water conditions (400 °C for 60 min), while no remarkable changes were found on total organic matter conversion to aqueous and gas products. Such enhancement in hydrochar yield could be attributed to devolatilization of biomass or early polymerization when the moisture content is low (Gong et al., 2014a; Karayıldırım et al., 2008; Xu et al., 2012). Wang et al. (2019) also indicated that increased moisture content (82–90%) promoted the hydrolysis of MS biomass to produce water-soluble organics and suppressed tar and char formation under supercritical conditions (400 °C for 30 min). Aragón-Briceño et al. (2020) found that increasing solids content (2.5 to 30 wt%) of DS for HTC treatment (250 °C for 30 min) gradually enhanced yield (68 to 76%, db), HHV (15.4 to 16.5 MJ/kg), and energy recovery (65.9 to 76.7%) of hydrochar; it also increased pH, organics, ammonia, total phosphorus, total solids, and total carbon contents in HTC aqueous. From the engineering perspective, using a high solids content (10–25 wt%) of feedstock for HTP is critical to enhance the process energy efficiency, achieve net positive energy

recovery, and improve concentrations of nutrients (e.g., N and P) in hydrochar and aqueous phase to allow efficient recovery.

2.3.2. Temperature, pressure, and residence time (severity factor)

Reaction temperature and pressure are the governing parameters of HTP as they control the water state and thus essentially determine the reaction mechanisms. When temperature and pressure are both above the critical point, reaction mechanism alters from ionic in subcritical condition to free-radical reactions under supercritical condition (He et al., 2014a). However, at full-scale with a continuous flow system (often configured as plug flow), pressure is mostly formed autogenously and not controlled but only monitored. To date, no one has systematically studied the impact of pressure on the HTP of MS. Several reviews have suggested that pressure has no major effects on the product distribution from HTP when conditions are within the subcritical or supercritical zone (Gu et al., 2020; Ibrahim and Akilli, 2019). Therefore, the effect of pressure is not further discussed in this review.

From the thermodynamic viewpoint, the degradation of organic macromolecules and recombination of chemical bonds require a significant amount of energy, and therefore temperature is a crucial and limiting factor for HTP treatment. When insufficient energy is provided at low temperatures, the reaction of HTP is often restricted to hydrolysis, while higher temperatures can promote subsequent reactions. The reported optimal temperature range for thermal hydrolysis of MS is 160–180 °C (Barber, 2016). It is also suggested that carbohydrates and proteins can be hydrothermally decomposed at above 180 °C, while lignin requires higher temperatures (280–500 °C) for degradation (He et al., 2013). The complete decomposition of proteins and lipids also requires high temperatures (300 and 640 °C, respectively). Under the subcritical conditions, a competition between depolymerization and polymerization occurs with increasing temperature and residence time. However, when temperature is above 375 °C, reactions are heavily shifted to the free radical mechanism, including water-gas shift reaction (Watson et al., 2020). Therefore, the yield of gaseous products (CO₂, CO, H₂, and alkane gases) can be significantly enhanced.

The distribution of products from HTP is affected by both temperature and residence time to the ultimate extent. To analyze the collective effects of temperature and residence time, a combined

parameter, the concept of severity factor was developed by Ruyter (1982). The calculation of severity factor (f , dimensionless) in terms of reaction temperature (T , in Kelvin) and residence time (t , in seconds) is expressed in Eq. (2):

$$f=50t^{0.2}exp((-3500)/T) \quad (2)$$

Fig. 5 illustrates the distribution of HTP products as a function of severity factor from numerous studies. The figure demonstrates that the hydrochar yield significantly decreases with an increase in the reaction severity up to a certain extent. Some variations can be attributed to the use of solvents (e.g., methanol, ethanol, and acetone) and MS compositions (e.g., high ash content) (Huang et al., 2014; Li et al., 2012). Enhanced severity for HTC treatment could promote the decarboxylation process and improve hydrochar quality (e.g., HHV increase and O reduction), but the overall energy recovery of hydrochar may be decreased due to lower yields (Gaur et al., 2020). After a certain severity factor is reached at supercritical water conditions, the hydrochar yield remains around 10%. The reason for this trend is because hydrochar can be converted into other phases at higher reaction severities. Hydrochar tends to accumulate at a low severity factor. It is worth noting that the maximum biocrude yield can be achieved at a point of severity (around 0.5–1) where hydrochar, gas, and aqueous byproducts are all minimized when aiming for an energy-condensed product. A previous study noted that lower hydrochar yields and higher syngas yields with the intensified reaction severity when temperature increased from 170 °C to 500 °C for HTP of DS (Ekpo et al., 2016). Qian et al. (2020) studied HTL of primary sludge at various severities. They proposed two possible phases during the HTL: First is the conversion of solids in the PS into biocrude and aqueous phase products, which are then converted to volatiles and gas. The rapidly reduced yield of hydrochar probably resulted from cell rupture and hydrolysis of PS that occurred within several minutes at 300 °C. The hydrochar yield remained constant near the end (10.8 wt%) when it reached the ash content in the feedstock (10.3 wt%) (Qian et al., 2020). Tasca et al. (2019) suggested that condensation of a carbonaceous matrix occurred at higher reaction severity (i.e., higher reaction temperature and residence time), while lower severity did not favor the formation of highly condensed

aromatic structure. It is also indicated that humus and protein are the main precursors of hydrochar produced at 300–400 °C (Wang et al., 2019).

=====
Please Insert Fig. 5 Here
=====

2.3.3. Heating rate

Heating rate is another parameter that can affect the HTP products. Mostly a high heating rate can favor the destruction of biomass and inhibit the formation of hydrochar. Wang et al. (2019) studied the effects of heating rate (8–50 °C/min) on the HTG of MS (400 °C for 30 min). Lower yields of char, tar, and water-soluble phase on a carbon basis were observed with higher heating rates. It was suggested that a reduced heating rate could cause a longer reaction period at lower temperatures, which would promote the formation of hydrochar because of insufficient decomposition. However, no effects on gas yield (carbon basis) were reported (Wang et al., 2019). Gong et al. (2018) investigated the effects of both heating rate (3–20 °C/min) and cooling rate (18–50 °C/min) on the formation of PAHs at the reaction temperature of 400 °C (24 MPa) and residence time of 0 min. Total PAHs decreased in both liquid and solid phases with faster heating and cooling. It was also observed that low heating (≤ 6 °C/min) and cooling rate (≤ 28 °C/min) promoted the formation of 6-ring PAHs, while more light fractions of PAHs (2-ring and 3-ring) were formed under higher heating and cooling rate (Gong et al., 2018). However, the impacting mechanisms of heating rate have not been clarified in detail. It is generally assumed that slow heating could enhance the reactions of re-polymerization, condensation, oligomerization, etc., and therefore promote the production of hydrochar.

2.3.4. Co-processing of municipal sludge

Co-processing of MS with other types of biomass using HTP has attracted much interest recently. It plays the role of utilizing various waste biomass for energy conversion, reforming the properties of feedstock, modifying the yield and quality of products, and creating synergistic effects. [Table 3](#)

summarizes research works on co-HTP of MS with different biomass. The co-processing has been studied for producing energy-condensed hydrochar, biocrude, and syngas via co-HTC, co-HTL, and co-HTG, respectively.

=====

Please Insert Table 3 Here

=====

Most coprocessing studies for MS were done under HTC conditions. It was reported that co-HTC (220 °C for 12 h) of MS with peanut shell could improve HHV and hydrophobicity of the corresponding hydrochar, compared to HTC of MS only (He et al., 2019). Such hydrochar showed a more stable and durable combustion profile. Synergistic decarboxylation and favorable aromatization were reported during the co-HTC process (He et al., 2019). Kim et al. (2017) also suggested that there were enhanced dehydration and decarboxylation reactions for co-HTC of DS with peat. It was indicated that waste biomass with abundant cellulose and lignin could promote decarboxylation, dehydration, and demethylation during the co-HTC with DS (Zhai et al., 2017). Several researchers have also conducted co-HTL of MS with lignocellulosic and microalgae. Some studies found synergistic effects with a higher yield of biocrude and better energy recovery from co-HTL of PS or other MS with lignocellulose compared to individual feedstock (Biller et al., 2018; Leng et al., 2018). It was implied that the cause might be from interactions between the intermediates from MS and lignocellulosic biomass during co-processing (Leng et al., 2018). However, Huang et al. (2019) did not observe synergistic effects on biocrude yield or conversion rate by co-HTL of MS with rice straw or wood sawdust, probably due to the low contents of protein and lipid in MS. The addition of microalgae in co-HTL with MS was also reported to have beneficial synergistic effects on biocrude yield (Mishra and Mohanty, 2020; Xu et al., 2019). It seems that co-HTL could promote the production of low-boiling fractions in biocrude (Huang et al., 2019; Mishra and Mohanty, 2020). Co-HTG of MS with other biomass seems to lack research interest. To date, only Xu and Antal (1998) studied the co-gasification of DS with corn starch at 340 °C in the

presence of a catalyst (coconut shell activated carbon). However, no clear results could be obtained to conclude if there were synergistic effects during the co-HTG.

In summary, co-processing of MS with other types of biomass generally provides synergistic effects on produced hydrochar or biocrude. However, such effects rely on the chemical compositions of the feedstocks and hydrothermal conditions. Co-HTP also creates a novel strategy to overcome the drawbacks of different biomass. For example, adding wood biomass could improve the concentrations of biomass in MS and thus enhance the conversion rate. It is believed that co-HTP of various biomass is beneficial over HTP of individual feedstock. Nevertheless, the mechanisms behind the co-HTP are very limited due to the lack of systematic studies. Therefore, more investigation on chemical interactions during the co-HTP should be performed, which would provide a road map for future process design and optimization.

2.3.5. Catalyst

To optimize the yield and quality of featured products and facilitate the conversion rate, various catalysts have been applied to the HTP of MS. A comprehensive summary of recent studies conducted with different catalysts is presented in [Table 4](#). As shown in the table, catalysts applied to HTP of MS include but are not limited to inorganic and organic acids, bases, mineral salts, metal oxides, activated carbon, Ni, and H₂O₂.

=====

Please Insert Table 4 Here

=====

Generally, an acidic environment could promote the hydrolysis, deamination, and dehydration of MS during HTP, while alkaline catalysts mainly facilitate water-gas shift reaction, denitrogenating, and capturing CO₂ under supercritical water conditions (Becker et al., 2019; Gong et al., 2014b; Liu et al., 2020; Zhai et al., 2013). Alkali, as well as other bases, such as ammonia, can catalyze the condensation reactions (Aldol) to produce aromatic compounds from lighter oxygenates, while acid catalyzes the formation of char from carbohydrates. Also, Chen et al. (2020) suggested that an acid environment of

HTC could promote the protonation effect and enhance structural stability of SS-derived hydrochar with diverse morphology, showing a high removal rate (84%) of phenols for adsorption. Liu et al. (2020) found that ash content tended to decrease in hydrochar with the increase of initial pH by adding KOH during the HTC treatment (270 °C for 2 h). However, Li et al. (2017) found that raising initial pH (9–11) by Ca(OH)₂ increased ash content in hydrochar (160 °C for 1 h), possibly due to enhanced mineral precipitation. An acidic environment was found to promote the production of fatty substances, while the formation of N-containing organic compounds and ketone organics was enhanced at alkaline conditions (Liu et al., 2020). The addition of K₂CO₃ could increase biocrude yield and energy recovery from SS under both subcritical (350 °C for 15 min) and supercritical (400 °C for 15 min) conditions (Shah et al., 2020). However, several studies of HTL and HTG have stated that adding Na₂CO₃ or K₂CO₃ had no significant effects on the quality or yield of biocrude (Suzuki et al., 1988; Suzuki and Nakamura, 1989; Wang et al., 2013). This could be attributed to the high alkalinity of MS, as shown in [Table 2](#). Regardless of the initial reaction pH (2–12), the nearly neutral pH of hydrochar also suggested the high buffering capacity of MS (Liu et al., 2020; Wang et al., 2017).

The change of initial pH by acid or alkaline catalysts could also affect the species of nutrients and heavy metals during HTP. Decreased pH could transform organic phosphorus (OP) to inorganic phosphorus (IP), and apatite phosphorus (AP) to non-apatite inorganic phosphorus (NAIP), while increased pH can foster the precipitation of P during HTC (Shi et al., 2019; Wang et al., 2017; Xu et al., 2018). Studies have suggested using hydrochloric acid (HCl) and sulfuric acid (H₂SO₄) to solubilize N and P in HTP aqueous phase, which can be subsequently recovered as fertilizer (e.g., struvite) by precipitation under alkaline conditions (Aragón-Briceño et al., 2021a; Shi et al., 2019). Nevertheless, the high acid consumption to achieve a low pH (e.g., 1.9) only for the sake of P release would not be economically desirable (Lühmann and Wirth, 2020). Increased pH could immobilize heavy metals in hydrochar from HTL (320 °C) of MS and therefore reduce the associated ecological risk (Huang et al., 2011). However, an opposite observation of the mobilization of Cu and Cr was reported with increasing pH under HTC condition (270 °C for 2 h) (Zhai et al., 2016). Other catalysts such as FeCl₃, Al(OH)₃, and

sludge-based activated carbon can also inhibit the migration of heavy metals (Xu and Jiang, 2017; Zhai et al., 2014a).

Mineral salts and oxides have been reported to enhance the hydrothermal conversion of MS. Combined magnesium citrate and H_2SO_4 led to more abundant carboxyl groups (C–N, C–O, and O=C–O) in hydrochar from HTC (260 °C for 1 h). Using FeCl_3 and $\text{Al}(\text{OH})_3$ promoted the decomposition and hydrolysis of WAS at 180 °C (Xu and Jiang, 2017). Adding CaO facilitated the hydrolysis and deamination of organics and the break of aromatic (C–C/C–H) and anomeric (C–H, C–O, O–C–O, and C–N) bonds at 380 °C (He et al., 2016, 2015a). Besides, the CaO additive also promoted the formation of aromatic C–O and O=C–O (He et al., 2016). However, some catalysts (NiMo/ Al_2O_3 , CoMo/ Al_2O_3 , activated carbon felt) showed negative effects on energy recovery in HTL, although HHV values of biocrude were improved compared to non-catalytic runs (Prestigiacomio et al., 2019). Therefore, energy recovery rate should be considered as an important criterion in evaluating the impacts of catalysts.

Nickel catalysts are well reported in the enhancement of gasification efficiency. Numerous studies have demonstrated that increased load of nickel could enhance methane and hydrogen yields as well as carbon gasification ratio significantly under HTG conditions due to the promotion of water-gas shift reaction (Afif et al., 2011; Gong et al., 2014b; Sawai et al., 2014; Wang et al., 2017). Other co-catalysts (e.g., NaOH, K_2CO_3 , and H_2O_2) with Ni have also been reported to further augment the enhancement. The addition of alkaline catalysts to HTG of MS could further promote the water-gas shift reaction and favor H_2 production by seizing CO_2 (Gong et al., 2014b). Ni catalyst can effectively decrease the generation of phenols, while H_2O_2 can promote the degradation of PAHs to form intermediates (Wang et al., 2017). Therefore, the combination of Ni/ H_2O_2 could favor the gasification of intermediates to avoid re-polymerization to new PAHs. NaOH and H_2O_2 catalysts could also inhibit the formation of char and tar, and thus relieve the fouling of Ni catalysts caused by char (Sawai et al., 2014; Wang et al., 2019). However, adding certain H_2O_2 alone would dramatically reduce the yield of combustible gases (H_2 , CO, and CH_4) to 0, even though it can achieve the carbon gasification efficiency of 90% (Qian et al., 2015). One significant drawback of Ni catalysts is their pricy cost and deactivation with service time. It has been

reported that their catalytic performance is degraded with time due to sulfur fouling and surface deposition of char and tar (Sawai et al., 2014). Therefore, future studies should not just focus on the efficiency of catalysts but also on enhancing their reusability.

From the gathered remarks from HTP studies, catalysts have shown outstanding effects on the reactions in MS treatment. However, detailed reaction pathways caused by various catalysts are still limited. Given the complex compositions of MS, such as high alkalinity and diverse minerals and heavy metals, it is worth investigating the particular mechanism of each potential catalyst. Synergetic effects of co-catalysts are promising to enhance their performance and durability and therefore demand further exploration. It is also more reasonable to incorporate the energy recovery rate into the evaluation criteria.

2.3.6.Solvent or co-solvent

Noticeably, most solvents or co-solvents (solvent mixed with water) applied to HTP of MS were for the liquefaction and the production of biocrude. [Table 5](#) summarizes HTP studies that utilized organic solvents as reaction media in MS treatment. The studied solvents include acetone, ethanol, methanol, and n-hexane. It has been demonstrated that the application of solvents or co-solvents could moderate the reaction conditions and enhance the yield and/or caloric value of biocrude at lower reaction temperatures.

=====

Please Insert Table 5 Here

=====

There are several advantages of utilizing solvents in HTP. Firstly, the critical points of these organic solvents are much lower than water and, therefore, can depolymerize biomass at milder temperature and pressure conditions (Perkins et al., 2019). For acetone, ethanol, methanol, and n-hexane, their critical temperatures are 234.9, 243.1, 239.5, and 234.5 °C, respectively, while their critical pressures are 4.8, 6.3, 8.1, and 3.0 MPa, respectively. Secondly, organic solvents could dissolve liquefied products with high-molecular-weight more easily than using pure water due to the lower dielectric constants (Lai et al., 2018). Thirdly, polar solvents (e.g., ethanol and methanol) can donate active hydrogen and facilitate the free

radical and dehydration reactions (Huang et al., 2014). Thus, the produced biocrude would have lower oxygen content. However, when using dipolar solvents, such as acetone, the dehydration reactions are mainly responsible for the deoxygenation process (Leng et al., 2015a). Lastly, using ethanol or methanol can convert acidic components into esters through esterification reaction, and therefore enhance the biocrude quality (Huang et al., 2013). However, the biocrude obtained with acetone is primarily consisted of ketones and N-containing compounds with relatively low calorific values (e.g., 26.7 MJ/kg), although acetone treatments consistently lead to higher biocrude yields (Huang et al., 2014; Leng et al., 2015a).

Beneficial synergistic effects of ethanol-water co-solvents on biocrude yield and energy recovery have been reported (Lai et al., 2018). Li et al. (2010) also found that increasing ethanol-water ratios could improve the yield and reduce the O contents of biocrude. However, Prajitno et al. (2018) pointed out that the addition of solvents should be counted for the enhancement since solvents were consumed during the HTL treatment. Therefore, solvents should be considered in the feedstock when calculating yield and energy conversion. Besides, ethanol-water co-solvent could also promote the production of esters (69.1%) in biocrude compared to pure ethanol (57.4%) and pure water (43.3%) HTL (220 °C for 30 min) (Lai et al., 2018). This improvement may be attributed to combined ionic, polar non-ionic, and free-radical reactions.

Indeed, the utilization of organic solvents or co-solvents in HTP of MS has significant impacts on the reaction mechanisms. However, the biggest barriers are the industrial implementation and the recovery and recycle of solvents, which requires further validation and investigation. The other consideration is that the higher quality of reactor material may be required due to the supercritical conditions created by solvents. It has been observed that the corrosion of the reactor wall (316 stainless steel) can be caused by supercritical ethanol at 300 and 350 °C (Chen et al., 2014). Lastly, there are limited studies about the influence of organic solvents on MS-derived hydrochar. Consequently, to comprehensively understand the effects of solvents and evaluate the potential utilization of the corresponding hydrochar, more research should be conducted in hydrochar characterization.

3. Characterization of hydrochar

Diverse MS properties and hydrothermal conditions would result in a hydrochar with various physical and chemical characteristics. It is of critical significance to characterize MS-derived hydrochar since the properties of hydrochar essentially determine its potential applications.

3.1. The proximate and ultimate analyses

The proximate and ultimate analyses have been widely applied to the characterization of solid fuels, such as coal. These analyses are also frequently utilized for evaluating the potential use of hydrochar as a fuel resource. The proximate analysis measures the contents of ash, VM, and FC by recording the mass change of hydrochar while heating at high temperatures. Mostly used methods include the American Society for Testing and Materials (ASTM) D3174 (for ash), D3175 (for VM), and D7582 (for proximate analysis) (Danso-Boateng et al., 2015; He et al., 2014b; Lee et al., 2019). FC is usually estimated by calculating the difference between sample mass and ash and VM contents. The ultimate analysis of C, H, N, and S can be determined using an elemental analyzer, while O content is typically estimated by the difference between sample mass and contents of C, H, N, S, and ash (Zheng et al., 2019). The ASTM D5373 can be referred to as a standard method for the ultimate analysis.

[Fig. 6a](#) summarizes the physicochemical properties of MS-derived hydrochar reported in numerous studies. Detailed data and reaction conditions of selected studies are presented in [Table 6](#). Due to the heterogeneous nature of MS and substantial range of hydrothermal conditions, the corresponding hydrochar exhibits properties with large varieties. Most studies (80%) reported hydrochar with ash, VM, FC, and HHV values of 29.3–79.6%, 14.2–63.3%, 1.1–13.3%, and 3.9–18.9 MJ/kg on a dry basis, respectively. It seems that high HTP temperatures (e.g., >280 °C) generally cause very high contents, low carbon, low VM, and low HHV in hydrochar. Apart from ash, MS-derived hydrochar is comprised of 12–44.3% C, 1.7–5.6% H, 4.6–25.1% O, 0.9–4.6% N, and 0.2–1.7% S on a dry basis. Many studies also reported that the pH of hydrochar was around neutral (5.8–7.6), with an average of 6.6, regardless of the initial pH prior to the reaction. [Fig. 6b](#) compares properties of MS to its derived hydrochar based on the sludge type used in HTP. For DS, PS, and SS, the derived hydrochar tends to have relatively lower C,

while hydrochar derived from mixed primary and secondary sludge (MPS) has higher C probably due to mild reaction temperatures (mostly $<280\text{ }^{\circ}\text{C}$) and relatively low ash contents in MPS (averagely 31.2%, db). Regardless of sludge type, hydrochar tends to have lower H, O, N, and VM but higher ash contents, while S remains at a similar level to those in MS. Such changes could be caused by the dehydration, decarboxylation, and decomposition of organic matter (e.g., protein), dissolution of low-molecular components, and the transformation into organic vapors or gaseous products. Wang et al. (2020) suggested that nearly 90% of S in SS after HTP ($180\text{--}300\text{ }^{\circ}\text{C}$) remained in hydrochar, and increasing temperature reduced S in hydrochar and aqueous phase (mainly sulfate) and enhanced gaseous S formation (e.g., SO_2 and H_2S). FC represents the stable components of char, which increases with the rank of coal. Interestingly we found that average FC contents in hydrochar derived from PS, SS, and MPS all decreased, but it increased in DS-derived hydrochar. Regarding the energy density, PS, SS, and MPS could be good candidates for their relatively high C, VM, and HHV but low ash contents, while SS may lead to high S contents in hydrochar (averagely 1.2%, db). Therefore, combining DS with PS/SS for HTC treatment could potentially produce high-quality coal-like hydrochar. It should also be noted that HTP conditions could largely affect the properties of hydrochar. Fig. 6c compares properties of hydrochar by HTP types. It is found that the properties (mean) in the feedstock MS are at the similar levels, but they are quite different in the derived hydrochar from HTC vs. HTL/HTG. Generally, high reaction temperatures in HTL and HTG intensify the dehydration, decarboxylation, deamination, and decomposition reactions, which lead to further reduction of C, H, O, N, and VM and increase of remaining ash. HTL and HTG minimize the HHV of hydrochar because most C is distributed into biocrude and syngas, respectively. Cyclization, aromatization, and re-polymerization are responsible for the enhanced FC due to the formation of stable carbon. Lee et al. (2019) observed that increasing temperature from 180 to $270\text{ }^{\circ}\text{C}$ decreased the contents of C, O, N and VM, but increased ash and FC values of PS-derived hydrochar, with an HHV of $16.68\text{--}19.70\text{ MJ/kg}$. Wang et al. (2019) also reported the same inclination when reaction temperature increased from 170 to $350\text{ }^{\circ}\text{C}$. However, the corresponding hydrochar had a fairly low HHV

of 3.27–4.77 MJ/kg. It should be noted that the raw MS used by Lee et al. had an initial HHV of 19.68 MJ/kg, compared to only 5.53 MJ/kg used by Wang et al. Therefore, the properties of hydrochar are highly dependent on the characteristics of the corresponding MS and HTP conditions. Therefore, the usage of hydrochar will be dependent on how it is formed and the resulted compositions.

=====

Please Insert Fig. 6 Here

=====

=====

Please Insert Table 6 Here

=====

With the determination of C, H, and O, the atomic ratios of H/C and O/C are commonly calculated to evaluate the transformation of biomass during the HTP treatment. Specifically, the van Krevelen diagram is graphed to assist the evaluation, where anthracite, coals, lignite, and peat could be applied to compare the coalification extent of hydrochar. Fig. 7 displays the H/C and O/C ratios of MS and its derived hydrochar reported by numerous studies. Generally, these ratios are lower in hydrochar than in original MS, and the H/C ratio is much higher than O/C of hydrochar. This indicates that the reaction pathway of HTP is predominantly regulated by dehydration, followed by decarboxylation, while demethylation is mostly minor (Wang et al., 2018). These reactions can enhance the performance of hydrochar by removing oxygen. Low ratios of H/C and O/C also suggest high aromaticity of hydrochar (Zhuang et al., 2018). Wang et al. (2019b) studied the impacts of reaction severity on H/C and O/C ratios and found a strong correlation between the reduction of both ratios and the increase of severity factor (120–300 °C for 30–180 min). Due to the decarboxylation process in HTP, CO₂ has been reported as the major gas phase under subcritical conditions. However, it should be noted that there is a lack of study on the properties of hydrochar obtained at supercritical conditions. It has been observed that HTC temperatures of 150–

280 °C could generate desirable H/C and O/C ratios of hydrochar derived from all types of sludge close to the quality of lignite and coal, while higher HTL/HTG temperatures may lead to very low H/C but high O/C values.

=====

Please Insert Fig. 7 Here

=====

3.2. Distribution of macronutrients in hydrochar

Macronutrients are abundantly distributed in hydrochar, such as N, P, Na, K, Al, Ca, Fe, and Mg. Their distributions are closely related to the compositions of MS. [Fig. 8a](#) illustrates the percentage of each element distributed in hydrochar from various studies (it is noted that some data were over 100% probably due to experimental errors). Basically, all macronutrients have shown large variations in terms of their presence in MS-derived hydrochar. However, most studies have displayed that P (>82%), Al (>86%), Ca (>80%), Fe (>72%), and Mg (>82%) incline to accumulate in hydrochar, while N (~39%), Na (~42%), and K (~52%) seem not. The majority of C could also be distributed to hydrochar, but it can be significantly reduced by increased HTP temperature (e.g., >280 °C). It is known that Al, Ca, Fe, and Mg have strong affinity with P, which would form mineral phosphate precipitates during HTP treatment. Therefore, the concentrations of most macronutrients in hydrochar could be significantly increased compared to the substrate (MS). Considering the substantial mass loss of solids after HTP, the total contents of N, Na, and K would not decrease much but may even increase (Zhang et al., 2014). However, Zhang et al. (2014) discovered that HTP at 190 and 260 °C could essentially inhibit the bioavailability of N, P and K. The concentrations of extractable $\text{NH}_4^+\text{-N}$ (by 2M KCl), $\text{NO}_3^-\text{-N}$ (by 2M KCl), P (by 0.5M NaHCO_3), and K (by 1M NH_4OAC) in hydrochar reduced by over 1, 8, 8, and 9 times, respectively, compared to those in MS. The low availability of these nutrients in hydrochar may enhance its behaviors as soil nutrients due to the extended durability.

=====
Please Insert Fig. 8 Here
=====

As shown in [Fig. 8b](#), the concentrations of macronutrients seem to remain unchanged or increase in hydrochar compared to its original MS. P and Ca exhibit the largest variety in hydrochar with a content range of 0.14–8.1% and 0.3–22% on a dry basis, respectively. Most reported ranges of each nutrient in hydrochar are also identified: Al (0.3–3.5%), Ca (0.4–4.8%), Fe (0.3–4.2%), K (0.2–0.8%), Mg (0.3–1.3%), Na (0.03–0.4%), and P (0.7–5.3%) on the dry basis. In most cases, SS and DS and their derived hydrochar could have above mean levels of Al, Fe, Mg, and P in reported MS. High concentrations of cations could provide hydrochar with adsorption ability for cationic pollutants due to cation exchange (Leng et al., 2015b). The hydrochar with the highest concentration of P (8.1%, db) was reported from the HTC of WAS (initial P of 4.1%, db) at 225 °C for 16 h (Huang and Tang, 2016). Such hydrochar with high contents of P could be a promising candidate for fertilizer or nutrient recovery. To further evaluate the nutrient values of hydrochar, atomic ratios of N:P versus C:N and N:P versus C:P are plotted in [Fig. 9](#). It appears that most hydrochar has high C:N (>10) but low N:P (<10) ratios ([Fig. 9a](#)), which signifies its potential as P-rich fertilizer (Huang et al., 2018). In some cases, hydrochar can also have high C:P (>100) and N:P (~9) ratios ([Fig. 9b](#)), representing a potential N-rich fertilizer (Huang et al., 2018).

=====
Please Insert Fig. 9 Here
=====

3.3. Contaminants of concern

Due to the heterogeneous nature of MS, the ultimate destiny of its derived hydrochar is not clear. It has been found that thermal treatment can cause some contaminants to remain in hydrochar. Mostly

reported contaminants of concern include heavy metals and persistent organic pollutants (POPs), such as PAHs, PCBs, polychlorinated dibenzo-dioxins/-furans (PCDD/Fs) as well as pharmaceuticals.

3.3.1. Heavy metals

Heavy metals are known to accumulate in the environment and food chain for their non-biodegradability. Many municipalities (e.g., British Columbia in Canada) have regulated their concentrations when using stabilized and dewatered MS (biosolids) for land application as fertilizer. Owing to the common presence and toxicity of heavy metals, Canada, the European Union (EU), and the US have implemented criteria for As, Cd, Cr, Co, Cu, Hg, Mo, Ni, Pb, Se, and Zn (Table 7). These limits should also be adopted for MS-hydrochar before a specific guideline is formed. Table 7 summarizes the total concentration of each heavy metal in MS-derived hydrochar reported in Canada, China, Japan, the EU, and the US. It demonstrates that Cr, Cu, Hg, Ni, and Zn are found to exceed the land application criteria, while the data of Se are lacking. Previous studies have verified that most heavy metals are concentrated in hydrochar compared to other products from HTP of MS. Fig. 10a compares the total concentrations of commonly found heavy metals in various types of MS and the corresponding hydrochar. It is observed that all MS samples show low mean levels of As, Cd, Co, and Mo, with slightly lower or unchanged concentrations in hydrochar. However, the average contents of Cr, Cu, Ni, and Zn could be sustainably raised in hydrochar compared to the original MS. A previous study ranked the accumulation rate of heavy metals in hydrochar in the following order: Zn > Cu > Cr > Ni > Pb > As > Hg > Cd (L. Wang et al., 2019b). Particularly, concerning amount of heavy metals could be present in hydrochar derived from PS (Cu, Ni, and Zn), SS (Cr, Cu, Hg, Ni, Pb, and Zn), MPS (Cu and Hg), and DS (Cu, Hg, and Ni), which should attract more attention.

=====

Please Insert Table 7 Here

=====

=====
Please Insert Fig. 10 Here
=====

Besides the measurement of total metals, chemical species and leachability are commonly used to determine the mobility and toxicity of heavy metals (Chen et al., 2020; Shao et al., 2020). The chemical speciation of heavy metals has been widely used to evaluate the mobility and bioavailability to the environment and biosphere, while the leaching characteristics can reflect the stability of heavy metals under extreme environmental conditions. To determine the chemical speciation of heavy metals in hydrochar, sequential extraction procedures (SEPs) developed by Tessier and the Community Bureau of Reference (BCR) have been adopted (Li et al., 2012; Yuan et al., 2011). According to the Tessier SEPs, heavy metals are classified into five fractions: Exchangeable fraction (F1), carbonate-bound fraction (F2), Fe-Mn oxides fraction (F3), organic matter/sulfide fraction (F4), and residual fraction (F5). According to the BCR extraction, heavy metals are categorized into four fractions: Acid soluble fraction (f1), reducible fraction (f2), oxidizable fraction (f3), and residual fraction (f4). Both procedures have identical categories of metal species. Based on the extraction methods, these fractions can be further described as three groups: readily bioavailable (F1+F2 or f1+f2), potentially bioavailable (F3+F4 or f3), and non-bioavailable (F5 or f4) (Shi et al., 2013).

[Fig. 10b](#) illustrates the ternary plot of the fractional distribution of various heavy metals reported in MS and the consequent hydrochar. Most metals (As, Cd, Cr, Cu, Ni, Pb, and Zn) have demonstrated that their readily bioavailable forms can be converted into potentially bioavailable and/or non-bioavailable fractions during the HTP treatment, therefore reducing the toxicity and bioavailability. It also displays that increasing reaction temperature and residence time could further inhibit the bioavailability of heavy metals in hydrochar (Chen et al., 2014; Fei et al., 2019b). However, such a trend seems to be reversed after approaching the critical point of water. Li et al. (2012) found that the readily bioavailable forms of Cd, Pb, and Zn, as well as their total contents, increased with increasing temperature (from 375 to 400 °C).

Xu et al. (2011) also reported the readily bioavailable Cd, Cr, and As dramatically enhanced from 0.7% to 14%, 0.4% to 3%, and 1.3% to 12.6%, respectively, after reaction condition raised from subcritical (350 °C) to supercritical (400 °C). Huang et al. (2021) found that HTC treatment (150–275 °C) could transform metals into insoluble sulfides (e.g., Cu-Fe- or Zn-Fe-sulfides) and completely reduce high-toxic Cr(VI) into low-toxic Cr(III) in hydrochar derived from WAS and DS. Besides, Lu et al. (2021) reported that co-HTC of MS with lignocellulosic biomass (e.g., cellulose, lignin, and xylan) could further promote the immobilization of heavy metals (e.g., Cr, Cu, Ni, and Zn) along with improved fuel quality of hydrochar. In general, the bioavailability and toxicity of heavy metals are highly reduced after HTP compared to raw MS.

With the availability of characterizing metal fractions, various risk assessment methods are established. The ecological risk index assessment, geo-accumulation index, and risk assessment code have been used to evaluate the risks associated with heavy metals. Detailed explanations have been summarized by Huang and Yuan (2016). By applying these methods, numerous studies have found the overall bioavailability and ecotoxicity of heavy metals in hydrochar are decreased compared to raw MS (Chen et al., 2014; Shao et al., 2015; Shi et al., 2014, 2013; Zhai et al., 2016). Therefore, HTP can be considered as a promising detoxification technology for municipal biosolids.

Toxicity characteristic leaching procedure (TCLP) is another approach to assess the leachability of heavy metals under various conditions (acidic, neutral, and alkaline). The US Environmental Protection Agency (EPA) Method 1311 can be referred to as a standard procedure. Liu et al. found that HTC at 200 °C for 30 min reduced the leachable amount of Cd, Cr, Cu, Mn, Ni, Pb, and Zn from 0.77, 2.84, 3.1, 154.57, 23, 11.44, and 25.39 mg/kg in digested sludge to 0.26, 1.36, 0.7, 121.34, 7.25, 10.34 and 12.58 mg/kg in hydrochar, respectively. However, the leachable Hg slightly increased from 0.2 to 0.3 mg/kg (Liu et al., 2018b). Fei et al. (2019b) identified the decreased leachability of Cu, Ni, and Zn with the increasing reaction temperature of HTP for MPS-derived hydrochar. It was also discovered that HTP had greater inhibition on leachable Zn than pyrolysis. Shi et al., (2014) obtained a decline of Cd, Cr, Cu, Ni, Pb, and Zn in the leachate from DS-derived hydrochar with 94%, 74%, 97%, 72%, 11%, and 86%,

respectively, after HTC at 280 °C for 1 h, compared to raw digested sludge. It was also found that hydroxyapatite addition could further reduce the leachability of Cd during the HTC treatment (200 and 280 °C) (Shi et al., 2014). Adding NaOH also showed a reduction in leachable Cu and Zn in hydrochar generated at 320 °C (Huang et al., 2011). In summary, the HTP process has demonstrated effective ways for immobilizing heavy metals and thus reducing the toxicity of hydrochar. However, the challenge is if the abovementioned risks will be changed when hydrochar is applied to soil under potential synergetic effects from the environment. This requires additional efforts to be clarified prior to land utilization.

3.3.2. Persistent organic pollutants (POPs)

Many organic compounds have been identified in MS with over 100 pollutants attributed to pharmaceuticals, personal care products (PPCPs), pesticides, and their metabolites. Many of these contaminants are known to be highly persistent, even under intensive thermal treatment conditions. The presence of PAHs, PCBs, PCDDs, and PCDFs has brought researchers' concerns to the surface when considering the utilization of hydrochar.

3.3.2.1. Polycyclic aromatic hydrocarbons (PAHs)

The US EPA has identified 16 PAHs as priority contaminants, including acenaphthene, acenaphthylene, anthracene, benzo[a]anthracene, benzo[a]pyrene, benzo[b]fluoranthene, benzo[g,h,i]perylene, benzo[k]fluoranthene, chrysene, dibenz[a,h]anthracene, fluoranthene, fluorene, indeno[1,2,3-c,d]pyrene, naphthalene, phenanthrene, and pyrene (Hu et al., 2021). Those PAHs with four or more benzene rings are considered carcinogenic, i.e., benzo[a]anthracene, benzo[a]pyrene, benzo[b]fluoranthene, benzo[g,h,i]perylene, benzo[k]fluoranthene, chrysene, dibenz[a,h]anthracene, indeno[1,2,3-c,d]pyrene, and pyrene. [Fig. 11](#) illustrates the total PAHs in MS and its derived hydrochar from hydrothermal studies. Most current studies have confirmed that HTP treatment causes concentrated PAHs (4.2–19 mg/kg) in hydrochar under both subcritical and supercritical water conditions. Wiedner et al. (2013) investigated various types of feedstock for HTC and found MS-derived hydrochar had the highest total PAHs (12.1 mg/kg) over any other types of biomass (e.g., maize, food waste, manure digestate, and grass greenery). They also reported that hydrochar had a higher portion of 2-ring PAHs

compared to raw biomass. Gong et al. (2018) studied the PAHs formation from MS through HTP at subcritical (220–325 °C) and supercritical (375–400 °C) water conditions. It was found that total PAHs in hydrochar increased gradually with increasing reaction temperature and reached the highest (12.1 mg/kg) at 400 °C. Interestingly, slow heating and cooling processes could enhance the formation of heavy PAHs (4–6 rings), which essentially was resulted from the extended total reaction time and severity (Gong et al., 2018). They also examined the changes of PAHs during the HTG of MPS from various WWTPs (Gong et al., 2016b). These MPS samples were initially dominated by 3-ring and 4-ring PAHs, but then shifted to 2-ring and 3-ring PAHs after HTG at 400 °C for 1 h. A positive linear correlation was identified between the total PAHs in hydrochar and the initial contents of VM, humic substances and lignin, and crude fat and carbohydrate in MPS. However, an opposite trend was found with the initial pH of MPS (Gong et al., 2016b). The wide range of total PAHs in MPS (3–15.5 mg/kg) also caused a large variety in hydrochar (3.8–28.5 mg/kg) under the same HTG condition. The possible reaction pathway of the formation of PAHs is included in Fig. 4. Wang et al. (2017) discovered adding catalysts such as Ni and H₂O₂ could inhibit the formation of PAHs. Liu et al. (2021) found adding 3–9 %, db of CaO to MS for HTC (200 °C for 10 h) could reduce PAHs (by 5.6–16%) and TEQ (by 2.9–3.5%) of hydrochar by inhibiting free radical reaction. Melo et al. (2019) reported a significant rise of almost each PAH compound in hydrochar (190 °C) compared to initial biosolids feedstock, with the total PAHs increased from 3.7 mg/kg to 21.2 mg/kg. However, one study found that most PAHs (> 89%) from HTL (240–360 °C for 0–60 min) were distributed into biocrude produced, while MS-derived hydrochar only contained 1.4–1.8 mg/kg of PAHs possibly due to the solvent (dichloromethane) extraction, thus leachable contents and toxic equivalent (TEQ) of PAHs of hydrochar and associated environmental risk were reduced compared to MS (Chang et al., 2021). It seems that the formation of PAHs in hydrochar is governed by the feedstock compositions (e.g., initial PAHs and organic components) and HTP treatment conditions (mainly reaction temperature and severity). European Biochar Foundation (EBC) has established a guideline for the application of biochar and defined a threshold of PAHs (12 mg/kg) for basic grade biochar (EBC, 2019). Such a limit is set specifically for biochar, which has shown effective binding of PAHs. However, to date, there is no

research available about the PAHs released from MS-derived hydrochar. Therefore, further research on the risks associated with PAHs is necessary to provide a legal framework and benchmark prior to the application of hydrochar.

=====

Please Insert Fig. 11 Here

=====

3.3.2.2. Polychlorinated biphenyls (PCBs) and polychlorinated dibenzo-dioxins/-furans (PCDD/Fs)

Low levels of PCBs and PCDD/Fs have been commonly detected in MS, which are mainly originated from disinfectants, solvents, oil and grease, pesticides, and other industrial and household products (Fijalkowski et al., 2017). For soil protection, PCBs, dioxins, and furans in biochar are also regulated by the EBC: 0.2 mg/kg for PCBs and 20 ng/kg by international toxic equivalent (I-TEQ) for dioxins and furans (EBC, 2019). Some researchers have started the investigation of how PCBs and PCDD/Fs react during the HTP treatment of MS. Wiedner et al., (2013) examined various types of feedstock for HTP at 230 °C for 15 min, followed by 180 °C for 75 min. MS-derived hydrochar showed the top level of I-TEQ (14.2 ng/kg) for PCDD/Fs among all tested biomass (all others below 6 ng/kg). Brookman et al. (2018) investigated the effects of HTC (200–240 °C for 5 h) on PCBs and PCDD/Fs. Results presented that total PCDDs increased from 1.24 mg/kg in raw DS to 1.43 mg/kg in hydrochar obtained at 200 °C, but then suddenly decreased with increasing temperature to 0.12 mg/kg at 240 °C. Differently, the total PCDFs in hydrochar gradually decreased with increasing temperature and reached a minimum of 0.012 mg/kg at 240 °C compared to that of MS (0.11 mg/kg). However, total PCBs remained identical in hydrochar from all conditions (4.33–4.43 mg/kg), compared to 4.81 mg/kg in MS. When considering the toxicity by TEQ, the total TEQ of PCBs and PCDD/Fs was raised 9 times with increasing temperature from 5.36 ng/kg in MS to 46.09 ng/kg in hydrochar obtained at 240 °C. This was mostly contributed by PCDDs, whose TEQ increased significantly from an initial 2.72 ng/kg to a final 44.5 ng/kg (Brookman et al., 2018). On one hand, it appears that HTC could dechlorinate POPs. On the other hand, the low chlorinated congeners

with high toxicity index raise the overall TEQ of these contaminants. However, the overall risk from PCBs and PCDD/Fs cannot be concluded due to limited studies. Therefore, the toxicity of POPs in hydrochar should be carefully examined prior to its utilization. Detailed studies of various reaction conditions should also be further explored.

3.3.2.3. *Other persistent organic pollutants (POPs)*

Emerging contaminants, such as PPCPs and perfluorinated compounds (PFCs), have attracted more attention recently (Fijalkowski et al., 2017). The reason is related to their wide use in industrial and consumer applications and associated health concerns, such as endocrine disruption resulted from PPCPs and reduced female fertility and sperm quality caused by PFCs. vom Eyser et al. (2015) spiked various pharmaceuticals into SS to investigate the impacts of HTC (210 for 4 h) on them. They found that HTC could remove over 68% of carbamazepine, clarithromycin, diclofenac, erythromycin, propranolol, and roxithromycin, and 42% of metoprolol from hydrochar compared to raw feedstock. However, the content of phenazone rather slightly increased from 210 $\mu\text{g}/\text{kg}$ to 230 $\mu\text{g}/\text{kg}$ after HTC. It was indicated that the precursors might be converted to phenazone by reversible chemical bonds and thus caused such an increase (vom Eyser et al., 2015). However, there was no convincing evidence. Due to the persistence, hydrophobicity, and electrostatic interactions, PFAs can accumulate in MS and their fate in HTP is of great interest. A recent study investigated the effects of HTL on PFAs in mixed primary and secondary sludge and found that: 1) High reaction severity (350 °C for 90 min) degraded >99% fluorinated carboxylic acid structures but limited sulfonic acid structures; 2) minerals in sludge solids could catalyze the transformation of PFAs; and 3) hydrochar and aqueous had minimal undegraded PFAs, which were mostly distributed into biocrude, demanding monitoring/purification during upgrading (Yu et al., 2020). The Pacific Northwest National Laboratory observed that all analyzed PFCs and most PPCPs in PS and SS were removed after the HTL process (reaction conditions not reported) (Mitroshkov et al., 2019). However, some PPCPs, such as ibuprofen, diclofenac, and 4-tert-octylphenol were still present in wet hydrochar (comparable to initial contents). The differences of PFAs from the above two studies may be attributed to the initial concentrations. One pilot-scale HTL (at 325 or 350 °C for 5 min) study achieved

99% destruction for most pharmaceuticals and pesticides detected in the original MS (Silva Thomsen et al., 2020). With limited studies, we can infer that although HTP treatment can destroy most PPCPs and PFCs, there is a considerable amount of POPs remaining in hydrochar. Therefore, further investigation is necessary for guiding the establishment of environmental criteria.

3.4. Characterization of surface functionality and structure

3.4.1. *Fourier-transform infrared spectroscopy (FTIR)*

FTIR is the most used technique for characterizing the surface functionality of hydrochar. It can semi-quantitatively display the change of surface functional groups and thus explain potential reactions during the HTP treatment. Table 8 summarizes the observed peaks in FTIR spectra of MS-derived hydrochar and potential corresponding components. Compared to the MS feedstock, the -OH stretching between $3600\text{--}3200\text{ cm}^{-1}$ in hydrochar tends to be weakened, which is typically caused by dehydration reactions (Gai et al., 2016a). This is consistent with the reduced H/C and O/C ratios shown in the van Krevelen diagram (Fig. 7). The disappeared or declined -C-H stretching may suggest the demethylation or condensation reactions during the HTP treatment (Leng et al., 2015b). After HTP, the absence of band at $1120\text{--}1050\text{ cm}^{-1}$ could be attributed to decarboxylation reactions, which causes the break of -C-O bond (Kim et al., 2017). The decreased intensity of the -C=N stretching could reflect the hydrolysis reaction during the HTP (Peng et al., 2016). The enhanced intensity of -C=C stretching generally indicates the formation of aromatic compounds (Kim et al., 2017; Peng et al., 2016). It was suggested that the decomposition of amides should be responsible for the fading -N-H band by the formation of ammonia (Chen et al., 2013b). The decomposition of amide I may also enhance the -C=O peaks and form CO_2 and CO (Chen et al., 2013b). By comparing the intensity changes of FTIR bands between MS and its derived hydrochar, potential reactions could be inferred. However, it should be noted that some peaks may be overlapped by others. For example, the vibration of carboxylates (-C=O) and carboxylic acids (-C-O) can cause overlaps to amide I and amide III bands, respectively (Zhao et al., 2013). Overall, FTIR spectra have shown the reduced oxygenated surface functional groups but increased aromatic functional groups in hydrochar compared to the MS feedstock. The condensed carbon structure and abundant functional

groups could improve the C sequestration, C stability, and surface activity of hydrochar, indicating high potential of water and nutrient retention for soil amendment and decent adsorption capacity for water remediation.

=====

Please Insert Table 8 Here

=====

3.4.2. Two-dimensional perturbation correlation infrared spectroscopy (2D-PCIS)

As abovementioned, the peak overlapping in FTIR spectra limits its analytical discussion, whereas the 2D-PCIS can provide an enhanced resolution of significant peaks and overcome this issue. 2D-PCIS elucidates the quantitative similarity or dissimilarity variations and explains chemical bonds according to Noda's rules (Harvey et al., 2012). Zhuang et al. (2018) first applied this technique to characterize MS and its derived hydrochar. The synchronous and asynchronous spectra of $-C-H$ were reflected in $3100-2800\text{ cm}^{-1}$, while stretches of $-C=O$, $-C-C$, and $-C-O$ were displayed in the ranges of $1800-1650$, $1650-1500$, and $1300-1000\text{ cm}^{-1}$, respectively. With the assistance of the 2D-PCIS and calculated relative intensities, they were able to deduce that the aliphatic chain was cyclized before the demethylation from aromatics during the HTP. The demethylation started first at low temperature ($120\text{ }^{\circ}\text{C}$), while aliphatic methylene was cracked at higher temperatures ($180-300\text{ }^{\circ}\text{C}$), and subsequently bound onto the aromatic structures through polymerization and condensation. Over $180\text{ }^{\circ}\text{C}$, the intensity of aromatic $-C-C$ decreased with the increase of polyaromatic $-C-C$ simultaneously, possibly due to the accelerated aromatization. The rapid reduction of $-C-O$ bonds was also observed with increasing reaction temperature, indicating the route of aromatic condensation (Zhuang et al., 2018). Overall, 2D-PCIS can effectively display the changes of surface functional groups and thus facilitate the explanation of reaction pathways during HTP.

3.4.3. X-ray photoelectron spectroscopy (XPS)

XPS is a useful tool to analyze the outer surface of hydrochar and determine the atomic composition and functional forms more accurately than FTIR. Depending on the spectra used, such as C1s (Zhuang et al., 2018), N1s (He et al., 2015b), S2p (Wang et al., 2020), and Fe(2p) (Zhang and Hay, 2020), C, N, S, and Fe containing compounds can be identified, respectively. Zhuang et al. (2018) detected five C-functional groups in MS and the corresponding hydrochar (180–300 °C for 30–120 min): $\text{--}\underline{\text{C}}\text{--H}$, $\text{--}\underline{\text{C}}\text{--(C, H)}$ / $\text{--}\underline{\text{C}}\text{=C}$, $\text{--}\underline{\text{C}}\text{--(O, N)}$, $\text{--}\underline{\text{C}}\text{=O}$ and $\text{O}=\underline{\text{C}}\text{--O}$. Based on the calculated relative intensity, it was found that the sum of $\text{--}\underline{\text{C}}\text{--C}$ and $\text{--}\underline{\text{C}}\text{=C}$ fractions in derived hydrochar significantly increased with reaction severity and reached the maximum (43%) at 300 °C for 120 min. Such enhancement was attributed to the decomposition of aliphatic carbon in carbohydrates or proteins and the formed aromatic compounds by condensation and polymerization (Zhuang et al., 2018). He et al. (2016) also observed these same carbon peaks between 280–290 eV. They found that $\text{--}\underline{\text{C}}\text{--(C, H)}$ (60.24%) was initially dominant in MS but without the presence of $\text{O}=\underline{\text{C}}\text{--O}$. With the increasing temperature from 260 to 380 °C, the portions $\text{--}\underline{\text{C}}\text{--H}$ and $\text{--}\underline{\text{C}}\text{--(O, N)}$ gradually raised and became principal at 380 °C, while the $\text{O}=\underline{\text{C}}\text{--O}$ group was not present until the addition of CaO during the reaction. It was indicated that CaO catalyst could promote the hydrolysis of nitrile-N and deamination of pyridine-N (He et al., 2016). However, Melo et al. (2019) only identified three carbon groups in biosolids and hydrochar: Hydroxyl (--C--OH / --C--O), aliphatic/aromatic (--C--C / --C--H), and sp^2 C. They stated more O-rich functional groups and aliphatic and aromatic C in hydrochar (obtained at 190 °C and pH=4.5 for 4 h) than the feedstock (Melo et al., 2019).

The N1s XPS spectra (390–410 eV) can present the evolution of N-containing functional groups during HTP treatment. Zhuang et al. (2017) found only two N groups (amino and inorganic N) in MS but three more new peaks (quaternary-N, pyrrole-N, and pyridine-N) in hydrochar obtained at 210–300 °C for 0.5–8 h. It was observed that the inorganic N was completely dissolved and disappeared in hydrochar after 240 °C. The conversion of amino-N to quaternary-N was also displayed, possibly resulted from the enhanced hydrolysis and polymerization and ring condensation of amino-N (Zhuang et al., 2017). He et al. (2015b) used digested sludge with mostly protein-N (90.3%) and some pyridine-N and inorganic N. The pyridine-N content raised gradually with increasing reaction temperature and became dominant (25.2%)

at 380 °C, with the reduced protein-N (18.5%). The Diels–Alder reaction was inferred in charge (He et al., 2015b). Liu et al. (2017a) obtained compositions of mainly protein-N, pyridine-N, pyrrole-N, and some inorganic-N in MS. A new peak (nitrile-N) was identified in hydrochar with the absence of inorganic-N after HTC at 200 °C for 30 min. Generally, deamination is attributed to the inorganic-N and some protein-N, while polymerization and cyclization promoted by high HTP temperatures (e.g., 300–350 °C) would form more stable nitrile-N and heterocyclic-N (pyrrole-N and pyridine-N) that are mainly concentrated in hydrochar (T. Liu et al., 2017a; Wu et al., 2020).

Similarly, the S2p spectra (160–175 eV) are used to identify S-containing compounds. So far, only Wang et al. (2020) attempted to discover the transformation pathway of S for HTP of secondary sludge at 180–300 °C for 30 min. Six organic (mercaptan, sulfide, sulfone, sulfoxide, and thiophene) and one inorganic (sulfate) S-compounds were found in the secondary sludge. Sulfide which was major in the sludge (39.44%) decreased rapidly with the increasing reaction temperature and reached a minimum of 17.14% in hydrochar (200 °C). On the contrary, the portion of thiophene enhanced from 22.19% in the sludge to 37.48% in hydrochar (300 °C) which was the dominant species. This change may result from poly-condensation of sulfide, sulfoxide, and sulfone. Meanwhile, the decomposition and transformation of organic S forms into inorganic species was also indicated by the significantly increased sulfate content (from 0.07% to 20.96%). In the end, Wang et al. (2020) proposed a potential reaction pathway for sulfur during HTP treatment. In summary, XPS analysis can identify specific elemental compounds and thus reflect potential evolution associated with these elements.

3.4.4. Nuclear magnetic resonance (NMR) spectroscopy

NMR spectra is an advanced technology to quantify the species distribution of various elements (e.g., C, N, and P) in both solid and liquid phases. The ¹³C NMR provides the relative contribution of each carbon molecular such as alkyl C, O-alkyl C, alkene C, anomeric C, aryl C, carboxyl C, and carbonyl C by the chemical shifts (Zhang et al., 2017). Similarly, ¹⁵N NMR presents the distribution of N species, e.g., pyrrole N and amide N. Paneque et al. (2017) applied both ¹³C and ¹⁵N NMR and found that both primary and secondary sludge were mainly composed of alkyl C (43.1% and 37.6%, respectively) and amide N

(77.6% and 82.8%, respectively). With increasing reaction severity (200–260 °C and 0.5–3 h), hydrochar had continuously increased contents of alkyl C, O/N-aryl C, aryl C, and pyrrole N, but decreased proportions of carboxyl/amide C and O-alkyl C and amide N. These findings indicated that higher reaction severity of HTC promoted the hydrolysis, dehydration, decarboxylation, and aromatization (Paneque et al., 2017). Zhang et al. (2018) also obtained enhanced aromaticity of hydrochar (44.3%) after HTP at 300 °C for 30 min compared to MS (7.0%) feedstock by using ^{13}C NMR. Wiedner et al. compared the C groups in hydrochar derived from HTC of different biomass. They found that MS-derived hydrochar was one of the groups with the highest alkyl C (39%) and carboxyl C (18%) but the lowest O-alkyl C (24%) and aryl C (19%), compared to those generated from maize silage and grass greenery (except for the biogas digestate) (Wiedner et al., 2013). Generally, the ^{13}C NMR shows that MS-derived hydrochar has reduced oxygen-containing organic C but improved aromaticity than its feedstock (Wang et al., 2017; Zhang et al., 2014).

^{31}P NMR has been used to determine the speciation of P in hydrochar. Huang and Tang (2015) found both WAS and its derived hydrochar (at 225 °C for 24 h) were primarily composed of orthophosphate (ortho-P), but a low portion of P in hydrochar was observed (30.9%) in solid-state NMR analysis. This suggested that more P was formed with metal complexes. However, the liquid-state NMR spectra of the extract showed that the hydrochar contained 100% of ortho-P (Huang and Tang, 2015). Shi et al. (2019) combined ^{31}P NMR spectra with the NaOH/EDTA extraction. It was reported that the pyrophosphate (pyro-P) was more in hydrochar obtained at 170–260 °C than that of MS feedstock. This is probably caused by the hydrolysis of organic phosphorus (monoester-P) into pyro-P. However, the pyro-P disappeared in hydrochar from 320 °C. Besides, most P was transferred into inorganic forms (nearly 100%) after HTP treatment (Shi et al., 2019). It seems that liquid-state ^{31}P NMR combined with extraction is a better way to characterize the speciation of P in hydrochar owing to the dominance of inorganic P.

3.4.5. X-ray diffractometry (XRD)

XRD is commonly used for the analysis of the crystal structure of hydrochar. Wang et al. (2017) observed various minerals in both digested sludge and its derived hydrochar (200–230 °C for 2 h), such as quartz (SiO₂), kaolinite, and muscovite. With XRD analysis, they investigated the behaviors of P minerals among different hydrothermal conditions. It was found that AlPO₄ was the predominant P form at all conditions, while AP increased in an alkaline environment. However, it should be noted that XRD cannot detect the phosphate minerals in amorphous phase, which is combined with Ca, Al, Fe, and others (Wang et al., 2017). XRD results also indicated that at supercritical water conditions (400 °C for 30 min) alkaline additives (Na₂CO₃ and K₂CO₃) could react with Ca²⁺ and Al³⁺ to form calcium carbonate, analcime, and kalsilite, while phosphate originally combined with Ca and Al minerals could be mobilized into aqueous (Wang et al., 2019). XRD could verify the transformation of mineral species. Minerals of Ca₃(PO₄)₂ and Ca₇Mg₂(PO₄)₆ were found in MS-derived hydrochar when CaO was added in HTC treatment (200–260 °C), suggesting a directional production of Ca-P (Xu et al., 2018). Wang et al. (2020) also used XRD and observed higher intensity and more peaks of CaSO₄ in hydrochar than that in MS, reflecting that HTC (180–300 °C) was likely to transform unstable organic sulfur species (mercaptan and sulfide) to sulfate. XRD patterns also showed the presence of complex combinations of alkali and alkaline earth metals (AAEMs) in MS-derived hydrochar obtained at 600 °C and 23 MPa for 1 h (Sawai et al., 2014). Mostly, XRD analysis is used to assist the elucidation of reactions related to various minerals during HTP treatment.

3.5. Characteristics of morphology

Scanning electron microscopy (SEM) or SEM coupled with energy dispersive X-ray spectrometry (SEM-EDS) is mostly applied to visualize the surface morphology of hydrochar and the present elements. Wang et al. (2018) utilized SEM-EDS and observed many granular and massive substances (such as coke and char) attached to the surface of Ni catalyst for HTG treatment, which eventually led to the deactivated catalyst. Zhang et al. (2017) found the structure features of hydrochar (220 °C) derived from MS and pinewood sawdust were distinctly different. MS-derived hydrochar MS was fragmented of clustered aggregates, while hydrochar resulted from pinewood sawdust still had sharp edges and flat plates, similar

to the features of raw sawdust. Chen et al. (2013b) reported the formation of porous structures and bubbles in hydrochar obtained at 350 °C compared to the close-knit structure of MS. However, more porous structures were formed with the destroying of bubbles when reaction temperature raised to 425 °C, probably caused by the release of gas. On the contrary, hydrochar produced at low temperature (260 °C) was mostly non-porous (Khoshbouy et al., 2019). Other studies also observed dense and low porosity of hydrochar obtained at low temperatures (180–200 °C). However, the structure of hydrochar was ruptured with a rougher surface after HTC, compared to MS (Saetea and Tippayawong, 2013; Zhuang et al., 2020c). Liu et al. (2017b) suggested that acid washing (HCl and HF) of hydrochar could largely enhance pore size and develop a multiple-pores structure with rich mesopores. Generally, SEM results show that MS-derived structure shifts from dense to more porous with increasing reaction temperature.

Transmission electron microscope (TEM) is another technique that can display the surface morphology. Liu et al. (2017b) used TEM imaging to investigate the effects of acid washing on MS-derived hydrochar. A higher amount of mesopores and channels were found in hydrochar after washing with 2M of HCl and 20 wt% of HF, compared to that washed with HCl only. El-Deen and Zhang also used TEM analysis to prove the coating of dense nanoparticles on hydrochar after HTC of MS at 200 °C with catalysts (glucose and $\text{FeSO}_4 \cdot 7\text{H}_2\text{O}$) (El-Deen and Zhang, 2012). However, to date, there is a lack of HTP studies investigated with TEM.

4. Valorization of hydrochar

Initial studies on sludge-to-hydrochar were primarily focused on carbonization to provide alternative solid fuel. However, considering the abundant characteristics of hydrochar, the applications of hydrochar have been broadened in recent studies. MS-derived hydrochar has been valorized in energy production, agricultural application, water remediation, catalysis, and nutrient recovery. Nevertheless, many other potential applications have not been adopted to MS-derived hydrochar, such as carbon sequestration, gas adsorption, energy storage (batteries, supercapacitors, and fuel cells), and biochemical applications (Titirici et al., 2012).

4.1. Energy production

4.1.1. Biofuel for combustion

Hydrothermal treatment has been proven to convert waste biomass into promising solid fuels with high energy density, i.e., a coal-like material. In recent studies, MS-derived hydrochar has shown both HHV and H/C, and O/C ratios moving towards natural lignite (He et al., 2014b). As a result, many researchers have attempted to apply hydrochar in combustion or co-combustion mostly via thermogravimetry (TG) and derivative thermogravimetry (DTG) tests (Ahn et al., 2020). [Table 9](#) catalogs the application of MS-derived hydrochar to energy production with key findings. As shown in the table, most studies focused on combustion. Considering the low hydrochar yield at high temperature and corresponding energy investment, it is suggested to use a mild HTC condition (≤ 280 °C) to produce solid biofuel. Among reported studies, the best potential hydrochar fuel was produced from a SS at 260 °C for 1 h (Khoshbouy et al., 2019). It showed the highest HHV (23.3 MJ/kg) and relatively low ash content (26.6%) and ratios of H/C (1.15) and O/C (0.13). Compared to the feedstock (MS), hydrochar has shown several improvements during combustion: Reduced ignition temperature and burnout temperature, lower activation energies, more stable flame, longer combustion process, and significant NO_x and SO₂ emission reduction (He et al., 2013; Wang et al., 2019). The reasons include but are not limited to the enhancement of HHV, FC, and C content, and the reduction of N and S contents, VM, H/C, and O/C ratios. Some studies also compared hydrochar with coals regarding combustion performance. Parshetti et al. (2013) added hydrochar to low-rank coal and found a reduction in emission gas (CO₂, CO, and CH₄). He et al. (2014b) blended hydrochar with different coals. In terms of the combustion performance and burnout efficiency, co-combustion showed positive synergistic effects with moderate-rank coal, but negative synergistic effects with low/high-rank coals. However, the detailed mechanisms behind the co-combustion should be further studied.

=====

Please Insert Table 9 Here

=====

Challenges are also expected when using MS-derived hydrochar for combustion. Firstly, to produce energy-dense hydrochar, the feedstock should be highly selective. As demonstrated in [Section 2.1](#), MS has a large variability in properties, such as C, O, HHV, VM, and ash contents. Statistical analysis shows that the HHV of hydrochar is substantially related to the properties of MS. [Fig. 12](#) explains the correlations among properties of hydrochar and the corresponding MS. The HHV of hydrochar is negatively governed by its ash content (adjusted $R^2 = 0.70$, [Fig. 12a](#)). The ash content of hydrochar is positively impacted by that of the feedstock (adjusted $R^2 = 0.69$, [Fig. 12b](#)), and thus the HHV of hydrochar is negatively correlated to the ash content of MS (adjusted $R^2 = 0.48$, [Fig. 12c](#)). Meanwhile, the HHV of hydrochar is positively affected by the HHV of its feedstock (adjusted $R^2 = 0.74$, [Fig. 12d](#)). Consequently, a feedstock with high HHV but low ash content is preferable to produce a promising solid biofuel through HTP treatment. Some studies showed that co-HTC of MS with other types of biomass might overcome the drawback of low HHV but high ash content of hydrochar (He et al., 2019; C. Zheng et al., 2019). Secondly, the balance between HHV value of hydrochar and the corresponding energy recovery rate (defined as the percentage of energy in hydrochar recovered from MS) should be maintained. As shown in [Fig. 13a](#), more than half of the studies reported a low HHV (< 15 MJ/kg, db) or low energy recovery rate ($< 60\%$) of MS-derived hydrochar. It also seems that the energy recovery rate is positively related to the HHV of hydrochar with a polynomial relationship (adjusted $R^2=0.93$). Therefore, future studies should pay attention to optimize the treatment conditions to enhance both hydrochar HHV and energy recovery rate. Besides, energy densification expressed as the HHV ratio between hydrochar and the feedstock MS is targeted to be >1 for solid fuel production. Through a scatter matrix analysis ([Fig. 13b](#)), it is found that to achieve energy densification, the preferable HTC conditions should be controlled at $150\text{--}300$ °C and severity factor <0.5 . Thirdly, issues of ash slagging and fouling and the generation of harmful gases seem to be inevitable while combusting hydrochar. Due to the ash accumulation and concentrated AAEMs, such as Ca, K, Mg, and Na, hydrochar can have a high alkali index (> 0.34), which would certainly cause slagging and fouling during combustion (Smith et al., 2016). Even though HTP

reduces the N and S contents in hydrochar, high NO_x and SO₂ emission of hydrochar combustion was found comparable to coal and wood pellet (Ahn et al., 2020). On the other hand, high deformation (1220–1240 °C) and flow (1440–1470 °C) temperatures of hydrochar ash could inhibit the formation of NO_x (Smith et al., 2016). Thus, future studies should focus on balancing the ash content of hydrochar and the potential emission. Blending low-ash biomass (e.g., lignocellulose) with MS for co-HTC could probably mitigate the concerning of ash, along with syncretistic effects on the improvement of hydrochar quality. Lastly, potential nutrient loss and secondary contamination can be caused by combustion. Due to the low melting point of P₂O₅ (340 °C), P is likely to spread in fly ash by complexing with other elements, including Al, Ca, Fe, Mg, and Si (Ahn et al., 2020). The highest P concentration in hydrochar, derived from WAS, was reported as 8.1%, db, which can be the best candidate for P fertilizer or P recovery (Huang and Tang, 2016). Direct burning such hydrochar would cause a significant loss and higher cost for recollecting P. Besides, combustion of MS-derived hydrochar can also cause emissions of heavy metals concentrated fly ash, such as Hg and Cd (Lumley et al., 2014; Shi et al., 2014). Therefore, nutrient loss and emission control must be considered when evaluating the combustion behaviors of hydrochar. Also, not all hydrochar products apply to combustion. In HTL/HTG treatment, minerals are concentrated in hydrochar while carbon is minimized, causing the hydrochar with poor quality as solid fuel. It is preferred to process such hydrochar for P recovery.

=====

Please Insert Fig. 12 Here

=====

=====

Please Insert Fig. 13 Here

=====

In conclusion, MS-derived hydrochar has many limitations to be a solid biofuel, which needs to be optimized with low ash contents, high energy density, and improved combustion performance. Co-HTC and co-combustion seem to be a trend of overcoming the drawbacks of MS-derived hydrochar and valorizing the asset for combustion. Moreover, challenges during combustion, such as ash slagging and fouling, harmful emissions, and nutrient loss, require more comprehensive evaluation.

4.1.2. Hydrochar for syngas production

Syngas production via pyrolysis or steam gasification is another process to utilize energy in MS-derived hydrochar. As shown in [Table 9](#), numerous studies have examined the gasification of hydrochar for generating gas rich with H₂, CO, and CH₄. Most hydrochar used in gasification or pyrolysis was produced with a low hydrothermal temperature (≤ 240 °C) and residence time (≤ 1 h). It is suggested that high hydrothermal severity (e.g., high reaction temperature and long residence time) could reduce H₂ production as a result of the sharp decline of carboxyl and hydroxyl groups in hydrochar (Zheng et al., 2019). Compared to direct gasification of MS, hydrochar could result in gases with better quality (up to 9.6 MJ/Nm³ of lower heating value and 56% of H₂ in the product) and gasification efficiency (up to 91%) (Gai et al., 2016b; Zhuang et al., 2020b). Unlike the fouling effects of AAEMs in combustion, metals such as Ca, Fe, K, Mg, Na, and Ni in hydrochar have been reported to show catalytic effects on gasification (Gai et al., 2016b). Zhuang et al. reported that their impacts on gasification conversion rates followed the order: Na > K > Mg > Ca > Fe (Zhuang et al., 2020c). They also found that Na and K mainly contributed to CO₂ generation during gasification. Regarding syngas production, only one study analyzed pyrolysis, and it seems the gas was mainly composed of CO₂ (more than half of the total gas). Most studies have shown that gasification can produce high-quality syngas and achieve a high carbon conversion rate or gasification efficiency. Besides, one study also suggested that gasification can be coupled with P recovery through thermochemical conversion. It was reported that P₂O₅ could be completely converted into gas phase after 600 °C, and a total P recovery of over 80% can be achieved (Feng et al., 2018).

However, considering the high temperature required for gasification (typically 700–1000 °C), there is a concern about both capital investment and energy consumption. An energy return on investment is urgently required to evaluate the performance of gasification of MS-derived hydrochar. The catalytic effect of AAEMs in hydrochar also needs further exploration, as it could be inhibited by the melting of abundant Si and Al and resulted in the blocking of active sites (Zhuang et al., 2020c). Besides, the gasified residue could be concentrated with PAHs and heavy metals, which requires proper management (Zhuang et al., 2020b).

4.2. Agricultural applications

With abundant nutrients and functionality, the valorization of hydrochar as a sustainable fertilizer and soil amendment has attracted attention. Fei et al. (2019b) suggested that hydrochar (150–300 °C for 2 h) tended to have lower available nutrients (i.e., 1.58–6.87 g/kg of N, 0.27–0.9 g/kg of P, and 0.26–0.87 g/kg of K), compared to MS feedstock and pyrochar. These values are still far higher than those of typical agricultural soil: N (0.01–0.49 g/kg), P (<0.02 g/kg), and K (<0.1–0.27 g/kg). High cation exchange capacity (CEC) values (11.8–25.3 cmol/kg) of hydrochar were also obtained. It should be noted that 20 cmol/kg is very high for soil CEC, which represents a high capacity of attracting ammonium and trace elements (Fei et al., 2019b). Fei et al. also found that most P was immobilized with an available portion of 0.42 g/kg in hydrochar after HTC treatment (150–250 °C for 2 h). Interestingly, hydrochar turned into a P adsorbent when environmental P content was above 20 mg/L, which can be readily released. Adding P-rich hydrochar also nearly doubled soil available P by 8.9 mg/kg during 1–10 days incubation (Fei et al., 2019a). Therefore, hydrochar is considered a feasible and value-added soil amendment. Also, the inhibited availability of nutrients could benefit the long-term application of hydrochar due to the slow release of nutrients (Fei et al., 2019a). It should be noted that most MS-derived hydrochar has low N/P ratios (e.g., less than 10) (Fig. 9a), and therefore complementary N fertilizers may be required for better fertilization when using hydrochar as a fertilizer.

Some lab-scale experiments have been done to evaluate the feasibility of hydrochar application as a soil amendment. Chu et al. (2020) applied digested sludge-derived hydrochar (260 °C for 1 h) as N-

fertilizer (240 kg urea-N/ha) to paddy soil columns for rice (*Oryza sativa* L. Nangeng 46) growth. It was found that the addition of hydrochar could significantly enhance the soil ammonium-N retention, inhibit the ammonium-N loss in floodwater, and thus improve rice production. These effects could be due to the low surface pH (7.09–7.78) and pore diameter (1.19–3.05 nm), large adsorption pore volume (0.14–0.20 cm³/g), and abundant carboxyl functional groups of hydrochar (Chu et al., 2020). Melo et al. (2018) conducted a pot experiment to assess the plant and soil response to biosolids-derived hydrochar (190 °C for 4 h). The soil CEC, water holding capacity and the availability of nutrients (organic C, hot water extractable C, ammonium, nitrate, total N and P, Ca and Fe) and trace elements (Cu and Zn) were found to be positively correlated with hydrochar application rates (0.2–1.6 wt%) by the end of harvest. However, the Mg availability and soil C/N ratio decreased with increasing hydrochar addition. Applying 0.8 wt% of hydrochar resulted in equal and 96% higher total dry matter of plant biomass (*Phaseolus* beans), compared to that of the mineral fertilizer, during the first and second harvest, respectively (Melo et al., 2018). Melo et al. also investigated the influence of hydrochar on the germination of rice, beans, and radish. Adding 0.5 wt% and 3 wt% of hydrochar resulted in the maximum yields of beans and rice, respectively. However, the yield of radish linearly decreased with increasing application rates of hydrochar (Melo et al., 2019). MS-derived hydrochar appears to be beneficial as a soil amendment for its positive impacts on soil properties and crop yield, but it would vary depending on the soil and plants. Therefore, more assessments, including both pot and field trials, are necessary for a comprehensive evaluation and understanding of long-term impacts, prior to the application of hydrochar to the agricultural scale.

Besides the uncertainty of hydrochar performance on agricultural production, potential toxic effects associated with the concentrated contaminants, such as heavy metals and POPs, are creating concerns. Yue et al. (2017) examined the transformation of heavy metals during a 60-day incubation with MS-derived hydrochar as a soil amendment. Adding 5 wt% of hydrochar to the agricultural soil (non-contaminated) significantly increased total metals (As, Cd, Cr, Cu, Pb, and Zn) in soil. Additionally, after 60 days of incubation, the oxidable and residual fractions of heavy metals were greatly mobilized into

readily bioavailable forms (acid-soluble and reducible fractions) (Yue et al., 2017). It seems that although heavy metals are highly immobilized in hydrochar initially, they can be re-mobilized during soil application. This could particularly pose risks to the food chain when applying hydrochar to agriculture. On the contrary, another study showed that the application of hydrochar derived from WAS could promote the immobilization of Cd in contaminated soil (Ren et al., 2017). With the favor of hydrochar amendment, Cd was restrained from being assimilated from contaminated soil to the aboveground (up to 15% reduction) and underground (up to 58% reduction) parts of cabbage. It was also found that hydrochar addition largely enhanced the abundance of soil microorganisms (Ren et al., 2017). So far, only one study has conducted a limited ecotoxicological assessment. With the application of biosolids-derived hydrochar (190 °C for 4 h) up to 80 Mg/ha or 4 wt%, no acute toxicity to earthworms was identified, although earthworms showed significant preference to control soil rather than hydrochar amended (Melo et al., 2017). Limited reports have shown that using MS-derived hydrochar may pose environmental and human health risks but probably depending on the hydrochar properties, soil properties, and soil biota. More detailed studies are required to address such concerns for the valorization of hydrochar.

Last but not least, public and farmer perception is another big challenge when using MS-derived hydrochar for agricultural application. Historically, MS (biosolids) presents a negative public perception due to the environmental concerns from its contaminants. It is not surprising that Melo et al. found only 51% of surveyed rural producers would use biosolids-derived hydrochar (Melo et al., 2019). In the future, long-term field trials should be performed to clarify the interactions among hydrochar, soil properties, plant growth, and crop quality. More investment in the safe use of hydrochar in agriculture is also beneficial for its valorization.

4.3. Adsorption: Water remediation

MS-derived hydrochar with abundant oxygen-functional groups makes it promising for adsorption or as a precursor of activated carbon. Several researchers have directly applied hydrochar for water remediation or convert hydrochar into activated carbon. [Table 10](#) summarizes available isotherms or models for the evaluation of adsorption performance. The adsorption isotherms are used to quantify the

affinity of an adsorbent to the adsorbate and describe adsorbent-adsorbate interactions. Langmuir isotherm describes the equilibrium as a reversible chemical reaction, assuming a fixed number of sites on a monolayer where adsorption can take place without adsorbate interactions (Leng et al., 2015b). Freundlich isotherm describes heterogeneous surfaces and multilayer adsorption, which allows for adsorbate interactions (Ferrentino et al., 2020a). Sips isotherm is the combined Langmuir-Freundlich form that also predicts heterogeneous adsorption, but it describes the process with a finite limit at high enough concentrations (Alatalo et al., 2013). Temkin isotherm considers the adsorbent-adsorbate interactions, assuming that the adsorption heat or free energy is dependent on the surface coverage (Xia et al., 2019). Adsorption kinetics modeling has been widely used to indicate adsorption mechanisms. Pseudo-first-order describes the adsorption occurring through interface diffusion, assuming that the adsorption rate is directly proportional to the difference of equilibrium concentration and adsorption time. Pseudo-second-order represents an adsorption process controlled by chemisorption. Intraparticle-diffusion model can be used to identify the rate-limiting step in the three-stage adsorption process: 1) Surface diffusion through interparticle or boundary layer; 2) intra-particle diffusion into micropores; and 3) equilibrium stage with pore diffusion or solid surface diffusion of adsorbate molecules to interior surface/sites of adsorbent (T. Liu et al., 2017b). Most kinetics studies have shown that the adsorption of MS-derived hydrochar follows pseudo-second-order, and intra-particle diffusion is the rate-limiting step.

=====

Please Insert Table 10 Here

=====

Table 11 compares the physicochemical properties of hydrochar based adsorbents in current studies and their application. Alatalo et al. (2013) directly applied DS-derived hydrochar to heavy metals removal from wastewater. It was reported that the hydrochar can only effectively remove Pb(II) (up to 80%) but not Cr(VI), As(III), or As(V). The adsorption for Pb(II) well fitted Sips (Langmuir-Freundlich) isotherm ($R^2 = 0.86$) with a maximum adsorption capacity of 12.97 mg/g (Alatalo et al., 2013). Luo et al. (2020)

also showed that HTC of WAS at a low temperature (120 °C) could produce hydrochar with MgAl-layered double hydroxides composites, an efficient adsorbent of Pb(II) ($q_m = 19\text{--}86$ mg/g). This indicates that MS-derived hydrochar is a capable adsorbent. Leng et al., (2015b) also demonstrated that hydrochar had effective adsorption of Malachite green and Methylene blue from the liquid. Although hydrochar had low surface area and pore volume, the abundant oxygen-functional groups (e.g., carboxyl, carboxylic, lactonic, and phenolic groups) were found responsible for the adsorption, plus exchanging hydrochar cations (e.g., releasing Ca^{2+} , K^+ , Mg^{2+} , Na^+ , and Zn^{2+}) with cationic Malachite green (Leng et al., 2015b). Ferrentino et al. (2020) also found that DS-derived hydrochar was efficient in adsorbing Methylene blue, and they suggested a complex sorption process of physical-chemical adsorption, acid-base, and redox equilibria. However, it is noted that, without activation, hydrochar from HTC treatment tends to have a low surface area (≤ 31 m²/g), which could restrict its adsorption capacity (<71 mg/g of Methylene blue). El-Deen and Zhang (2012) first converted MS into a carbon nanocomposite with HTC treatment. They found that the novel nanocomposite could completely remove 0.5 mg/L of As(V) within 30 min at a wastewater pH of 5–7. The adsorbed As could also be easily released later; thus, the nanocomposite can be reused (El-Deen and Zhang, 2012). However, the adsorption capability (2.1 mg/g) was still limited.

=====

Please Insert Table 11 Here

=====

To improve the performance of SS-derived hydrochar, several studies utilized chemical, thermal, and thermochemical processes to produce activated carbon. Through chemical activation with 2M KOH solution, DS-derived hydrochar showed nearly 3 times higher adsorption capacity of Methylene blue (140.1 mg/g) and much higher adsorption rate than inactivated; such improvement was favored by the enhanced homogenization of hydrochar surface by alkali washing, although the surface area was not significantly improved (Ferrentino et al., 2020a). Thermal and thermochemical activation processes have

been found to significantly improve the surface area (up to 270 times) and pore volume (up to 58 times), providing intensive active sites, thus enhancing the adsorption capacity of hydrochar. The pore size of hydrochar (2–20 nm) has been found mostly in the range of mesopores (2–50 nm), and activation has not been discovered effective in improving it. Khoshbouy et al. (2019) generated SS-based activated hydrochar under various conditions. They reported that thermochemically activated hydrochar had the best adsorption properties and results compared to non-activated and thermally activated hydrochar. The activated hydrochar showed superior results ($q_m = 588.2$ mg/g) for methylene blue removal compared with commercial activated carbons ($q_m = 210$ mg/g) (Khoshbouy et al., 2019). Liu et al. (2017b) also performed a thermochemical activation to MS-derived hydrochar and observed more abundant mesopores and large pores after activation. The activated hydrochar exhibited excellent adsorption capacity of azo dye (440.5 mg/g). Tu et al. (2021) reported that thermochemical activation of MS/coconut shell-derived hydrochar enhanced the adsorption capacity of Methylene blue from 140 to 623 mg/g by highly improved surface area (from 22 to 874 m²/g) and pore volume (from 0.13 to 0.57 cm³/g) of hydrochar. They also found that the activated hydrochar could be reused for ten cycles by washing with 25% ethanol solution without affecting the adsorption properties significantly. Noticeably, all reported non-activated hydrochar and activated hydrochar were found to well fit Langmuir isotherm and pseudo-second-order model, indicating that hydrochar based adsorbents likely adsorb organic pollutants and metal cations as a monolayer with chemisorption as the rate limiting step.

Indeed, MS-derived hydrochar has shown a gifted ability in adsorption application due to the oxygen-rich functional groups. However, its capacity is typically restricted for the very low surface area and porosity. Most studied hydrochar was generated under mild conditions (≤ 280 °C), while the performance of hydrochar from a more severe environment should also be analyzed since more porous structures could be formed. Limited studies have shown that activated hydrochar could have comparable performance to commercial activated carbons. Therefore, further efforts are required to develop cost-effective and promising adsorbent from MS-derived hydrochar. Last but not least, the release of pre-existing contaminants (e.g., heavy metals and POPs) remains unknown during the adsorption process.

4.4. Heterogeneous catalysis

The development of green catalysts has attracted extensive interest for a sustainable environment. Many studies suggest that hydrochar derived from biomass, such as macroalgae and lignocellulose, as a catalyst could promote H₂ production during gasification and facilitate the degradation of organic pollutants (Khan et al., 2019). Concurrently, previous studies also demonstrated that AAEMs existed in MS-derived hydrochar significantly contributed to gas composition from gasification, with catalytic effects observed (Zhuang et al., 2020c). More details can be found in Section 4.1.2. However, there is a lack of validation of using MS-derived hydrochar as a catalyst for gasification or HTG process.

Magnetic hydrochar converted from MS provides another alternative environmentally friendly reuse approach. Such material acts as a heterogeneous catalyst in Fenton and Fenton-like treatment of organic pollutants, e.g., textile wastewater (Zhang et al., 2018). However, many catalysts face issues of iron leaching and deactivation, with a large amount of ferric sludge produced after reaction (Zhou et al., 2015). Yuan and Dai (2014) first developed a facile synthesis of mesoporous material from MS with Fe(II) solution and calcination at 350 °C. The magnetic material exhibited significant improvement and stability as a catalyst for photo-Fenton reaction. Following similar protocols, Zhou et al. (2015) also obtained a magnetic catalyst from paper mill sludge. The excellent stability of catalytic activity and negligible iron leaching were reported during the degradation of Methylene blue through a Fenton-like treatment. Favored by these previous studies, Zhang et al. successfully produced a magnetic hydrochar by coprocessing SS with ferric sludge under various HTC conditions (160–240 °C for 2–10 h). The sludge-based magnetic hydrochar showed great catalytic effects on the Methylene blue degradation in Fenton reaction. However, the removal efficiencies of chemical oxygen demand (COD) and total organic carbon (TOC) only reached 47% and 49%, respectively, when it was applied to real wastewater from a dyeing process (Zhang et al., 2018). Similarly, Zhang and Hay (2020) synthesized a magnetic hydrochar from biosolids with Fe(III) and glucose under HTC condition (180 °C for 6 h at pH=11). It was found that the magnetic hydrochar had 10 times bigger pores (180 nm) than that of non-magnetic hydrochar (17 nm), although they showed close surface area (around 49 m²/g). The magnetic hydrochar also presented an

improved enzyme immobilization, which was likely contributed by the larger pores. After 10 wash cycles, magnetic hydrochar still maintained a high activity (> 60%) on enzymes (laccase and horseradish peroxidase). Moreover, much lower acute toxicity was identified for magnetic hydrochar compared to previously reported carbon-based materials (Zhang and Hay, 2020).

In summary, MS-derived hydrochar seems to be a promising alternative heterogeneous catalyst, which can have high catalytic activity, long-term stability, and low toxicity produced from an economically friendly condition. However, limited studies are available to validate these advantages.

4.5. Nutrient recovery

Nutrient (particularly P) recovery is a promising approach to valorize hydrochar. P has been included in the Critical Raw Material List by EU (European Commission, 2018). Its recovery and recycling from waste streams, such as MS and its derived hydrochar, is practical in replacing primary phosphate rock consumption and mitigating eutrophication. Previous studies have demonstrated that most P (>81%) is accumulated in hydrochar after HTP of MS, with a reported average concentration of 2.8%, db (see Section 3.2). Among reported studies, the highest P content (8.1%, db) in hydrochar was derived from WAS, which was comparable to commercial P source, phosphate rock (a mineral deposit containing 11–15% of P) (Huang and Tang, 2016; Kroiss et al., 2011). Such abundant P resource could be irretrievably lost without proper recovery, causing both environmental challenges and nutrient loss. Previous studies have demonstrated the potential of P recovery from hydrochar (Huang et al., 2017). Recently, some traditional and emerging technologies have been applied to MS-derived hydrochar for P and/or N recovery: Wet chemical extraction, thermochemical process, and integrated biological recovery (Table 12).

=====

Please Insert Table 12 Here

=====

4.5.1. Wet-chemical extraction

Wet-chemical extraction and/or coupled with precipitation is the most common method for nutrient recovery from MS-derived hydrochar, as shown in [Table 12](#). The reason is because of its simple procedure and relatively low expenditure (Meng et al., 2019). Our recent review article has detailed the feasibilities and challenges of P recovery from hydrochar using wet-chemical processes (H. Liu et al., 2021). P can be leached from hydrochar by both acidic and alkali solutions. Followed by precipitation or crystallization of liquid extracts, P and/or N can be recovered in the form of struvite and calcium phosphates (Ca-P), by adding Mg^{2+} and NH_4^+ or Ca^{2+} solutions, respectively, with adjusted pH. Detailed recovery mechanisms can be found elsewhere (Meng et al., 2019; Peng et al., 2018; Tansel et al., 2018). A typical nutrient recovery procedure for MS-derived hydrochar is illustrated in [Fig. 14](#).

=====

Please Insert Fig. 14 Here

=====

Among the studies of nutrient recovery from MS-derived hydrochar, acidic extraction ($pH \leq 2$) is commonly used due to its high efficiency. One study found that oxalic and sulfuric acids can effectively extract P from hydrochar with 80–95% of P leached, but no further precipitation of solid fertilizer was conducted (Acelas et al., 2014). Several studies have performed struvite production with acidic leachate from hydrochar and ammonium-rich HTP aqueous phase (320–2,970 mg/L) (Becker et al., 2019; Ovsyannikova et al., 2020; Zhai et al., 2014b). A high P recovery rate (82–98%) can be reached in batch scales. It was also suggested that the obtained P precipitate could be further purified into struvite ($MgNH_4PO_4 \cdot 6H_2O$) (Becker et al., 2019). However, co-dissolution of heavy metals along with P is inevitable during acidic extraction, which causes the concerns of heavy metals contents in recovery products as fertilizers. Detailed studies about heavy metals co-leaching and co-precipitation are necessary to address such concerns.

An improved extraction procedure was developed to minimize the risk of having heavy metals in the recovered Ca-P (Zhai et al., 2014b). Activated alumina powder was added into the acidic leachate of

hydrochar to adsorb P, which was subsequently released in an acid solution. Followed by the calcium precipitation, the recovered calcium phosphate was found to have less than 5% of Cu, Pb, and Zn. A high recovery rate (> 85% of P from MS) was also achieved (Zhai et al., 2014b). Compared to acidic extraction, direct alkaline extraction is a promising alternative to avoid the co-recovery of heavy metals. However, this process is highly selective on P species in hydrochar, as only NAIP can be extracted at alkalic conditions ($\text{pH} \geq 12$) (Cao et al., 2019; Falayi, 2019). Therefore, NAIP content indicates if it is feasible to use alkalic extraction for P recovery. One study showed a very high extraction efficiency (> 89% of total P) from hydrochar (200 °C for 4 h) using KOH solution ($\text{pH} \geq 12$), which was probably caused by the use of poly-aluminum sulfate during sludge sedimentation in the WWTP. A solid K-P fertilizer, K-struvite ($\text{MgKPO}_4 \cdot 6\text{H}_2\text{O}$), was produced by subsequent precipitation with a high P recovery efficiency (> 92% from raw sludge) (Li et al., 2020). Many studies found that alkaline-extractable P in sludge-derived hydrochar was below 60% (especially for those produced under higher HTP temperatures), limiting the wide application of alkalic extraction (Shi et al., 2019; Y. Xu et al., 2018; Zhai et al., 2014b). Our previous review identified that sequential procedures by coupling acidic and alkalic extraction (e.g., procedures established by Zhai et al. (2014b)) could achieve promising P extraction efficiencies (70–91%), separate metals from P extracts, and produce qualified P fertilizers and potentially clean hydrochar (H. Liu et al., 2021).

Compared to batch-scale-based hydrochar, the nutrient recovery rate in the continuous flow operation does not seem satisfactory. Ovsyannikova et al. (2020) used hydrochar and aqueous phase from a pilot-scale continuous flow HTL treatment (350 °C, 22 MPa, and 60 L/h) of primary sludge for nutrient recovery. The total recovery for N and P based on the original sludge was only 6.8% and 23.7%, respectively. It should be noted that the recovery rates were high based on precipitation (99% of P and 79% of $\text{NH}_4\text{-N}$). Interestingly, there was also 2% of K recovered from the sludge in the struvite precipitates. The low overall recovery rate was attributed to the dispersion of P-containing particles into the biocrude (Ovsyannikova et al., 2020).

Overall, wet-chemical technology is promising to recover nutrients from hydrochar and associated HTP aqueous phase. Laboratory studies have demonstrated that a high extraction rate and total recovery rate of P can be achieved simultaneously. It is believed that a way to higher P recovery rate can be accomplished with the optimization of the continuous-flow HTP operations. However, preliminary cost analysis has shown that struvite precipitation coupled with HTC treatment of MPS can marginally make a profit, and the costliest part was the use of expensive Mg chemicals (Munir et al., 2017). Therefore, alternative methods should be developed for optimizing nutrient recovery. Many other research gaps are required to be filled, such as the risk of contaminant accumulation in the recovered fertilizer, the reusability and disposal of post-recovery filtrate, the utilization of processed residue (i.e., hydrochar after P leaching), the profitability of each extraction process, etc. After P recovery, additional improvements of hydrochar should be counted to provide integrated benefits. For example, acid washing (1N HCl) could reduce ash in DS-derived hydrochar by 50%, thus enhancing C, FC, and HHV by 70%, 167%, and 53%, respectively, and providing high-quality solid biofuel (Marin-Batista et al., 2020). By removing most heavy metals with acidic extraction, hydrochar may also be directly used as soil amendment. Moreover, a sound hydrochar adsorbent could be formed due to the improved adsorption performance by both acid and alkaline treatments (see Section 4.3).

4.5.2. Thermochemical process

Thermochemical technique provides an alternative method for P recovery from MS-derived hydrochar. It can avoid the problematic metals present in wet-chemical extraction process. Favored by the low melting point of P_2O_5 (340 °C), P in hydrochar can be vaporized under heated conditions, and thus recovered in the form of settled ash (Ahn et al., 2020). So far, only Feng et al. evaluated the feasibility of P recovery through thermochemical process, steam gasification of hydrochar derived from waste activated sludge (Feng et al., 2018). It was found that phosphorus oxides can be completely converted into gas phase after 560 °C, and AP was the primary form in the gasification ash. However, compared to direct gasification of MS, the total P recovery rate was not enhanced and stayed low (22–56%) (Feng et al., 2018). Chlorine donor is widely used to improve the thermochemical recovery process, but no further

studies about its application to hydrochar. Besides, it remains invalid whether heavy metals are eliminated from P-rich ash produced by hydrochar. Lastly, high energy demand and equipment requirements also limit the application of thermochemical treatment for P recovery.

4.5.3. *Integrated biotechnology*

With the growing interest in green and sustainable infrastructures, emerging technologies of coupling HTP with biological treatment have received much attention. Aida et al. (2016) first designed a system of algal cultivation using hydrochar and HTL aqueous. The scheme was mainly composed of: 1) HTC treatment of MS to produce nutrient-rich liquid; 2) conversion of P and cellulose-rich hydrochar into nutrient-rich glucose solution; 3) cultivation of microalgae with HTC aqueous and glucose solution; 4) production of biocrude from grown microalgae using HTL process. The preliminary results showed positive growth of microalgae using the integrated biological process (Aida et al., 2016). Therefore, nutrients can be cycled for microalgae cultivation during continuous treatment. The new green biotechnology provides an effective solid reduction approach with feasible ability of recycling nutrients. However, as an emerging technology, it also faces many challenges: The nutrient utilization efficiencies are unknown; the cultivation procedure requires care to balance nutrients; the contaminants in MS may inhibit the algal growth; the associated costs are not analyzed. Concurrently, another study integrated algal growth using MS, and HTL of cultivated algae followed by struvite extraction and showed promising performance (5.9% of N and 71.6% of P recovery) (Abeyisiriwardana-Arachchige et al., 2020). Therefore, the potential of emerging biotechnology, such as integrated algae cultivation, should not be underestimated.

4.6. Evaluation of valorization technologies for hydrochar

The abundant functions of MS-derived hydrochar provide numerous opportunities for its valorization. The utilization approaches for hydrochar are compared in **Fig. 15**. A summary of technical prospects for these processes is provided below:

=====

Please Insert Fig. 15 Here

=====

- I. Combustion using hydrochar as a biofuel is a promising direction in terms of the commercialization potential. Further optimization of energy density and combustion performance by co-HTC or co-combustion of hydrochar shows a way to enhance its market value. Addressing issues of ash slagging and fouling and harmful emissions is also beneficial. Besides, it is necessary to identify the nutrient potential and hazardous components of the post-combustion products, such as fly ash and bottom ash, from the perspective of a sustainable environment.
- II. Gasification to syngas production undergoes a high energy demand and expenditure (both capital and operating costs) associated with rigorous reactor requirements and catalyst assistance. Coupling energy gas production with P recovery through gasification may relieve the cost issue. However, gas separation/purification processes are required to become a mainstream treatment. Many other quandaries are still surrounding the understanding of gasification reactions, yield enhancement, ideal design, continuous feeding techniques, gas cleanup, and byproducts (ash) disposal.
- III. Agricultural application of hydrochar has shown its positive effects on soil properties and crop yield. However, such impacts may largely rely on the soil and plants, and thus require extensive and long-term studies to validate prior to field application. The relationships are not clarified between hydrochar application and the response of soil, microbial community, and plants. It appears that the availability of nutrients in hydrochar is inhibited, which will benefit the slow release process and long-term application. However, the fertilization efficiency and associated runoff issues need further investigation. Moreover, since pre-existing contaminants, such as heavy metals and POPs, are likely to accumulate in hydrochar, the safe use of hydrochar in agriculture must be developed and demonstrated. This will also help address public and specifically farmers' concerns.
- IV. Adsorption capacity is an important feature of hydrochar. It has shown positive effects in water remediation, with excellent activated carbon derived from hydrochar. However, the direct adsorption

of hydrochar is still limited and thus requires further optimization and systematic investigation. It is also necessary to recognize the potential release of pre-existing contaminants, such as heavy metals and POPs, during the adsorption process.

- V. Utilized as a heterogeneous catalyst is a special ability of hydrochar. Due to the presence of AAEMs, hydrochar displays the catalytic potential in gasification process. Magnetic hydrochar derived from MS provides a green and sustainable catalyst in Fenton-like reactions. However, there are limited studies about the catalytic mechanisms and application. Certainly, hydrochar is worthy of investigation as a catalyst for its high catalytic activity, long-term stability, and low toxicity.
- VI. Nutrient recovery is a sound promise for the valorization of hydrochar. It could lead to a cost-effective, efficient, profitable, easy, and simple operation. Wet-chemical extraction and precipitation are mostly used for their simple process, low expenditure, and high efficiency. However, they do require additional chemicals and equipment. Optimization of the chemical usage and search for cheap alternative chemicals would improve the profitability. Towards a sustainable approach, other gaps should also be fulfilled: The purity of recovered fertilizer, the reusability and disposal of post-recovery filtrate, and the usage of hydrochar after extraction. Following P recovery, the modified hydrochar could be investigated for solid biofuel, soil amendment, adsorbent, and catalyst to develop an integrated utilization approach.

5. Prospects towards sustainable waste management

Hydrothermal conversion is a promising technology in dealing with the challenges of MS treatment. The valorization of its byproducts, such as hydrochar and aqueous phase, is a critical and necessary first step. Among hydrothermal processes, HTC and HTL have shown their promising commercial potential for sludge decomposition and energy production. Through the literature review, a research trend of coupling HTP (particularly HTC/HTL) of MS and AD of HTP aqueous is identified, which could enhance the overall energy recovery, sustainability, environmental performance, and upscaling potential. Despite the energy recovered into hydrochar and biocrude by HTC and HTL, respectively, a large amount of organic matter is converted into the aqueous phase (with an average dry basis yield of 39 and 23%,

respectively), requiring proper treatment or valorization. **Fig. 16** compares the main characteristics of HTC aqueous and HTL aqueous from various types of sludge. Despite the MS type, both HTC and HTL aqueous showed high contents of COD (13–98 vs. 48–83 g/L) and TOC (9–38 vs. 14–27 g/L) on average, suggesting that further valorization of aqueous (e.g., biogas production by AD) would benefit the energy recovery of the HTP system. It should be noted that COD and TOC could proportionally increase with feedstock TS contents, which raised from 9.6 to 72.3 g/L and from 3.6 to 29.8 g/L, respectively, in HTC aqueous from DS when sludge TS increased from 2.5 to 30% (Aragón-Briceño et al., 2020). Previous literature review has reported that AD of HTP aqueous typically could achieve a specific methane yield of 200 mL CH₄/g COD, corresponding to over 50% energy recovery from the aqueous (Watson et al., 2020). Due to the hydrolysis and deamination of protein in MS, HTC and HTL aqueous also contains a large amount of ammonia (0.6–4.1 vs. 2.2–5 g/L), which are typically higher in SS and DS derived aqueous. Meanwhile, most P (>82%) is concentrated in hydrochar, which can be extracted and mixed with ammonia rich HTP aqueous to produce struvite as a fertilizer for N/P recovery. Studies have found that the recovery of N/P by struvite from HTP aqueous could enhance the performance of AD, probably due to the removal of ammonia and co-precipitation of other inhibitors (e.g., phenolics) (P. Wang et al., 2021; W. Wang et al., 2017). Conceptual designs of integrating HTC-AD or HTL-AD, nutrient recovery, and subsequent hydrochar valorization are illustrated in **Fig. 17**.

=====

Please Insert Fig. 16 Here

=====

=====

Please Insert Fig. 17 Here

=====

HTC is mostly applied to DS that contains a high content of non-biodegradable organics, which can be solubilized into HTC aqueous and recycled into AD with enhanced biodegradability. Consequently, the volume of remaining solids (hydrochar) for management could be significantly reduced. Many studies have suggested that HTC at mild conditions (e.g., 180–250 °C for < 1h) could compromise between energy consumption, dewaterability, hydrochar production, and methane production (92–356 mL CH₄/g COD) from HTC aqueous (Ahmed et al., 2021a, 2021b; Aragón-Briceño et al., 2017, 2021a, 2021b, 2020; Ferrentino et al., 2020b; Gaur et al., 2020; Medina-Martos et al., 2020). Danso-Boateng et al. (2015) found that Maillard reactions between monosaccharides and amino acids initiated at HTC of 180 °C for over 15 min, which could form non-biodegradable and/or AD inhibitors (e.g., aldehydes, furans, pyrroles, pyrazines, and pyridines) in the aqueous. However, increasing temperature from 160 to 250 °C (30 min) could enhance the formation of 191 to 716 mg COD/L equivalent volatile fatty acids from DS HTC aqueous, which are intermediate compounds in methane production (Aragón-Briceño et al., 2017). Therefore, HTC reaction conditions should be optimized for coupling HTC-AD. Through a system energy balance study for HTC-AD, Aragón-Briceño et al. (2020) found that higher TS contents in feedstock DS were favorable for net system electricity and heat production, which became positive at TS ≥10% when energy (>65% based on feedstock) in hydrochar was included. However, if hydrochar contained energy was omitted, HTC-AD would consume 0.01 kW of electricity and 0.06 kW of heat per kg of solids input even at 30% TS. Example of overall C and energy distribution is shown in **Fig. 17a**. Energy production and valorization of hydrochar in the HTC-AD scenario are critical steps for building a sustainable system in WWTPs. We recommend integrating nutrient recovery to the system to enhance the overall benefits and sustainability, especially in regions lack of P resource (e.g., EU). More importantly, the ash removal during P extraction step could make hydrochar a more capable solid biofuel. The potential of using hydrochar as a soil amender, absorbent, and heterogeneous catalyst has been demonstrated in the Section 4. However, the concerns of transferring POPs and heavy metals from hydrochar to struvite should be addressed before it can be used as a fertilizer.

MPS is a preferable feedstock for HTL as it likely contains balanced protein (dominant in SS) and carbohydrates (major in PS), which promotes Maillard reactions to achieve high yields and energy recovery into biocrude (Basar et al., 2021). Using HTL, where C is maximized to biocrude and P is enriched in hydrochar to allow its recovery, represents a justifiable operation for MS treatment. Through several techno-economic analyses, Pacific Northwest National Laboratory in the US has concluded that HTL of MPS (20–25% TS) is very promising in producing economically competitive and environmentally sustainable biocrude, while significantly reducing management costs and environmental risks associated to sludge solids (Li et al., 2021; Seiple et al., 2020, 2017; Snowden-Swan et al., 2017, 2016). However, HTL aqueous still contains a large portion of solubilized C (e.g., 20% of total input), which could contribute 9% BOD and 18% ammonia load to the WWTP (Snowden-Swan et al., 2017). Simply return HTL aqueous to the WWTP headworks would significantly increase aeration cost and may lead to toxicity impacts and exceed discharge limits due to high ammonia concentrations. Many studies have proposed to valorize HTL aqueous by AD, with a specific methane yield of 36–259 mL CH₄/g COD (Hao et al., 2020; Posmanik et al., 2017b; Usman et al., 2019b, 2020; P. Wang et al., 2021). However, inhibitory effects, such as delay, reduced rate, or even complete inhibition on AD performance, have been widely reported by the increase of HTL aqueous loading rates (Watson et al., 2020). Many organics (e.g., furans, ketones, phenols, and N-heterocyclic compounds) and inorganics (e.g., ammonia and chloride salts) in HTL aqueous can inhibit AD activities (mainly acetogenesis and methanogenesis). High temperatures (e.g., 300–350 °C) used in HTL could promote the formation of recalcitrant compounds, such as melanoidins, N-heterocyclics, and phenols, which are mainly responsible for AD inhibition. Wang et al. (2021) observed no methane generation and 1–8% COD removal for AD (at 35 °C, pH 7–8 for 28 days) of raw HTL aqueous from MS (325 °C for 30 min). Most other studies were conducted on diluted (4–10 times) HTL aqueous to obtain positive methane yields. Therefore, efficient treatment of HTL aqueous is considered the critical step in HTL-AD configuration. Studies have shown that adding granular activated carbon (Usman et al., 2019b) and hydrochar (Usman et al., 2020) to diluted HTL aqueous for AD could improve methane yield by up to 30 and 52%, respectively, due to enhanced

degradation of aromatic, N-heterocyclic, and phenolic compounds. A promising treatment was achieved by Wang et al. (2021), who used struvite precipitation for ammonia removal (82%) and biochar for phenols removal (70%) and reached a specific methane yield up to 225 mL CH₄/g COD from non-diluted HTL aqueous by mesophilic AD, while only struvite precipitation could achieve a specific methane yield up to 115 mL CH₄/g COD. Shanmugam et al. (2017) also found struvite precipitation improved methane production by 3.5 times from AD of diluted HTL aqueous from algae compared to non-treated. To achieve sustainable management of MS, an interwoven system is conceptually designed to integrate HTL-AD and nutrient recovery with hydrochar valorization in **Fig. 17b**. However, the long-term operation of AD for HTL aqueous is still challenging due to the accumulation of inhibitors and possible operational failure. This need to be addressed before the system can be applied to full-scale.

6. Conclusions

HTP has been recognized as one of the most efficient technologies in sludge-to-energy conversion for handling the challenge of waste MS management. Hydrochar, as the solid residue, is the main product of all three hydrothermal processes (i.e., HTC, HTL, and HTG). Its valorization improves the environmental and financial sustainability of sludge treatment by HTP. This review aims to guide future studies by summarizing the effects of reaction conditions on hydrochar formation, comparing the key characteristics of hydrochar, and highlighting the potential valorization routes with critical evaluations. The major findings of this review are listed below.

- High TS content (10–25 wt%) in MS feedstock for HTP is beneficial to hydrochar yields, process energy efficiency and energy recovery, and concentrated nutrients in hydrochar (e.g., P) and aqueous phase (e.g., organics and N) for efficient recovery.
- Hydrothermal temperature is crucial in determining reaction pathways, while combined effects of temperature and residence time govern hydrochar yields, which significantly decrease with increasing severity factor and remain around 10%, db at severity factor >1.
- Co-HTC and co-HTL of MS with other types of biomass have synergistic effects on quality and/or yield of hydrochar and biocrude, respectively. Co-HTC with low-ash biomass, such as lignocellulose,

could reduce ash, enhance HHV, and mitigate the concerns of heavy metals in hydrochar, representing a promising technique to generate desirable solid biofuel.

- Numerous catalysts have been examined in HTP to serve various purposes (e.g., dewaterability, conversion rate, and energy and nutrient recovery), but their reusability and the balance between costs and outcome should be evaluated.
- Using organic solvents or co-solvents in HTL could reduce reaction temperature and enhance biocrude yield and energy recovery. However, the biggest barriers of industrial implementation and solvent recycling should be addressed. The impacts of solvents on MS-derived hydrochar also lack studies.
- Hydrochar has diverse physicochemical properties that highly depend on initial characteristics of MS and treatment conditions. Therefore, the assignment of hydrochar utilization should be different from case to case. Mixing various types of sludge to achieve low ash and high C, FC, and HHV could be desirable for producing biofuel hydrochar under HTC conditions, while DS and SS derived hydrochar from HTL/HTG treatment could be suitable for efficient P recovery.
- Hydrochar has been extensively studied for solid biofuel production, but its other application means should be expanded for valorization, including but not limited to land application, adsorption, catalysis, and nutrient recovery.
- Energy densification (>1) of hydrochar likely occurs at HTP temperature of 150–300 °C and severity factor <0.5 . However, the high ash contents (19–57%, db) could limit the direct combustion of hydrochar due to possible ash fouling.
- Energy production from hydrochar is necessary for net positive energy recovery in HTC-AD scenario, while proper treatment for HTL aqueous is challenging for HTL-AD case.
- Coupling P extraction from hydrochar and struvite precipitation with HTP aqueous is critical for both HTC-AD and HTL-AD scenarios for multiple benefits: 1) Recycling non-renewable critical material (P); 2) reducing ammonia level in HTP aqueous and enhancing biogas production from AD; 3)

decreasing contents of ash and heavy metals in hydrochar to promote its subsequent valorization, such as upgraded biofuel, soil amender, activated carbon, and catalyst; and 4) improving the overall energy recovery, environmental performance, system sustainability, and commercialization potential.

Declaration of Competing Interest

The authors declare that they have no known competing financial interests or personal relationships that could have appeared to influence the work reported in this paper.

Acknowledgments

This research was funded by the Natural Sciences and Engineering Research Council of Canada (NSERC) and Metro Vancouver Industrial Research Chair Program in Advanced Resource Recovery from Wastewater (IRCPJ 548816-18). The authors would also like to thank the handling Editor and anonymous reviewers for their insightful comments and suggestions, which greatly improved this article.

References

- Abeywardana-Arachchige, I.S.A., Munasinghe-Arachchige, S.P., Delanka-Pedige, H.M.K., Nirmalakhandan, N., 2020. Removal and recovery of nutrients from municipal sewage: Algal vs. conventional approaches. *Water Res.* 175, 115709. <https://doi.org/10.1016/j.watres.2020.115709>
- Acelas, N.Y., López, D.P., Wim Brilman, D.W.F., Kersten, S.R.A., Kootstra, A.M.J., 2014. Supercritical water gasification of sewage sludge: Gas production and phosphorus recovery. *Bioresour. Technol.* 174, 167–175. <https://doi.org/10.1016/j.biortech.2014.10.003>
- Afif, E., Azadi, P., Farnood, R., 2011. Catalytic hydrothermal gasification of activated sludge. *Appl. Catal. B Environ.* 105, 136–143. <https://doi.org/10.1016/j.apcatb.2011.04.003>
- Ahmed, M., Andreottola, G., Elagroudy, S., Negm, M.S., Fiori, L., 2021a. Coupling hydrothermal carbonization and anaerobic digestion for sewage digestate management: Influence of hydrothermal treatment time on dewaterability and bio-methane production. *J. Environ. Manage.* 281, 111910. <https://doi.org/10.1016/j.jenvman.2020.111910>
- Ahmed, M., Sartori, F., Merzari, F., Fiori, L., Elagroudy, S., Negm, M.S., Andreottola, G., 2021b. Anaerobic degradation of digestate based hydrothermal carbonization products in a continuous hybrid fixed bed anaerobic filter. *Bioresour. Technol.* 330, 124971. <https://doi.org/10.1016/j.biortech.2021.124971>
- Ahn, H., Kim, D., Lee, Y., 2020. Combustion characteristics of sewage sludge solid fuels produced by drying and hydrothermal carbonization in a fluidized bed. *Renew. Energy* 147, 957–968. <https://doi.org/10.1016/j.renene.2019.09.057>
- Aida, T.M., Nonaka, T., Fukuda, S., Kujiraoka, H., Kumagai, Y., Maruta, R., Ota, M., Suzuki, I., Watanabe, M.M., Inomata, H., Smith, R.L., 2016. Nutrient recovery from municipal sludge for microalgae cultivation with two-step hydrothermal liquefaction. *Algal Res.* 18, 61–68. <https://doi.org/10.1016/j.algal.2016.06.009>

- Alatalo, S.M., Repo, E., Mäkilä, E., Salonen, J., Vakkilainen, E., Sillanpää, M., 2013. Adsorption behavior of hydrothermally treated municipal sludge & pulp and paper industry sludge. *Bioresour. Technol.* 147, 71–76. <https://doi.org/10.1016/j.biortech.2013.08.034>
- Ali Shah, A., Sohail Toor, S., Hussain Seehar, T., Sadetmahaleh, K.K., Helmer Pedersen, T., Haaning Nielsen, A., Aistrup Rosendahl, L., 2021. Bio-crude production through co-hydrothermal processing of swine manure with sewage sludge to enhance pumpability. *Fuel* 288. <https://doi.org/10.1016/j.fuel.2020.119407>
- Alipour, M., Asadi, H., Chen, C., Rashti, M.R., 2021. Bioavailability and eco-toxicity of heavy metals in chars produced from municipal sewage sludge decreased during pyrolysis and hydrothermal carbonization. *Ecol. Eng.* 162, 106173. <https://doi.org/10.1016/j.ecoleng.2021.106173>
- Amrullah, A., Matsumura, Y., 2018. Supercritical water gasification of sewage sludge in continuous reactor. *Bioresour. Technol.* 249, 276–283. <https://doi.org/10.1016/j.biortech.2017.10.002>
- Anastasakis, K., Biller, P., Madsen, R.B., Glasius, M., Johannsen, I., 2018. Continuous Hydrothermal Liquefaction of Biomass in a Novel Pilot Plant with Heat Recovery and Hydraulic Oscillation. *Energies* 11, 1–23. <https://doi.org/10.3390/en11102695>
- Aragón-Briceño, C., Ross, A.B., Camargo-Valero, M.A., 2017. Evaluation and comparison of product yields and bio-methane potential in sewage digestate following hydrothermal treatment. *Appl. Energy* 208, 1357–1369. <https://doi.org/10.1016/j.apenergy.2017.09.019>
- Aragón-Briceño, C.I., Grasham, O., Ross, A.B., Dupont, V., Camargo-Valero, M.A., 2020. Hydrothermal carbonization of sewage digestate at wastewater treatment works: Influence of solid loading on characteristics of hydrochar, process water and plant energetics. *Renew. Energy* 157, 959–973. <https://doi.org/10.1016/j.renene.2020.05.021>
- Aragón-Briceño, C.I., Pozarlik, A.K., Bramer, E.A., Niedzwiecki, L., Pawlak-Kruczek, H., Brem, G., 2021a. Hydrothermal carbonization of wet biomass from nitrogen and phosphorus approach: A review. *Renew. Energy* 171, 401–415. <https://doi.org/10.1016/j.renene.2021.02.109>
- Aragón-Briceño, C.I., Ross, A.B., Camargo-Valero, M.A., 2021b. Mass and energy integration study of hydrothermal carbonization with anaerobic digestion of sewage sludge. *Renew. Energy* 167, 473–483. <https://doi.org/10.1016/j.renene.2020.11.103>
- Azadi, P., Afif, E., Foroughi, H., Dai, T., Azadi, F., Farnood, R., 2013. Catalytic reforming of activated sludge model compounds in supercritical water using nickel and ruthenium catalysts. *Appl. Catal. B Environ.* 134–135, 265–273. <https://doi.org/10.1016/j.apcatb.2013.01.022>
- Barber, W.P.F., 2016. Thermal hydrolysis for sewage treatment: A critical review. *Water Res.* 104, 53–71. <https://doi.org/10.1016/j.watres.2016.07.069>
- Basar, I.A., Liu, H., Carrere, H., Trably, E., Eskicioglu, C., 2021. A review on key design and operational parameters to optimize and develop hydrothermal liquefaction of biomass for biorefinery applications. *Green Chem.* <https://doi.org/10.1039/D0GC04092D>
- Becker, G.C., Wüst, D., Köhler, H., Lautenbach, A., Kruse, A., 2019. Novel approach of phosphate-reclamation as struvite from sewage sludge by utilising hydrothermal carbonization. *J. Environ. Manage.* 238, 119–125. <https://doi.org/10.1016/j.jenvman.2019.02.121>
- Belete, Y.Z., Leu, S., Boussiba, S., Zorin, B., Posten, C., Thomsen, L., Wang, S., Gross, A., Bernstein, R., 2019. Characterization and utilization of hydrothermal carbonization aqueous phase as nutrient source for microalgal growth. *Bioresour. Technol.* 290, 121758. <https://doi.org/10.1016/j.biortech.2019.121758>
- Berge, N.D., Ro, K.S., Mao, J., Flora, J.R.V., Chappell, M.A., Bae, S., 2011. Hydrothermal carbonization of municipal waste streams. *Environ. Sci. Technol.* 45, 5696–5703.

<https://doi.org/10.1021/es2004528>

- Bhatt, D., Shrestha, A., Dahal, R.K., Acharya, B., Basu, P., MacEwen, R., 2018. Hydrothermal carbonization of biosolids from Waste water treatment plant. *Energies* 11. <https://doi.org/10.3390/en11092286>
- Biller, P., Johannsen, I., dos Passos, J.S., Ottosen, L.D.M., 2018. Primary sewage sludge filtration using biomass filter aids and subsequent hydrothermal co-liquefaction. *Water Res.* 130, 58–68. <https://doi.org/10.1016/j.watres.2017.11.048>
- Breulmann, M., van Afferden, M., Müller, R.A., Schulz, E., Fühner, C., 2017. Process conditions of pyrolysis and hydrothermal carbonization affect the potential of sewage sludge for soil carbon sequestration and amelioration. *J. Anal. Appl. Pyrolysis* 124, 256–265. <https://doi.org/10.1016/j.jaap.2017.01.026>
- Brookman, H., Gievers, F., Zelinski, V., Ohlert, J., Loewen, A., 2018. Influence of hydrothermal carbonization on composition, formation and elimination of biphenyls, dioxins and furans in sewage sludge. *Energies* 11. <https://doi.org/10.3390/en11061582>
- Cao, J., Wu, Y., Zhao, J., Jin, S., Aleem, M., Zhang, Q., Fang, F., Xue, Z., Luo, J., 2019. Phosphorus recovery as vivianite from waste activated sludge via optimizing iron source and pH value during anaerobic fermentation. *Bioresour. Technol.* 293, 122088. <https://doi.org/10.1016/j.biortech.2019.122088>
- Cao, X., Peng, X., Sun, S., Zhong, L., Chen, W., Wang, S., Sun, R.C., 2015. Hydrothermal conversion of xylose, glucose, and cellulose under the catalysis of transition metal sulfates. *Carbohydr. Polym.* 118, 44–51. <https://doi.org/10.1016/j.carbpol.2014.10.069>
- Catallo, W.J., Comeaux, J.L., 2008. Reductive hydrothermal treatment of sewage sludge. *Waste Manag.* 28, 2213–2219. <https://doi.org/10.1016/j.wasman.2007.10.005>
- Chanaka Udayanga, W.D., Veksha, A., Giannis, A., Lisak, G., Chang, V.W.C., Lim, T.T., 2018. Fate and distribution of heavy metals during thermal processing of sewage sludge. *Fuel* 226, 721–744. <https://doi.org/10.1016/j.fuel.2018.04.045>
- Chang, Y., Xiao, X., Huang, H., Xiao, Y.-D., Fang, H.-S., He, J.-B., Zhou, C.-H., 2021. Transformation characteristics of polycyclic aromatic hydrocarbons during hydrothermal liquefaction of sewage sludge. *J. Supercrit. Fluids* 170, 105158. <https://doi.org/10.1016/j.supflu.2020.105158>
- Channiwala, S.A., Parikh, P.P., 2002. A unified correlation for estimating HHV of solid, liquid and gaseous fuels. *Fuel* 81, 1051–1063. [https://doi.org/10.1016/S0016-2361\(01\)00131-4](https://doi.org/10.1016/S0016-2361(01)00131-4)
- Chen, C., Liu, G., An, Q., Lin, L., Shang, Y., Wan, C., 2020. From wasted sludge to valuable biochar by low temperature hydrothermal carbonization treatment: Insight into the surface characteristics. *J. Clean. Prod.* 263, 121600. <https://doi.org/10.1016/j.jclepro.2020.121600>
- Chen, D., Dou, Y., Tang, Q., Huang, Y., Song, M., Zhou, J., Fu, L., 2020. New insight on the combined effects of hydrothermal treatment and FeSO₄/Ca(ClO)₂ oxidation for sludge dewaterability improvement: From experimental to theoretical investigation. *Fuel Process. Technol.* 197. <https://doi.org/10.1016/j.fuproc.2019.106196>
- Chen, G., Tian, S., Liu, B., Hu, M., Ma, W., Li, X., 2020. Stabilization of heavy metals during co-pyrolysis of sewage sludge and excavated waste. *Waste Manag.* 103, 268–275. <https://doi.org/10.1016/j.wasman.2019.12.031>
- Chen, H., Rao, Y., Cao, L., Shi, Y., Hao, S., Luo, G., Zhang, S., 2019. Hydrothermal conversion of sewage sludge: Focusing on the characterization of liquid products and their methane yields. *Chem. Eng. J.* 357, 367–375. <https://doi.org/10.1016/j.cej.2018.09.180>
- Chen, H., Zhai, Y., Xu, B., Xiang, B., Zhu, L., Qiu, L., Liu, X., Li, C., Zeng, G., 2014. Fate and risk

- assessment of heavy metals in residue from co-liquefaction of *Camellia oleifera* cake and sewage sludge in supercritical ethanol. *Bioresour. Technol.* 167, 578–581.
<https://doi.org/10.1016/j.biortech.2014.06.048>
- Chen, W.T., Zhang, Y., Zhang, J., Yu, G., Schideman, L.C., Zhang, P., Minarick, M., 2014. Hydrothermal liquefaction of mixed-culture algal biomass from wastewater treatment system into bio-crude oil. *Bioresour. Technol.* 152, 130–139. <https://doi.org/10.1016/j.biortech.2013.10.111>
- Chen, Y., Chen, H., Thring, R.W., Liu, H., Zhou, J., Tao, Y., Li, J., 2020. Immobilization of Chromium Contaminated Soil by Co-pyrolysis with Rice Straw. *Water, Air, Soil Pollut.* 231, 200.
<https://doi.org/10.1007/s11270-020-04581-3>
- Chen, Y., Guo, L., Cao, W., Jin, H., Guo, S., Zhang, X., 2013a. Hydrogen production by sewage sludge gasification in supercritical water with a fluidized bed reactor. *Int. J. Hydrogen Energy* 38, 12991–12999. <https://doi.org/10.1016/j.ijhydene.2013.03.165>
- Chen, Y., Guo, L., Jin, H., Yin, J., Lu, Y., Zhang, X., 2013b. An experimental investigation of sewage sludge gasification in near and super-critical water using a batch reactor, in: *International Journal of Hydrogen Energy*. pp. 12912–12920. <https://doi.org/10.1016/j.ijhydene.2013.05.076>
- Chen, Y.W., Lee, H.V., 2020. Recent progress in homogeneous Lewis acid catalysts for the transformation of hemicellulose and cellulose into valuable chemicals, fuels, and nanocellulose. *Rev. Chem. Eng.* 36, 215–235. <https://doi.org/10.1515/revce-2017-0071>
- Chu, Q., Xue, L., Singh, B.P., Yu, S., Müller, K., Wang, H., Feng, Y., Pan, G., Zheng, X., Yang, L., 2020. Sewage sludge-derived hydrochar that inhibits ammonia volatilization, improves soil nitrogen retention and rice nitrogen utilization. *Chemosphere* 245, 125558.
<https://doi.org/10.1016/j.chemosphere.2019.125558>
- Conti, F., Toor, S.S., Pedersen, T.H., Seehar, T.H., Nielsen, A.H., Rosendahl, L.A., 2020. Valorization of animal and human wastes through hydrothermal liquefaction for biocrude production and simultaneous recovery of nutrients. *Energy Convers. Manag.* 216, 112925.
<https://doi.org/10.1016/j.enconman.2020.112925>
- Couto, E.A., Pinto, F., Varela, F., Reis, A., Costa, P., Calijuri, M.L., 2018. Hydrothermal liquefaction of biomass produced from domestic sewage treatment in high-rate ponds. *Renew. Energy* 118, 644–653. <https://doi.org/10.1016/j.renene.2017.11.041>
- Danso-Boateng, E., Shama, G., Wheatley, A.D., Martin, S.J., Holdich, R.G., 2015. Hydrothermal carbonisation of sewage sludge: Effect of process conditions on product characteristics and methane production. *Bioresour. Technol.* 177, 318–327. <https://doi.org/10.1016/j.biortech.2014.11.096>
- De la Rubia, M.A., Villamil, J.A., Rodriguez, J.J., Borja, R., Mohedano, A.F., 2018. Mesophilic anaerobic co-digestion of the organic fraction of municipal solid waste with the liquid fraction from hydrothermal carbonization of sewage sludge. *Waste Manag.* 76, 315–322.
<https://doi.org/10.1016/j.wasman.2018.02.046>
- Do, T.X., Mujahid, R., Lim, H.S., Kim, J.-K., Lim, Y.-I., Kim, J., 2020. Techno-economic analysis of bio heavy-oil production from sewage sludge using supercritical and subcritical water. *Renew. Energy* 151, 30–42. <https://doi.org/10.1016/j.renene.2019.10.138>
- EBC, 2019. European Biochar Certificate - Guidelines for a Sustainable Production of Biochar, European Biochar Foundation (EBC). <https://doi.org/10.13140/RG.2.1.4658.7043>
- Ekpo, U., Ross, A.B., Camargo-Valero, M.A., Williams, P.T., 2016. A comparison of product yields and inorganic content in process streams following thermal hydrolysis and hydrothermal processing of microalgae, manure and digestate. *Bioresour. Technol.* 200, 951–960.
<https://doi.org/10.1016/j.biortech.2015.11.018>

- El-Deen, S.E.A.S., Zhang, F., 2012. Synthesis of Sludge@Carbon Nanocomposite for the Recovery of as (V) from Wastewater, in: *Procedia Environmental Sciences*. pp. 378–390. <https://doi.org/10.1016/j.proenv.2012.10.054>
- Elliott, D.C., Biller, P., Ross, A.B., Schmidt, A.J., Jones, S.B., 2015. Hydrothermal liquefaction of biomass: Developments from batch to continuous process. *Bioresour. Technol.* 178, 147–156. <https://doi.org/10.1016/j.biortech.2014.09.132>
- Escala, M., Zumbühl, T., Koller, C., Junge, R., Krebs, R., 2013. Hydrothermal carbonization as an energy-efficient alternative to established drying technologies for sewage sludge: A feasibility study on a laboratory scale. *Energy and Fuels* 27, 454–460. <https://doi.org/10.1021/ef3015266>
- European Commission, 2018. Report on Critical Raw Materials and the Circular Economy. Brussels.
- Fakkaew, K., Koottatep, T., Polprasert, C., 2018. Faecal sludge treatment and utilization by hydrothermal carbonization. *J. Environ. Manage.* 216, 421–426. <https://doi.org/10.1016/j.jenvman.2017.09.031>
- Falayi, T., 2019. Alkaline recovery of phosphorous from sewage sludge and stabilisation of sewage sludge residue. *Waste Manag.* 84, 166–172. <https://doi.org/10.1016/j.wasman.2018.11.041>
- Fan, Y.J., Zhu, W., Gong, M., Su, Y., Zhang, H.W., Zeng, J.N., 2016. Catalytic gasification of dewatered sewage sludge in supercritical water: Influences of formic acid on hydrogen production. *Int. J. Hydrogen Energy* 41, 4366–4373. <https://doi.org/10.1016/j.ijhydene.2015.11.071>
- Fei, Y., Zhao, D., Cao, Y., Huot, H., Tang, Y., Zhang, H., Xiao, T., 2019a. Phosphorous Retention and Release by Sludge-Derived Hydrochar for Potential Use as a Soil Amendment. *J. Environ. Qual.* 48, 502–509. <https://doi.org/10.2134/jeq2018.09.0328>
- Fei, Y., Zhao, D., Liu, Y., Zhang, W., Tang, Y., Huang, X., Wu, Q., Wang, Y., Xiao, T., Liu, C., 2019b. Feasibility of sewage sludge derived hydrochars for agricultural application: Nutrients (N, P, K) and potentially toxic elements (Zn, Cu, Pb, Ni, Cd). *Chemosphere* 236, 124841. <https://doi.org/10.1016/j.chemosphere.2019.124841>
- Feng, Y., Ma, K., Yu, T., Bai, S., Pei, D., Bai, T., Zhang, Q., Yin, L., Hu, Y., Chen, D., 2018. Phosphorus Transformation in Hydrothermal Pretreatment and Steam Gasification of Sewage Sludge. *Energy and Fuels* 32, 8545–8551. <https://doi.org/10.1021/acs.energyfuels.8b01860>
- Ferrentino, R., Ceccato, R., Marchetti, V., Andreottola, G., Fiori, L., 2020a. Sewage sludge hydrochar: An option for removal of methylene blue from wastewater. *Appl. Sci.* 10, 3445. <https://doi.org/10.3390/app10103445>
- Ferrentino, R., Merzari, F., Fiori, L., Andreottola, G., 2020b. Coupling hydrothermal carbonization with anaerobic digestion for sewage sludge treatment: Influence of HTC liquor and hydrochar on biomethane production. *Energies* 13, 6262. <https://doi.org/10.3390/en13236262>
- Fijalkowski, K., Rorat, A., Grobelak, A., Kacprzak, M.J., 2017. The presence of contaminations in sewage sludge – The current situation. *J. Environ. Manage.* 203, 1126–1136. <https://doi.org/10.1016/j.jenvman.2017.05.068>
- Fiori, L., Valbusa, M., Castello, D., 2012. Supercritical water gasification of biomass for H₂ production: Process design. *Bioresour. Technol.* 121, 139–147. <https://doi.org/10.1016/j.biortech.2012.06.116>
- Gai, C., Chen, M., Liu, T., Peng, N., Liu, Z., 2016a. Gasification characteristics of hydrochar and pyrochar derived from sewage sludge. *Energy* 113, 957–965. <https://doi.org/10.1016/j.energy.2016.07.129>
- Gai, C., Guo, Y., Liu, T., Peng, N., Liu, Z., 2016b. Hydrogen-rich gas production by steam gasification of hydrochar derived from sewage sludge. *Int. J. Hydrogen Energy* 41, 3363–3372. <https://doi.org/10.1016/j.ijhydene.2015.12.188>

- Gao, N., Kamran, K., Quan, C., Williams, P.T., 2020. Thermochemical conversion of sewage sludge: A critical review. *Prog. Energy Combust. Sci.* 79, 100843. <https://doi.org/10.1016/j.pecs.2020.100843>
- Gao, N., Li, Z., Quan, C., Miskolczi, N., Egedy, A., 2019. A new method combining hydrothermal carbonization and mechanical compression in-situ for sewage sludge dewatering: Bench-scale verification. *J. Anal. Appl. Pyrolysis* 139, 187–195. <https://doi.org/10.1016/j.jaap.2019.02.003>
- Gaur, R.Z., Khoury, O., Zohar, M., Poverenov, E., Darzi, R., Laor, Y., Posmanik, R., 2020. Hydrothermal carbonization of sewage sludge coupled with anaerobic digestion: Integrated approach for sludge management and energy recycling. *Energy Convers. Manag.* 224, 113353. <https://doi.org/10.1016/j.enconman.2020.113353>
- Gong, M., Nanda, S., Romero, M.J., Zhu, W., Kozinski, J.A., 2017. Subcritical and supercritical water gasification of humic acid as a model compound of humic substances in sewage sludge. *J. Supercrit. Fluids* 119, 130–138. <https://doi.org/10.1016/j.supflu.2016.08.018>
- Gong, M., Wang, Y., Fan, Y., Zhu, W., Zhang, H., Su, Y., 2018. Polycyclic aromatic hydrocarbon formation during the gasification of sewage sludge in sub- and supercritical water: Effect of reaction parameters and reaction pathways. *Waste Manag.* 72, 287–295. <https://doi.org/10.1016/j.wasman.2017.11.024>
- Gong, M., Zhu, W., Fan, Y., Zhang, H., Su, Y., 2016a. Influence of the reactant carbon-hydrogen-oxygen composition on the key products of the direct gasification of dewatered sewage sludge in supercritical water. *Bioresour. Technol.* 208, 81–86. <https://doi.org/10.1016/j.biortech.2016.02.070>
- Gong, M., Zhu, W., Xu, Z.R., Zhang, H.W., Yang, H.P., 2014a. Influence of sludge properties on the direct gasification of dewatered sewage sludge in supercritical water. *Renew. Energy* 66, 605–611. <https://doi.org/10.1016/j.renene.2014.01.006>
- Gong, M., Zhu, W., Zhang, H., Su, Y., Fan, Y., 2016b. Polycyclic aromatic hydrocarbon formation from gasification of sewage sludge in supercritical water: The concentration distribution and effect of sludge properties. *J. Supercrit. Fluids* 113, 112–118. <https://doi.org/10.1016/j.supflu.2016.03.021>
- Gong, M., Zhu, W., Zhang, H.W., Ma, Q., Su, Y., Fan, Y.J., 2014b. Influence of NaOH and Ni catalysts on hydrogen production from the supercritical water gasification of dewatered sewage sludge. *Int. J. Hydrogen Energy* 39, 19947–19954. <https://doi.org/10.1016/j.ijhydene.2014.10.051>
- Gu, X., Martinez-Fernandez, J.S., Pang, N., Fu, X., Chen, S., 2020. Recent development of hydrothermal liquefaction for algal biorefinery. *Renew. Sustain. Energy Rev.* 121. <https://doi.org/10.1016/j.rser.2020.109707>
- Guo, Y., Wang, S., Gong, Y., Xu, D., Tang, X., Ma, H., 2010. Partial oxidation of municipal sludge with activated carbon catalyst in supercritical water. *J. Hazard. Mater.* 180, 137–144. <https://doi.org/10.1016/j.jhazmat.2010.04.005>
- Hao, S., Ren, S., Zhou, N., Chen, H., Usman, M., He, C., Shi, Q., Luo, G., Zhang, S., 2020. Molecular composition of hydrothermal liquefaction wastewater from sewage sludge and its transformation during anaerobic digestion. *J. Hazard. Mater.* 383, 121163. <https://doi.org/10.1016/j.jhazmat.2019.121163>
- Harvey, O.R., Herbert, B.E., Kuo, L.-J., Louchouart, P., 2012. Generalized Two-Dimensional Perturbation Correlation Infrared Spectroscopy Reveals Mechanisms for the Development of Surface Charge and Recalcitrance in Plant-Derived Biochars. <https://doi.org/10.1021/es302971d>
- He, C., Chen, C.L., Giannis, A., Yang, Y., Wang, J.Y., 2014a. Hydrothermal gasification of sewage sludge and model compounds for renewable hydrogen production: A review. *Renew. Sustain. Energy Rev.* 39, 1127–1142. <https://doi.org/10.1016/j.rser.2014.07.141>
- He, C., Giannis, A., Wang, J.Y., 2013. Conversion of sewage sludge to clean solid fuel using

- hydrothermal carbonization: Hydrochar fuel characteristics and combustion behavior. *Appl. Energy* 111, 257–266. <https://doi.org/10.1016/j.apenergy.2013.04.084>
- He, C., Tang, C., Liu, W., Dai, L., Qiu, R., 2020. Co-pyrolysis of sewage sludge and hydrochar with coals: Pyrolytic behaviors and kinetics analysis using TG-FTIR and a discrete distributed activation energy model. *Energy Convers. Manag.* 203, 112226. <https://doi.org/10.1016/j.enconman.2019.112226>
- He, C., Wang, K., Giannis, A., Yang, Y., Wang, J.Y., 2015a. Products evolution during hydrothermal conversion of dewatered sewage sludge in sub- and near-critical water: Effects of reaction conditions and calcium oxide additive. *Int. J. Hydrogen Energy* 40, 5776–5787. <https://doi.org/10.1016/j.ijhydene.2015.03.006>
- He, C., Wang, K., Yang, Y., Amaniampong, P.N., Wang, J.Y., 2015b. Effective nitrogen removal and recovery from dewatered sewage sludge using a novel integrated system of accelerated hydrothermal deamination and air stripping. *Environ. Sci. Technol.* 49, 6872–6880. <https://doi.org/10.1021/acs.est.5b00652>
- He, C., Wang, K., Yang, Y., Wang, J.Y., 2014b. Utilization of sewage-sludge-derived hydrochars toward efficient cocombustion with different-rank coals: Effects of subcritical water conversion and blending scenarios. *Energy and Fuels* 28, 6140–6150. <https://doi.org/10.1021/ef501386g>
- He, C., Zhang, Z., Ge, C., Liu, W., Tang, Y., Zhuang, X., Qiu, R., 2019. Synergistic effect of hydrothermal co-carbonization of sewage sludge with fruit and agricultural wastes on hydrochar fuel quality and combustion behavior. *Waste Manag.* 100, 171–181. <https://doi.org/10.1016/j.wasman.2019.09.018>
- He, C., Zhao, J., Yang, Y., Wang, J.Y., 2016. Multiscale characteristics dynamics of hydrochar from hydrothermal conversion of sewage sludge under sub- and near-critical water. *Bioresour. Technol.* 211, 486–493. <https://doi.org/10.1016/j.biortech.2016.03.110>
- Hoşgün, E.Z., 2020. One-pot hydrothermal conversion of poppy stalks over metal chloride catalysts. *Biomass Convers. Biorefinery.* <https://doi.org/10.1007/s13399-020-00682-5>
- Hu, G., Liu, H., Chen, C., Hou, H., Li, J., Hewage, K., Sadiq, R., 2021. Low-temperature thermal desorption and secure landfill for oil-based drill cuttings management: Pollution control, human health risk, and probabilistic cost assessment. *J. Hazard. Mater.* 410, 124570. <https://doi.org/10.1016/j.jhazmat.2020.124570>
- Huang, H. jun, Chang, Y. chao, Lai, F. ying, Zhou, C. fei, Pan, Z. qian, Xiao, X. feng, Wang, J. xin, Zhou, C. huo, 2019. Co-liquefaction of sewage sludge and rice straw/wood sawdust: The effect of process parameters on the yields/properties of bio-oil and biochar products. *Energy* 173, 140–150. <https://doi.org/10.1016/j.energy.2019.02.071>
- Huang, H. jun, Yuan, X. zhong, Zhu, H. na, Li, H., Liu, Y., Wang, X. li, Zeng, G. ming, 2013. Comparative studies of thermochemical liquefaction characteristics of microalgae, lignocellulosic biomass and sewage sludge. *Energy* 56, 52–60. <https://doi.org/10.1016/j.energy.2013.04.065>
- Huang, H., Yuan, X., Zeng, G., Zhu, H., Li, H., Liu, Z., Jiang, H., Leng, L., Bi, W., 2011. Quantitative evaluation of heavy metals' pollution hazards in liquefaction residues of sewage sludge. *Bioresour. Technol.* 102, 10346–10351. <https://doi.org/10.1016/j.biortech.2011.08.117>
- Huang, H.J., Yuan, X.Z., 2016. The migration and transformation behaviors of heavy metals during the hydrothermal treatment of sewage sludge. *Bioresour. Technol.* 200, 991–998. <https://doi.org/10.1016/j.biortech.2015.10.099>
- Huang, H.J., Yuan, X.Z., Li, B.T., Xiao, Y.D., Zeng, G.M., 2014. Thermochemical liquefaction characteristics of sewage sludge in different organic solvents. *J. Anal. Appl. Pyrolysis* 109, 176–184. <https://doi.org/10.1016/j.jaap.2014.06.015>

- Huang, J., Wang, P., Niu, Y., Yu, H., Ma, F., Xiao, G., Xu, X., 2018. Changes in C:N:P stoichiometry modify N and P conservation strategies of a desert steppe species *Glycyrrhiza uralensis*. *Sci. Rep.* 8, 1–9. <https://doi.org/10.1038/s41598-018-30324-w>
- Huang, J., Wang, Z., Qiao, Y., Wang, B., Yu, Y., Xu, M., 2020. Transformation of nitrogen during hydrothermal carbonization of sewage sludge: Effects of temperature and Na/Ca acetates addition. *Proc. Combust. Inst.* 000, 1–10. <https://doi.org/10.1016/j.proci.2020.06.075>
- Huang, R., Fang, C., Lu, X., Jiang, R., Tang, Y., 2017. Transformation of phosphorus during (hydro)thermal treatments of solid Biowastes: Reaction mechanisms and implications for P reclamation and recycling. *Environ. Sci. Technol.* 51, 10284–10298. <https://doi.org/10.1021/acs.est.7b02011>
- Huang, R., Tang, Y., 2016. Evolution of phosphorus complexation and mineralogy during (hydro)thermal treatments of activated and anaerobically digested sludge: Insights from sequential extraction and P K-edge XANES. *Water Res.* 100, 439–447. <https://doi.org/10.1016/j.watres.2016.05.029>
- Huang, R., Tang, Y., 2015. Speciation Dynamics of Phosphorus during (Hydro)Thermal Treatments of Sewage Sludge. *Environ. Sci. Technol.* 49, 14466–14474. <https://doi.org/10.1021/acs.est.5b04140>
- Huang, R., Tang, Y., Luo, L., 2021. Thermochemistry of sulfur during pyrolysis and hydrothermal carbonization of sewage sludges. *Waste Manag.* 121, 276–285. <https://doi.org/10.1016/j.wasman.2020.12.004>
- Huang, R., Zhang, B., Saad, E.M., Ingall, E.D., Tang, Y., 2018. Speciation evolution of zinc and copper during pyrolysis and hydrothermal carbonization treatments of sewage sludges. *Water Res.* 132, 260–269. <https://doi.org/10.1016/j.watres.2018.01.009>
- Ibrahim, A.B.A., Akilli, H., 2019. Supercritical water gasification of wastewater sludge for hydrogen production. *Int. J. Hydrogen Energy* 44, 10328–10349. <https://doi.org/10.1016/j.ijhydene.2019.02.184>
- Inoue, S., Sawayama, S., Dote, Y., Ogi, T., 1997. Behaviour of nitrogen during liquefaction of dewatered sewage sludge. *Biomass and Bioenergy* 12, 473–475. [https://doi.org/10.1016/S0961-9534\(97\)00017-2](https://doi.org/10.1016/S0961-9534(97)00017-2)
- Itoh, S., Suzuki, A., Nakamura, T., Yokoyama, S. ya, 1994. Production of heavy oil from sewage sludge by direct thermochemical liquefaction. *Desalination* 98, 127–133. [https://doi.org/10.1016/0011-9164\(94\)00137-5](https://doi.org/10.1016/0011-9164(94)00137-5)
- Kacprzak, M., Neczaj, E., Fijałkowski, K., Grobelak, A., Grosser, A., Worwag, M., Rorat, A., Brattebo, H., Almås, Å., Singh, B.R., 2017. Sewage sludge disposal strategies for sustainable development. *Environ. Res.* 156, 39–46. <https://doi.org/10.1016/j.envres.2017.03.010>
- Kapusta, K., 2018. Effect of ultrasound pretreatment of municipal sewage sludge on characteristics of bio-oil from hydrothermal liquefaction process. *Waste Manag.* 78, 183–190. <https://doi.org/10.1016/j.wasman.2018.05.043>
- Karayıldırım, T., Sınağ, A., Kruse, A., 2008. Char and Coke Formation as Unwanted Side Reaction of the Hydrothermal Biomass Gasification. *Chem. Eng. Technol.* 31, 1561–1568. <https://doi.org/10.1002/ceat.200800278>
- Khan, T.A., Saud, A.S., Jamari, S.S., Rahim, M.H.A., Park, J.W., Kim, H.J., 2019. Hydrothermal carbonization of lignocellulosic biomass for carbon rich material preparation: A review. *Biomass and Bioenergy* 130, 105384. <https://doi.org/10.1016/j.biombioe.2019.105384>
- Khoshbouy, R., Takahashi, F., Yoshikawa, K., 2019. Preparation of high surface area sludge-based activated hydrochar via hydrothermal carbonization and application in the removal of basic dye. *Environ. Res.* 175, 457–467. <https://doi.org/10.1016/j.envres.2019.04.002>

- Kim, D., Lee, K., Park, K.Y., 2014. Hydrothermal carbonization of anaerobically digested sludge for solid fuel production and energy recovery. *Fuel* 130, 120–125. <https://doi.org/10.1016/j.fuel.2014.04.030>
- Kim, D., Park, S., Park, K.Y., 2017. Upgrading the fuel properties of sludge and low rank coal mixed fuel through hydrothermal carbonization. *Energy* 141, 598–602. <https://doi.org/10.1016/j.energy.2017.09.113>
- Kim, Y., Parker, W., 2008. A technical and economic evaluation of the pyrolysis of sewage sludge for the production of bio-oil. *Bioresour. Technol.* 99, 1409–1416. <https://doi.org/10.1016/j.biortech.2007.01.056>
- Kong, L., Li, G., Wang, H., He, W., Ling, F., 2008. Hydrothermal catalytic conversion of biomass for lactic acid production. *J. Chem. Technol. Biotechnol.* 83, 383–388. <https://doi.org/10.1002/jctb.1797>
- Koottatep, T., Fakkaew, K., Tajai, N., Pradeep, S. V., Polprasert, C., 2016. Sludge stabilization and energy recovery by hydrothermal carbonization process. *Renew. Energy* 99, 978–985. <https://doi.org/10.1016/j.renene.2016.07.068>
- Kor-Bicakci, G., Eskicioglu, C., 2019. Recent developments on thermal municipal sludge pretreatment technologies for enhanced anaerobic digestion. *Renew. Sustain. Energy Rev.* 110, 423–443. <https://doi.org/10.1016/j.rser.2019.05.002>
- Kroiss, H., Rechberger, H., Egle, L., 2011. Phosphorus in Water Quality and Waste Management, in: *Integrated Waste Management - Volume II*. InTech, pp. 181–214. <https://doi.org/10.5772/18482>
- Kumar, K., Parveen, F., Patra, T., Upadhyayula, S., 2018. Hydrothermal conversion of glucose to levulinic acid using multifunctional ionic liquids: Effects of metal ion co-catalysts on the product yield. *New J. Chem.* 42, 228–236. <https://doi.org/10.1039/c7nj03146g>
- Lai, F. ying, Chang, Y. chao, Huang, H. jun, Wu, G. qiang, Xiong, J. bo, Pan, Z. qian, Zhou, C. fei, 2018. Liquefaction of sewage sludge in ethanol-water mixed solvents for bio-oil and biochar products. *Energy* 148, 629–641. <https://doi.org/10.1016/j.energy.2018.01.186>
- Lee, J., Sohn, D., Lee, K., Park, K.Y., 2019. Solid fuel production through hydrothermal carbonization of sewage sludge and microalgae *Chlorella* sp. from wastewater treatment plant. *Chemosphere* 230, 157–163. <https://doi.org/10.1016/j.chemosphere.2019.05.066>
- Leng, L., Li, Jun, Yuan, X., Li, Jingjing, Han, P., Hong, Y., Wei, F., Zhou, W., 2018. Beneficial synergistic effect on bio-oil production from co-liquefaction of sewage sludge and lignocellulosic biomass. *Bioresour. Technol.* 251, 49–56. <https://doi.org/10.1016/j.biortech.2017.12.018>
- Leng, L., Yuan, X., Chen, X., Huang, H., Wang, H., Li, H., Zhu, R., Li, S., Zeng, G., 2015a. Characterization of liquefaction bio-oil from sewage sludge and its solubilization in diesel microemulsion. *Energy* 82, 218–228. <https://doi.org/10.1016/j.energy.2015.01.032>
- Leng, L., Yuan, X., Huang, H., Jiang, H., Chen, X., Zeng, G., 2014. The migration and transformation behavior of heavy metals during the liquefaction process of sewage sludge. *Bioresour. Technol.* 167, 144–150. <https://doi.org/10.1016/j.biortech.2014.05.119>
- Leng, L., Yuan, X., Huang, H., Shao, J., Wang, H., Chen, X., Zeng, G., 2015b. Bio-char derived from sewage sludge by liquefaction: Characterization and application for dye adsorption. *Appl. Surf. Sci.* 346, 223–231. <https://doi.org/10.1016/j.apsusc.2015.04.014>
- Li, C., Wang, X., Zhang, G., Yu, G., Lin, J., Wang, Y., 2017. Hydrothermal and alkaline hydrothermal pretreatments plus anaerobic digestion of sewage sludge for dewatering and biogas production: Bench-scale research and pilot-scale verification. *Water Res.* 117, 49–57. <https://doi.org/10.1016/j.watres.2017.03.047>
- Li, H., Yuan, X., Zeng, G., Huang, D., Huang, H., Tong, J., You, Q., Zhang, J., Zhou, M., 2010. The

- formation of bio-oil from sludge by deoxy-liquefaction in supercritical ethanol. *Bioresour. Technol.* 101, 2860–2866. <https://doi.org/10.1016/j.biortech.2009.10.084>
- Li, L., Xu, Z.R., Zhang, C., Bao, J., Dai, X., 2012. Quantitative evaluation of heavy metals in solid residues from sub- and super-critical water gasification of sewage sludge. *Bioresour. Technol.* 121, 169–175. <https://doi.org/10.1016/j.biortech.2012.06.084>
- Li, R., Ma, Z., Yang, T., Li, B., Wei, L., Sun, Y., 2018. Sub-supercritical liquefaction of municipal wet sewage sludge to produce bio-oil: Effect of different organic–water mixed solvents. *J. Supercrit. Fluids* 138, 115–123. <https://doi.org/10.1016/j.supflu.2018.04.011>
- Li, S., Jiang, Y., Snowden-Swan, L.J., Askander, J.A., Schmidt, A.J., Billing, J.M., 2021. Techno-economic uncertainty analysis of wet waste-to-biocrude via hydrothermal liquefaction. *Appl. Energy* 283, 116340. <https://doi.org/10.1016/j.apenergy.2020.116340>
- Li, S., Zeng, W., Jia, Z., Wu, G., Xu, H., Peng, Y., 2020. Phosphorus species transformation and recovery without apatite in FeCl₃-assisted sewage sludge hydrothermal treatment. *Chem. Eng. J.* 399, 125735. <https://doi.org/10.1016/j.cej.2020.125735>
- Lishan, X., Tao, L., Yin, W., Zhilong, Y., Jiangfu, L., 2018. Comparative life cycle assessment of sludge management: A case study of Xiamen, China. *J. Clean. Prod.* 192, 354–363. <https://doi.org/10.1016/j.jclepro.2018.04.171>
- Liu, C., Xu, J., Hu, J., Zhang, H., Xiao, R., 2017. Metal Ion-Catalyzed Hydrothermal Liquefaction of Calcium Lignosulfonate in Subcritical Water. *Chem. Eng. Technol.* 40, 1092–1100. <https://doi.org/10.1002/ceat.201600650>
- Liu, H., Hu, G., Basar, I.A., Li, J., Lyczko, N., Nzihou, A., Eskicioglu, C., 2021. Phosphorus recovery from municipal sludge-derived ash and hydrochar through wet-chemical technology: A review towards sustainable waste management. *Chem. Eng. J.* 417, 129300. <https://doi.org/10.1016/j.cej.2021.129300>
- Liu, M., Duan, Y., Bikane, K., Zhao, L., 2017. Effect of waste liquid produced from the hydrothermal treatment of both low-rank coal and sludge on the slurryability of coal sludge slurry. *Fuel* 203, 1–10. <https://doi.org/10.1016/j.fuel.2017.04.091>
- Liu, R., Tian, W., Kong, S., Meng, Y., Wang, H., Zhang, J., 2018. Effects of inorganic and organic acid pretreatments on the hydrothermal liquefaction of municipal secondary sludge. *Energy Convers. Manag.* 174, 661–667. <https://doi.org/10.1016/j.enconman.2018.08.058>
- Liu, T., Guo, Y., Peng, N., Lang, Q., Xia, Y., Gai, C., Liu, Z., 2017a. Nitrogen transformation among char, tar and gas during pyrolysis of sewage sludge and corresponding hydrochar. *J. Anal. Appl. Pyrolysis* 126, 298–306. <https://doi.org/10.1016/j.jaap.2017.05.017>
- Liu, T., Guo, Y., Peng, N., Lang, Q., Xia, Y., Gai, C., Zheng, Q., Liu, Z., 2018a. Identification and quantification of polycyclic aromatic hydrocarbons generated during pyrolysis of sewage sludge: Effect of hydrothermal carbonization pretreatment. *J. Anal. Appl. Pyrolysis* 130, 249–255. <https://doi.org/10.1016/j.jaap.2018.01.021>
- Liu, T., Lang, Q., Xia, Y., Chen, Z., Li, D., Ma, J., Gai, C., Liu, Z., 2019. Combination of hydrothermal carbonization and oxy-fuel combustion process for sewage sludge treatment: Combustion characteristics and kinetics analysis. *Fuel* 242, 265–276. <https://doi.org/10.1016/j.fuel.2019.01.035>
- Liu, T., Li, Y., Peng, N., Lang, Q., Xia, Y., Gai, C., Zheng, Q., Liu, Z., 2017b. Heteroatoms doped porous carbon derived from hydrothermally treated sewage sludge: Structural characterization and environmental application. *J. Environ. Manage.* 197, 151–158. <https://doi.org/10.1016/j.jenvman.2017.03.082>
- Liu, T., Liu, Z., Zheng, Q., Lang, Q., Xia, Y., Peng, N., Gai, C., 2018b. Effect of hydrothermal

- carbonization on migration and environmental risk of heavy metals in sewage sludge during pyrolysis. *Bioresour. Technol.* 247, 282–290. <https://doi.org/10.1016/j.biortech.2017.09.090>
- Liu, T., Tian, L., Liu, Z., He, J., Fu, H., Huang, Q., Xue, H., Huang, Z., 2021. Distribution and toxicity of polycyclic aromatic hydrocarbons during CaO-assisted hydrothermal carbonization of sewage sludge. *Waste Manag.* 120, 616–625. <https://doi.org/10.1016/j.wasman.2020.10.025>
- Liu, X., Zhai, Y., Li, S., Wang, B., Wang, T., Liu, Y., Qiu, Z., Li, C., 2020. Hydrothermal carbonization of sewage sludge: Effect of feed-water pH on hydrochar's physicochemical properties, organic component and thermal behavior. *J. Hazard. Mater.* 388, 122084. <https://doi.org/10.1016/j.jhazmat.2020.122084>
- Lopes, B.C., Machado, E.C., Rodrigues, H.F., Leal, D., Calábria De Araújo, J., Teixeira De Matos, A., 2020. Environmental Technology Effect of alkaline treatment on pathogens, bacterial community and antibiotic resistance genes in different sewage sludges for potential agriculture use Effect of alkaline treatment on pathogens, bacterial community and antibiotic. *Environ. Technol.* 41, 529–538. <https://doi.org/10.1080/09593330.2018.1505960>
- Lu, J., Zhang, J., Zhu, Z., Zhang, Y., Zhao, Y., Li, R., Watson, J., Li, B., Liu, Z., 2017. Simultaneous production of biocrude oil and recovery of nutrients and metals from human feces via hydrothermal liquefaction. *Energy Convers. Manag.* 134, 340–346. <https://doi.org/10.1016/j.enconman.2016.12.052>
- Lu, X., Ma, X., Chen, X., 2021. Co-hydrothermal carbonization of sewage sludge and lignocellulosic biomass: Fuel properties and heavy metal transformation behaviour of hydrochars. *Energy* 221, 119896. <https://doi.org/10.1016/j.energy.2021.119896>
- Lu, Xiuyang, Fu, J., Xu, X., Lu, Xilei, 2016. Hydrothermal Decomposition of Carbohydrates to Levulinic Acid with Catalysis by Ionic Liquids. *Ind. Eng. Chem. Res.* 55, 11044–11051. <https://doi.org/10.1021/acs.iecr.6b02478>
- Lühmann, T., Wirth, B., 2020. Sewage sludge valorization via hydrothermal carbonization: Optimizing dewaterability and phosphorus release. *Energies* 13, 1–16. <https://doi.org/10.3390/en13174417>
- Lumley, N.P.G., Ramey, D.F., Prieto, A.L., Braun, R.J., Cath, T.Y., Porter, J.M., 2014. Techno-economic analysis of wastewater sludge gasification: A decentralized urban perspective. *Bioresour. Technol.* 161, 385–394. <https://doi.org/10.1016/j.biortech.2014.03.040>
- Luo, X., Huang, Z., Lin, J., Li, X., Qiu, J., Liu, J., Mao, X., 2020. Hydrothermal carbonization of sewage sludge and in-situ preparation of hydrochar/MgAl-layered double hydroxides composites for adsorption of Pb(II). *J. Clean. Prod.* 258, 120991. <https://doi.org/10.1016/j.jclepro.2020.120991>
- Ma, H., Guo, Y., Qin, Y., Li, Y.Y., 2018. Nutrient recovery technologies integrated with energy recovery by waste biomass anaerobic digestion. *Bioresour. Technol.* 269, 520–531. <https://doi.org/10.1016/j.biortech.2018.08.114>
- Ma, J., Chen, M., Yang, T., Liu, Z., Jiao, W., Li, D., Gai, C., 2019a. Gasification performance of the hydrochar derived from co-hydrothermal carbonization of sewage sludge and sawdust. *Energy* 173, 732–739. <https://doi.org/10.1016/j.energy.2019.02.103>
- Ma, J., Luo, H., Li, Y., Liu, Z., Li, D., Gai, C., Jiao, W., 2019b. Pyrolysis kinetics and thermodynamic parameters of the hydrochars derived from co-hydrothermal carbonization of sawdust and sewage sludge using thermogravimetric analysis. *Bioresour. Technol.* 282, 133–141. <https://doi.org/10.1016/j.biortech.2019.03.007>
- Maddi, B., Panisko, E., Wietsma, T., Lemmon, T., Swita, M., Albrecht, K., Howe, D., 2017. Quantitative Characterization of Aqueous Byproducts from Hydrothermal Liquefaction of Municipal Wastes, Food Industry Wastes, and Biomass Grown on Waste. *ACS Sustain. Chem. Eng.* 5, 2205–2214. <https://doi.org/10.1021/acssuschemeng.6b02367>

- Malhotra, M., Garg, A., 2020. Hydrothermal carbonization of centrifuged sewage sludge: Determination of resource recovery from liquid fraction and thermal behaviour of hydrochar. *Waste Manag.* 117, 114–123. <https://doi.org/10.1016/j.wasman.2020.07.026>
- Malins, K., Kampars, V., Brinks, J., Neibolte, I., Murnieks, R., Kampare, R., 2015. Bio-oil from thermochemical hydro-liquefaction of wet sewage sludge. *Bioresour. Technol.* 187, 23–29. <https://doi.org/10.1016/j.biortech.2015.03.093>
- Marin-Batista, J.D., Mohedano, A.F., Rodríguez, J.J., de la Rubia, M.A., 2020. Energy and phosphorous recovery through hydrothermal carbonization of digested sewage sludge. *Waste Manag.* 105, 566–574. <https://doi.org/10.1016/j.wasman.2020.03.004>
- Marrone, P.A., 2016. Genifuel Hydrothermal Processing Bench-Scale Technology Evaluation Project. Alexandria, VA.
- Marrone, P.A., Elliott, D.C., Billing, J.M., Hallen, R.T., Hart, T.R., Kadota, P., Moeller, J.C., Randel, M.A., Schmidt, A.J., 2018. Bench-scale evaluation of hydrothermal processing technology for conversion of wastewater solids to fuels. *Water Environ. Res.* 90, 329–342. <https://doi.org/10.2175/106143017x15131012152861>
- Mathimani, T., Mallick, N., 2019. A review on the hydrothermal processing of microalgal biomass to bio-oil - Knowledge gaps and recent advances. *J. Clean. Prod.* 217, 69–84. <https://doi.org/10.1016/j.jclepro.2019.01.129>
- Medina-Martos, E., Istrate, I.R., Villamil, J.A., Gálvez-Martos, J.L., Dufour, J., Mohedano, Á.F., 2020. Techno-economic and life cycle assessment of an integrated hydrothermal carbonization system for sewage sludge. *J. Clean. Prod.* 277. <https://doi.org/10.1016/j.jclepro.2020.122930>
- Melo, T.M., Bottlinger, M., Schulz, E., Leandro, W.M., Botelho de Oliveira, S., Menezes de Aguiar Filho, A., El-Naggar, A., Bolan, N., Wang, H., Ok, Y.S., Rinklebe, J., 2019. Management of biosolids-derived hydrochar (Sewchar): Effect on plant germination, and farmers' acceptance. *J. Environ. Manage.* 237, 200–214. <https://doi.org/10.1016/j.jenvman.2019.02.042>
- Melo, T.M., Bottlinger, M., Schulz, E., Leandro, W.M., de Aguiar Filho, A.M., Ok, Y.S., Rinklebe, J., 2017. Effect of biosolid hydrochar on toxicity to earthworms and brine shrimp. *Environ. Geochem. Health* 39, 1351–1364. <https://doi.org/10.1007/s10653-017-9995-5>
- Melo, T.M., Bottlinger, M., Schulz, E., Leandro, W.M., Menezes de Aguiar Filho, A., Wang, H., Ok, Y.S., Rinklebe, J., 2018. Plant and soil responses to hydrothermally converted sewage sludge (sewchar). *Chemosphere* 206, 338–348. <https://doi.org/10.1016/j.chemosphere.2018.04.178>
- Meng, X., Huang, Q., Xu, J., Gao, H., Yan, J., 2019. A review of phosphorus recovery from different thermal treatment products of sewage sludge. *Waste Dispos. Sustain. Energy* 1, 99–115. <https://doi.org/10.1007/s42768-019-00007-x>
- Merzari, F., Goldfarb, J., Andreottola, G., Mimmo, T., Volpe, M., Fiori, L., 2020. Hydrothermal carbonization as a strategy for sewage sludge management: Influence of process withdrawal point on hydrochar properties. *Energies* 13, 2890. <https://doi.org/10.3390/en13112890>
- Merzari, F., Langone, M., Andreottola, G., Fiori, L., 2019. Methane production from process water of sewage sludge hydrothermal carbonization. A review. *Valorising sludge through hydrothermal carbonization. Crit. Rev. Environ. Sci. Technol.* 49, 947–988. <https://doi.org/10.1080/10643389.2018.1561104>
- Mishra, S., Mohanty, K., 2020. Co-HTL of domestic sewage sludge and wastewater treatment derived microalgal biomass – An integrated biorefinery approach for sustainable biocrude production. *Energy Convers. Manag.* 204, 112312. <https://doi.org/10.1016/j.enconman.2019.112312>
- Mitroshkov, A. V., Zhong, L., Thomas, L.M.P., 2019. Analysis of Perfluorinated, Pharmaceutical,

Personal Care Compounds and Heavy Metals in Waste Water Sludge using GC-MS/MS and Multicollector ICP-MS. U.S. Department of Energy, Richland, WA (United States).
<https://doi.org/10.2172/1494304>

- Mittapalli, S., Sharma, H.B., Dubey, B.K., 2021. Hydrothermal carbonization of anaerobic granular sludge and co-pelletization of hydrochar with yard waste. *Bioresour. Technol. Reports* 14, 100691. <https://doi.org/10.1016/j.biteb.2021.100691>
- Molton, P.M., Fassbender, A.G., Brown, M., 1986. STORS: the sludge-to-oil reactor system. Cincinnati, OH, USA.
- Moran, S., 2018. Sludge characterization and treatment objectives, in: *An Applied Guide to Water and Effluent Treatment Plant Design*. Elsevier, pp. 255–263. <https://doi.org/10.1016/b978-0-12-811309-7.00021-7>
- Moreno, J., Espada, J.J., 2019. Chapter 10 Environmental and techno-economic assessment of thermochemical treatment systems for sludge, in: *Wastewater Treatment Residues as Resources for Biorefinery Products and Biofuels*. Elsevier, pp. 201–223. <https://doi.org/10.1016/B978-0-12-816204-0.00010-2>
- Mujahid, R., Riaz, A., Insyani, R., Kim, J., 2020. A centrifugation-first approach for recovering high-yield bio-oil with high calorific values in biomass liquefaction: A case study of sewage sludge. *Fuel* 262, 116628. <https://doi.org/10.1016/j.fuel.2019.116628>
- Munir, M.T., Li, B., Boiarkina, I., Baroutian, S., Yu, W., Young, B.R., 2017. Phosphate recovery from hydrothermally treated sewage sludge using struvite precipitation. *Bioresour. Technol.* 239, 171–179. <https://doi.org/10.1016/j.biortech.2017.04.129>
- Nazari, L., Yuan, Z., Ray, M.B., Xu, C. (Charles), 2017. Co-conversion of waste activated sludge and sawdust through hydrothermal liquefaction: Optimization of reaction parameters using response surface methodology. *Appl. Energy* 203, 1–10. <https://doi.org/10.1016/j.apenergy.2017.06.009>
- Oliver-Tomas, B., Hitzl, M., Owsianiak, M., Renz, M., 2019. Evaluation of hydrothermal carbonization in urban mining for the recovery of phosphorus from the organic fraction of municipal solid waste. *Resour. Conserv. Recycl.* 147, 111–118. <https://doi.org/10.1016/j.resconrec.2019.04.023>
- Ovsyannikova, E., Arauzo, P.J., Becker, G., Kruse, A., 2019. Experimental and thermodynamic studies of phosphate behavior during the hydrothermal carbonization of sewage sludge. *Sci. Total Environ.* 692, 147–156. <https://doi.org/10.1016/j.scitotenv.2019.07.217>
- Ovsyannikova, E., Kruse, A., Becker, G.C., 2020. Feedstock-Dependent Phosphate Recovery in a Pilot-Scale Hydrothermal Liquefaction Bio-Crude Production. *Energies* 13, 379. <https://doi.org/10.3390/en13020379>
- Paneque, M., De la Rosa, J.M., Kern, J., Reza, M.T., Knicker, H., 2017. Hydrothermal carbonization and pyrolysis of sewage sludges: What happen to carbon and nitrogen? *J. Anal. Appl. Pyrolysis* 128, 314–323. <https://doi.org/10.1016/j.jaap.2017.09.019>
- Park, M., Kim, N., Lee, S., Yeon, S., Seo, J.H., Park, D., 2019. A study of solubilization of sewage sludge by hydrothermal treatment. *J. Environ. Manage.* 250, 109490. <https://doi.org/10.1016/j.jenvman.2019.109490>
- Parmar, K.R., Ross, A.B., 2019. Integration of hydrothermal carbonisation with anaerobic digestion; Opportunities for valorisation of digestate. *Energies* 12. <https://doi.org/10.3390/en12091586>
- Parshetti, G.K., Liu, Z., Jain, A., Srinivasan, M.P., Balasubramanian, R., 2013. Hydrothermal carbonization of sewage sludge for energy production with coal. *Fuel* 111, 201–210. <https://doi.org/10.1016/j.fuel.2013.04.052>
- Peng, C., Zhai, Y., Zhu, Y., Xu, B., Wang, T., Li, C., Zeng, G., 2016. Production of char from sewage

- sludge employing hydrothermal carbonization: Char properties, combustion behavior and thermal characteristics. *Fuel* 176, 110–118. <https://doi.org/10.1016/j.fuel.2016.02.068>
- Peng, L., Dai, H., Wu, Y., Peng, Y., Lu, X., 2018. A comprehensive review of phosphorus recovery from wastewater by crystallization processes. *Chemosphere* 197, 768–781. <https://doi.org/10.1016/j.chemosphere.2018.01.098>
- Perkins, G., Batalha, N., Kumar, A., Bhaskar, T., Konarova, M., 2019. Recent advances in liquefaction technologies for production of liquid hydrocarbon fuels from biomass and carbonaceous wastes. *Renew. Sustain. Energy Rev.* 115, 109400. <https://doi.org/10.1016/j.rser.2019.109400>
- Posmanik, R., Labatut, R.A., Kim, A.H., Usack, J.G., Tester, J.W., Angenent, L.T., 2017a. Coupling hydrothermal liquefaction and anaerobic digestion for energy valorization from model biomass feedstocks. *Bioresour. Technol.* 233, 134–143. <https://doi.org/10.1016/j.biortech.2017.02.095>
- Posmanik, R., Labatut, R.A., Kim, A.H., Usack, J.G., Tester, J.W., Angenent, L.T., 2017b. Coupling hydrothermal liquefaction and anaerobic digestion for energy valorization from model biomass feedstocks. *Bioresour. Technol.* 233, 134–143. <https://doi.org/10.1016/j.biortech.2017.02.095>
- Prajitno, H., Park, J., Ryu, C., Park, H.Y., Lim, H.S., Kim, J., 2018. Effects of solvent participation and controlled product separation on biomass liquefaction: A case study of sewage sludge. *Appl. Energy* 218, 402–416. <https://doi.org/10.1016/j.apenergy.2018.03.008>
- Prestigiacomio, C., Costa, P., Pinto, F., Schiavo, B., Siragusa, A., Scialdone, O., Galia, A., 2019. Sewage sludge as cheap alternative to microalgae as feedstock of catalytic hydrothermal liquefaction processes. *J. Supercrit. Fluids* 143, 251–258. <https://doi.org/10.1016/j.supflu.2018.08.019>
- Prestigiacomio, C., Laudicina, V.A., Siragusa, A., Scialdone, O., Galia, A., 2020. Hydrothermal liquefaction of waste biomass in stirred reactors: One step forward to the integral valorization of municipal sludge. *Energy* 201, 117606. <https://doi.org/10.1016/j.energy.2020.117606>
- Qian, L., Wang, S., Savage, P.E., 2020. Fast and isothermal hydrothermal liquefaction of sludge at different severities: Reaction products, pathways, and kinetics. *Appl. Energy* 260, 114312. <https://doi.org/10.1016/j.apenergy.2019.114312>
- Qian, L., Wang, S., Savage, P.E., 2017. Hydrothermal liquefaction of sewage sludge under isothermal and fast conditions. *Bioresour. Technol.* 232, 27–34. <https://doi.org/10.1016/j.biortech.2017.02.017>
- Qian, L., Wang, S., Xu, D., Guo, Y., Tang, X., Wang, L., 2015. Treatment of sewage sludge in supercritical water and evaluation of the combined process of supercritical water gasification and oxidation. *Bioresour. Technol.* 176, 218–224. <https://doi.org/10.1016/j.biortech.2014.10.125>
- Raheem, A., Sikarwar, V.S., He, J., Dastyar, W., Dionysiou, D.D., Wang, W., Zhao, M., 2018. Opportunities and challenges in sustainable treatment and resource reuse of sewage sludge: A review. *Chem. Eng. J.* 337, 616–641. <https://doi.org/10.1016/j.cej.2017.12.149>
- Ren, J., Wang, F., Zhai, Y., Zhu, Y., Peng, C., Wang, T., Li, C., Zeng, G., 2017. Effect of sewage sludge hydrochar on soil properties and Cd immobilization in a contaminated soil. *Chemosphere* 189, 627–633. <https://doi.org/10.1016/j.chemosphere.2017.09.102>
- Ruyter, H.P., 1982. Coalification model. *Fuel* 61, 1182–1187. [https://doi.org/10.1016/0016-2361\(82\)90017-5](https://doi.org/10.1016/0016-2361(82)90017-5)
- Saetea, P., Tippayawong, N., 2013. Recovery of Value-Added Products from Hydrothermal Carbonization of Sewage Sludge. *ISRN Chem. Eng.* 2013, 1–6. <https://doi.org/10.1155/2013/268947>
- Sawai, O., Nunoura, T., Yamamoto, K., 2014. Supercritical water gasification of sewage sludge using bench-scale batch reactor: Advantages and drawbacks. *J. Mater. Cycles Waste Manag.* 16, 82–92. <https://doi.org/10.1007/s10163-013-0144-7>

- Seiple, T.E., Coleman, A.M., Skaggs, R.L., 2017. Municipal wastewater sludge as a sustainable bioresource in the United States. *J. Environ. Manage.* 197, 673–680. <https://doi.org/10.1016/j.jenvman.2017.04.032>
- Seiple, T.E., Skaggs, R.L., Fillmore, L., Coleman, A.M., 2020. Municipal wastewater sludge as a renewable, cost-effective feedstock for transportation biofuels using hydrothermal liquefaction. *J. Environ. Manage.* 270, 110852. <https://doi.org/10.1016/j.jenvman.2020.110852>
- Sevilla, M., Fuertes, A.B., 2009. The production of carbon materials by hydrothermal carbonization of cellulose. *Carbon N. Y.* 47, 2281–2289. <https://doi.org/10.1016/j.carbon.2009.04.026>
- Shah, A.A., Toor, S.S., Conti, F., Nielsen, A.H., Rosendahl, L.A., 2020. Hydrothermal liquefaction of high ash containing sewage sludge at sub and supercritical conditions. *Biomass and Bioenergy* 135, 105504. <https://doi.org/10.1016/j.biombioe.2020.105504>
- Shan, Y.Q., Deng, X.Q., Luque, R., Xu, Z.X., Yan, L., Duan, P.G., 2020. Hydrothermal carbonization of activated sewage sludge over ammonia-treated Fenton sludge to produce hydrochar for clean fuel use. *Green Chem.* 22, 5077–5083. <https://doi.org/10.1039/d0gc01701a>
- Shanmugam, S.R., Adhikari, S., Shakya, R., 2017. Nutrient removal and energy production from aqueous phase of bio-oil generated via hydrothermal liquefaction of algae. *Bioresour. Technol.* 230, 43–48. <https://doi.org/10.1016/j.biortech.2017.01.031>
- Shao, J., Yuan, X., Leng, L., Huang, H., Jiang, L., Wang, H., Chen, X., Zeng, G., 2015. The comparison of the migration and transformation behavior of heavy metals during pyrolysis and liquefaction of municipal sewage sludge, paper mill sludge, and slaughterhouse sludge. *Bioresour. Technol.* 198, 16–22. <https://doi.org/10.1016/j.biortech.2015.08.147>
- Shao, S., Liu, H., Tai, X., Zheng, F., Li, J., Li, Y., 2020. Speciation and migration of heavy metals in sediment cores of urban wetland: bioavailability and risks. *Environ. Sci. Pollut. Res.* 27, 23914–23925. <https://doi.org/10.1007/s11356-020-08719-y>
- Shen, Z., Jin, F., Zhang, Y., Wu, B., Kishita, A., Tohji, K., Kishida, H., 2009. Effect of alkaline catalysts on hydrothermal conversion of glycerin into lactic acid. *Ind. Eng. Chem. Res.* 48, 8920–8925. <https://doi.org/10.1021/ie900937d>
- Shi, W., Feng, C., Huang, W., Lei, Z., Zhang, Z., 2014. Study on interaction between phosphorus and cadmium in sewage sludge during hydrothermal treatment by adding hydroxyapatite. *Bioresour. Technol.* 159, 176–181. <https://doi.org/10.1016/j.biortech.2014.02.108>
- Shi, W., Liu, C., Ding, D., Lei, Z., Yang, Y., Feng, C., Zhang, Z., 2013. Immobilization of heavy metals in sewage sludge by using subcritical water technology. *Bioresour. Technol.* 137, 18–24. <https://doi.org/10.1016/j.biortech.2013.03.106>
- Shi, Y., Luo, G., Rao, Y., Chen, H., Zhang, S., 2019. Hydrothermal conversion of dewatered sewage sludge: Focusing on the transformation mechanism and recovery of phosphorus. *Chemosphere* 228, 619–628. <https://doi.org/10.1016/j.chemosphere.2019.04.109>
- Silva, R.D.V.K., Lei, Z., Shimizu, K., Zhang, Z., 2020. Hydrothermal treatment of sewage sludge to produce solid biofuel: Focus on fuel characteristics. *Bioresour. Technol. Reports* 11, 100453. <https://doi.org/10.1016/j.biteb.2020.100453>
- Silva Thomsen, L.B., Carvalho, P.N., dos Passos, J.S., Anastasakis, K., Bester, K., Biller, P., 2020. Hydrothermal liquefaction of sewage sludge; energy considerations and fate of micropollutants during pilot scale processing. *Water Res.* 183, 116101. <https://doi.org/10.1016/j.watres.2020.116101>
- Smith, A.M., Singh, S., Ross, A.B., 2016. Fate of inorganic material during hydrothermal carbonisation of biomass: Influence of feedstock on combustion behaviour of hydrochar. *Fuel* 169, 135–145. <https://doi.org/10.1016/j.fuel.2015.12.006>

- Snowden-Swan, L.J., Zhu, Y., Bearden, M.D., Seiple, T.E., Jones, S.B., Schmidt, A.J., Billing, J.M., Hallen, R.T., Hart, T.R., Liu, J., Albrecht, K.O., Fox, S.P., Maupin, G.D., Elliott, D.C., 2017. Conceptual Biorefinery Design and Research Targeted for 2022: Hydrothermal Liquefaction Processing of Wet Waste to Fuels.
- Snowden-Swan, L.J., Zhu, Y., Jones, S.B., Elliott, D.C., Schmidt, A.J., Hallen, R.T., Billing, J.M., Hart, T.R., Fox, S.P., Maupin, G.D., 2016. Hydrothermal Liquefaction and Upgrading of Municipal Wastewater Treatment Plant Sludge: A Preliminary Techno-Economic Analysis. Richland, WA (United States). <https://doi.org/10.2172/1327165>
- Song, E., Park, S., Kim, H., 2019. Upgrading hydrothermal carbonization (HTC) hydrochar from sewage sludge. *Energies* 12. <https://doi.org/10.3390/en12122383>
- Su, Y., Liu, D., Gong, M., Zhu, W., Yu, Y., Gu, H., 2019. Investigation on the decomposition of chemical compositions during hydrothermal conversion of dewatered sewage sludge. *Int. J. Hydrogen Energy* 44, 26933–26942. <https://doi.org/10.1016/j.ijhydene.2019.08.182>
- Suzuki, A., Nakamura, T., 1989. Effect of Operating Parameters on Thermochemical Liquefaction of Sewage Sludge. *J. Chem. Eng. Japan* 23, 6–11.
- Suzuki, A., Nakamura, T., Yokoyama, S. ya, Ogi, T., Koguchi, K., 1988. Conversion of sewage sludge to heavy oil by direct thermochemical liquefaction. *J. Chem. Eng. Japan* 21, 288–293. <https://doi.org/10.1252/jcej.21.288>
- Syed-Hassan, S.S.A., Wang, Y., Hu, S., Su, S., Xiang, J., 2017. Thermochemical processing of sewage sludge to energy and fuel: Fundamentals, challenges and considerations. *Renew. Sustain. Energy Rev.* 80, 888–913. <https://doi.org/10.1016/j.rser.2017.05.262>
- Taboada-Santos, A., Braz, G.H.R., Fernandez-Gonzalez, N., Carballa, M., Lema, J.M., 2019. Thermal hydrolysis of sewage sludge partially removes organic micropollutants but does not enhance their anaerobic biotransformation. *Sci. Total Environ.* 690, 534–542. <https://doi.org/10.1016/j.scitotenv.2019.06.492>
- Tansel, B., Lunn, G., Monje, O., 2018. Struvite formation and decomposition characteristics for ammonia and phosphorus recovery: A review of magnesium-ammonia-phosphate interactions. *Chemosphere* 194, 504–514. <https://doi.org/10.1016/j.chemosphere.2017.12.004>
- Tasca, A.L., Puccini, M., Gori, R., Corsi, I., Galletti, A.M.R., Vitolo, S., 2019. Hydrothermal carbonization of sewage sludge: A critical analysis of process severity, hydrochar properties and environmental implications. *Waste Manag.* 93, 1–13. <https://doi.org/10.1016/j.wasman.2019.05.027>
- Tasca, A.L., Stefanelli, E., Raspolli Galletti, A.M., Gori, R., Mannarino, G., Vitolo, S., Puccini, M., 2020. Hydrothermal Carbonization of Sewage Sludge: Analysis of Process Severity and Solid Content. *Chem. Eng. Technol.* 43, 2382–2392. <https://doi.org/10.1002/ceat.202000095>
- Titirici, M.M., White, R.J., Falco, C., Sevilla, M., 2012. Black perspectives for a green future: Hydrothermal carbons for environment protection and energy storage. *Energy Environ. Sci.* 5, 6796–6822. <https://doi.org/10.1039/c2ee21166a>
- Tong, S., Zhang, S., Yin, H., Wang, J., Chen, M., 2021. Study on co-hydrothermal treatment combined with pyrolysis of rice straw/sewage sludge: Biochar properties and heavy metals behavior. *J. Anal. Appl. Pyrolysis* 155, 105074. <https://doi.org/10.1016/j.jaap.2021.105074>
- Tu, W., Liu, Y., Xie, Z., Chen, M., Ma, L., Du, G., Zhu, M., 2021. A novel activation-hydrochar via hydrothermal carbonization and KOH activation of sewage sludge and coconut shell for biomass wastes: Preparation, characterization and adsorption properties. *J. Colloid Interface Sci.* 593, 390–407. <https://doi.org/10.1016/j.jcis.2021.02.133>
- Usman, M., Chen, H., Chen, K., Ren, S., Clark, J.H., Fan, J., Luo, G., Zhang, S., 2019a. Characterization

and utilization of aqueous products from hydrothermal conversion of biomass for bio-oil and hydrochar production: A review. *Green Chem.* 21, 1553–1572. <https://doi.org/10.1039/c8gc03957g>

- Usman, M., Hao, S., Chen, H., Ren, S., Tsang, D.C.W., O-Thong, S., Luo, G., Zhang, S., 2019b. Molecular and microbial insights towards understanding the anaerobic digestion of the wastewater from hydrothermal liquefaction of sewage sludge facilitated by granular activated carbon (GAC). *Environ. Int.* 133, 105257. <https://doi.org/10.1016/j.envint.2019.105257>
- Usman, M., Shi, Z., Ren, S., Ngo, H.H., Luo, G., Zhang, S., 2020. Hydrochar promoted anaerobic digestion of hydrothermal liquefaction wastewater: Focusing on the organic degradation and microbial community. *Chem. Eng. J.* 399, 125766. <https://doi.org/10.1016/j.cej.2020.125766>
- Vardon, D.R., Sharma, B.K., Scott, J., Yu, G., Wang, Z., Schideman, L., Zhang, Y., Strathmann, T.J., 2011. Chemical properties of biocrude oil from the hydrothermal liquefaction of *Spirulina* algae, swine manure, and digested anaerobic sludge. *Bioresour. Technol.* 102, 8295–8303. <https://doi.org/10.1016/j.biortech.2011.06.041>
- Villamil, J.A., Mohedano, A.F., Rodriguez, J.J., De la Rubia, M.A., 2019. Anaerobic co-digestion of the aqueous phase from hydrothermally treated waste activated sludge with primary sewage sludge. A kinetic study. *J. Environ. Manage.* 231, 726–733. <https://doi.org/10.1016/j.jenvman.2018.10.031>
- Villamil, J.A., Mohedano, A.F., San Martín, J., Rodriguez, J.J., de la Rubia, M.A., 2020. Anaerobic co-digestion of the process water from waste activated sludge hydrothermally treated with primary sewage sludge. A new approach for sewage sludge management. *Renew. Energy* 146, 435–443. <https://doi.org/10.1016/j.renene.2019.06.138>
- vom Eyser, C., Palmu, K., Schmidt, T.C., Tuerk, J., 2015. Pharmaceutical load in sewage sludge and biochar produced by hydrothermal carbonization. *Sci. Total Environ.* 537, 180–186. <https://doi.org/10.1016/j.scitotenv.2015.08.021>
- Waldmüller, W., Herdzyk, S., Gaderer, M., 2021. Combined filtration and oxalic acid leaching for recovering phosphorus from hydrothermally carbonized sewage sludge. *J. Environ. Chem. Eng.* 9, 104800. <https://doi.org/10.1016/j.jece.2020.104800>
- Wang, C., Zhu, W., Chen, C., Zhang, H., Fan, Y., Mu, B., Zhong, J., 2019. Behavior of Phosphorus in Catalytic Supercritical Water Gasification of Dewatered Sewage Sludge: The Conversion Pathway and Effect of Alkaline Additive. *Energy and Fuels* 33, 1290–1295. <https://doi.org/10.1021/acs.energyfuels.8b04054>
- Wang, C., Zhu, W., Chen, C., Zhang, H., Lin, N., Su, Y., 2018. Influence of reaction conditions on the catalytic activity of a nickel during the supercritical water gasification of dewatered sewage sludge. *J. Supercrit. Fluids* 140, 356–363. <https://doi.org/10.1016/j.supflu.2018.07.018>
- Wang, C., Zhu, W., Fan, X., 2021. Char derived from sewage sludge of hydrothermal carbonization and supercritical water gasification: Comparison of the properties of two chars. *Waste Manag.* 123, 88–96. <https://doi.org/10.1016/j.wasman.2021.01.027>
- Wang, C., Zhu, W., Gong, M., Su, Y., Fan, Y., 2017. Influence of H₂O₂ and Ni catalysts on hydrogen production and PAHs inhibition from the supercritical water gasification of dewatered sewage sludge. *J. Supercrit. Fluids* 130, 183–188. <https://doi.org/10.1016/j.supflu.2017.08.009>
- Wang, C., Zhu, W., Zhang, H., Chen, C., Fan, X., Su, Y., 2019. Char and tar formation during hydrothermal gasification of dewatered sewage sludge in subcritical and supercritical water: Influence of reaction parameters and lumped reaction kinetics. *Waste Manag.* 100, 57–65. <https://doi.org/10.1016/j.wasman.2019.09.011>
- Wang, H., Yang, Z., Li, X., Liu, Y., 2020. Distribution and transformation behaviors of heavy metals and phosphorus during hydrothermal carbonization of sewage sludge. *Environ. Sci. Pollut. Res.* 27, 17109–17122. <https://doi.org/10.1007/s11356-020-08098-4>

- Wang, L., Chang, Y., Li, A., 2019a. Hydrothermal carbonization for energy-efficient processing of sewage sludge: A review. *Renew. Sustain. Energy Rev.* 108, 423–440. <https://doi.org/10.1016/j.rser.2019.04.011>
- Wang, L., Chang, Y., Liu, Q., 2019b. Fate and distribution of nutrients and heavy metals during hydrothermal carbonization of sewage sludge with implication to land application. *J. Clean. Prod.* 225, 972–983. <https://doi.org/10.1016/j.jclepro.2019.03.347>
- Wang, L., Chang, Y., Zhang, X., Yang, F., Li, Y., Yang, X., Dong, S., 2020. Hydrothermal co-carbonization of sewage sludge and high concentration phenolic wastewater for production of solid biofuel with increased calorific value. *J. Clean. Prod.* 255, 120317. <https://doi.org/10.1016/j.jclepro.2020.120317>
- Wang, L., Li, A., Chang, Y., 2017. Relationship between enhanced dewaterability and structural properties of hydrothermal sludge after hydrothermal treatment of excess sludge. *Water Res.* 112, 72–82. <https://doi.org/10.1016/j.watres.2017.01.034>
- Wang, L., Li, A., Chang, Y., 2016. Hydrothermal treatment coupled with mechanical expression at increased temperature for excess sludge dewatering: Heavy metals, volatile organic compounds and combustion characteristics of hydrochar. *Chem. Eng. J.* 297, 1–10. <https://doi.org/10.1016/j.cej.2016.03.131>
- Wang, L., Zhang, L., Li, A., 2014. Hydrothermal treatment coupled with mechanical expression at increased temperature for excess sludge dewatering: Influence of operating conditions and the process energetics. *Water Res.* 65, 85–97. <https://doi.org/10.1016/j.watres.2014.07.020>
- Wang, P., Sakhno, Y., Adhikari, S., Peng, H., Jaisi, D., Soneye, T., Higgins, B., Wang, Q., 2021. Effect of ammonia removal and biochar detoxification on anaerobic digestion of aqueous phase from municipal sludge hydrothermal liquefaction. *Bioresour. Technol.* 326, 124730. <https://doi.org/10.1016/j.biortech.2021.124730>
- Wang, R., Lei, H., Liu, S., Ye, X., Jia, J., Zhao, Z., 2021. The redistribution and migration mechanism of nitrogen in the hydrothermal co-carbonization process of sewage sludge and lignocellulosic wastes. *Sci. Total Environ.* 776, 145922. <https://doi.org/10.1016/j.scitotenv.2021.145922>
- Wang, R., Wang, C., Zhao, Z., Jia, J., Jin, Q., 2019. Energy recovery from high-ash municipal sewage sludge by hydrothermal carbonization: Fuel characteristics of biosolid products. *Energy* 186, 115848. <https://doi.org/10.1016/j.energy.2019.07.178>
- Wang, S., Persson, H., Yang, W., Jönsson, P.G., 2020. Pyrolysis study of hydrothermal carbonization-treated digested sewage sludge using a Py-GC/MS and a bench-scale pyrolyzer. *Fuel* 262, 116335. <https://doi.org/10.1016/j.fuel.2019.116335>
- Wang, T., Zhai, Y., Zhu, Y., Li, C., Zeng, G., 2018. A review of the hydrothermal carbonization of biomass waste for hydrochar formation: Process conditions, fundamentals, and physicochemical properties. *Renew. Sustain. Energy Rev.* 90, 223–247. <https://doi.org/10.1016/j.rser.2018.03.071>
- Wang, T.T., Zhai, Y., Zhu, Y., Peng, C., Wang, T.T., Xu, B., Li, C., Zeng, G., 2017. Feedwater pH affects phosphorus transformation during hydrothermal carbonization of sewage sludge. *Bioresour. Technol.* 245, 182–187. <https://doi.org/10.1016/j.biortech.2017.08.114>
- Wang, W., Ren, X., Yang, K., Hu, Z., Yuan, S., 2017. Inhibition of ammonia on anaerobic digestion of synthetic coal gasification wastewater and recovery using struvite precipitation. *J. Hazard. Mater.* 340, 152–159. <https://doi.org/10.1016/j.jhazmat.2017.07.002>
- Wang, W., Yu, Q., Meng, H., Han, W., Li, J., Zhang, J., 2018. Catalytic liquefaction of municipal sewage sludge over transition metal catalysts in ethanol-water co-solvent. *Bioresour. Technol.* 249, 361–367. <https://doi.org/10.1016/j.biortech.2017.09.205>

- Wang, X., Chi, Q., Liu, X., Wang, Y., 2019. Influence of pyrolysis temperature on characteristics and environmental risk of heavy metals in pyrolyzed biochar made from hydrothermally treated sewage sludge. *Chemosphere* 216, 698–706. <https://doi.org/10.1016/j.chemosphere.2018.10.189>
- Wang, Y., Chen, G., Li, Y., Yan, B., Pan, D., 2013. Experimental study of the bio-oil production from sewage sludge by supercritical conversion process. *Waste Manag.* 33, 2408–2415. <https://doi.org/10.1016/j.wasman.2013.05.021>
- Wang, Z., Lin, W., Song, W., 2012. Liquid product from hydrothermal treatment of cellulose by direct GC/MS analysis. *Appl. Energy* 97, 56–60. <https://doi.org/10.1016/j.apenergy.2011.11.077>
- Wang, Z., Zhai, Y., Wang, T., Peng, C., Li, S., Wang, B., Liu, X., Li, C., 2020. Effect of temperature on the sulfur fate during hydrothermal carbonization of sewage sludge. *Environ. Pollut.* 260, 114067. <https://doi.org/10.1016/j.envpol.2020.114067>
- Watson, J., Wang, T., Si, B., Chen, W.T., Aierzhati, A., Zhang, Y., 2020. Valorization of hydrothermal liquefaction aqueous phase: pathways towards commercial viability. *Prog. Energy Combust. Sci.* 77, 100819. <https://doi.org/10.1016/j.pecs.2019.100819>
- Weijin, G., Zizheng, Z., Yue, L., Qingyu, W., Lina, G., 2019. Hydrogen production and phosphorus recovery via supercritical water gasification of sewage sludge in a batch reactor. *Waste Manag.* 96, 198–205. <https://doi.org/10.1016/j.wasman.2019.07.023>
- Wiedner, K., Rumpel, C., Steiner, C., Pozzi, A., Maas, R., Glaser, B., 2013. Chemical evaluation of chars produced by thermochemical conversion (gasification, pyrolysis and hydrothermal carbonization) of agro-industrial biomass on a commercial scale. *Biomass and Bioenergy* 59, 264–278. <https://doi.org/10.1016/j.biombioe.2013.08.026>
- Wilk, M., 2016. A novel method of sewage sludge pre-treatment-HTC, in: *E3S Web of Conferences*. <https://doi.org/10.1051/e3sconf/20161000103>
- Wilk, M., Magdziarz, A., Jayaraman, K., Szymańska-Chargot, M., Gökalp, I., 2019. Hydrothermal carbonization characteristics of sewage sludge and lignocellulosic biomass. A comparative study. *Biomass and Bioenergy* 120, 166–175. <https://doi.org/10.1016/j.biombioe.2018.11.016>
- Wu, B., Berg, S.M., Remucal, C.K., Strathmann, T.J., 2020. Evolution of N-Containing Compounds during Hydrothermal Liquefaction of Sewage Sludge. *ACS Sustain. Chem. Eng.* 8, 18303–18313. <https://doi.org/10.1021/acssuschemeng.0c07060>
- Wu, S. yong, Liu, F. qi, Huang, S., Wu, Y. qing, Gao, J. sheng, 2017. Direct n-hexane extraction of wet sewage sludge at thermal and pressurized conditions: A preliminary investigation on its process and product characteristics. *Fuel Process. Technol.* 156, 90–97. <https://doi.org/10.1016/j.fuproc.2016.07.020>
- Xia, Y., Yang, T., Zhu, N., Li, D., Chen, Z., Lang, Q., Liu, Z., Jiao, W., 2019. Enhanced adsorption of Pb(II) onto modified hydrochar: Modeling and mechanism analysis. *Bioresour. Technol.* 288, 121593. <https://doi.org/10.1016/j.biortech.2019.121593>
- Xu, C., Lancaster, J., 2008. Conversion of secondary pulp/paper sludge powder to liquid oil products for energy recovery by direct liquefaction in hot-compressed water. *Water Res.* 42, 1571–1582. <https://doi.org/10.1016/j.watres.2007.11.007>
- Xu, D., Lin, G., Liu, L., Wang, Y., Jing, Z., Wang, S., 2018. Comprehensive evaluation on product characteristics of fast hydrothermal liquefaction of sewage sludge at different temperatures. *Energy* 159, 686–695. <https://doi.org/10.1016/j.energy.2018.06.191>
- Xu, D., Wang, Y., Lin, G., Guo, S., Wang, S., Wu, Z., 2019. Co-hydrothermal liquefaction of microalgae and sewage sludge in subcritical water: Ash effects on bio-oil production. *Renew. Energy* 138, 1143–1151. <https://doi.org/10.1016/j.renene.2019.02.020>

- Xu, X., Antal, M.J., 1998. Gasification of Sewage Sludge and Other Biomass for Hydrogen Production in Supercritical Water. *Environ. Prog.* 17, 215–220. <https://doi.org/10.1002/ep.670170411>
- Xu, X., Jiang, E., 2017. Treatment of urban sludge by hydrothermal carbonization. *Bioresour. Technol.* 238, 182–187. <https://doi.org/10.1016/j.biortech.2017.03.174>
- Xu, X., Matsumura, Y., Stenberg, J., Antal, M.J., 1996. Carbon-catalyzed gasification of organic feedstocks in supercritical water. *Ind. Eng. Chem. Res.* 35, 2522–2530. <https://doi.org/10.1021/ie950672b>
- Xu, Y., Yang, F., Zhang, L., Wang, X., Sun, Y., Liu, Q., Qian, G., 2018. Migration and transformation of phosphorus in municipal sludge by the hydrothermal treatment and its directional adjustment. *Waste Manag.* 81, 196–201. <https://doi.org/10.1016/j.wasman.2018.10.011>
- Xu, Z., Zhu, W., Bao, J., Chen, J., 2011. The fate of heavy metal during subcritical and supercritical water gasification of sewage sludge, in: 2011 International Symposium on Water Resource and Environmental Protection. IEEE, pp. 1260–1263. <https://doi.org/10.1109/ISWREP.2011.5893247>
- Xu, Z.R., Zhu, W., Gong, M., Zhang, H.W., 2013. Direct gasification of dewatered sewage sludge in supercritical water. Part 1: Effects of alkali salts. *Int. J. Hydrogen Energy* 38, 3963–3972. <https://doi.org/10.1016/j.ijhydene.2013.01.164>
- Xu, Z.R., Zhu, W., Li, M., 2012. Influence of moisture content on the direct gasification of dewatered sludge via supercritical water. *Int. J. Hydrogen Energy* 37, 6527–6535. <https://doi.org/10.1016/j.ijhydene.2012.01.086>
- Xu, Z.X., Shan, Y.Q., Zhang, Z., Deng, X.Q., Yang, Y., Luque, R., Duan, P.G., 2020a. Hydrothermal carbonization of sewage sludge: Effect of inorganic salts on hydrochar's physicochemical properties. *Green Chem.* 22, 7010–7022. <https://doi.org/10.1039/d0gc02615h>
- Xu, Z.X., Song, H., Li, P.J., He, Z.X., Wang, Q., Wang, K., Duan, P.G., 2020b. Hydrothermal carbonization of sewage sludge: Effect of aqueous phase recycling. *Chem. Eng. J.* 387, 123410. <https://doi.org/10.1016/j.cej.2019.123410>
- Xu, Z.X., Song, H., Zhang, S., Tong, S.Q., He, Z.X., Wang, Q., Li, B., Hu, X., 2019. Co-hydrothermal carbonization of digested sewage sludge and cow dung biogas residue: Investigation of the reaction characteristics. *Energy* 187, 115972. <https://doi.org/10.1016/j.energy.2019.115972>
- Xue, X., Chen, D., Song, X., Dai, X., 2015. Hydrothermal and Pyrolysis Treatment for Sewage Sludge: Choice from Product and from Energy Benefit, in: *Physics Procedia*. Elsevier B.V., pp. 301–304. <https://doi.org/10.1016/j.egypro.2015.02.064>
- Yang, G., Zhang, G., Wang, H., 2015. Current state of sludge production, management, treatment and disposal in China. *Water Res.* 78, 60–73. <https://doi.org/10.1016/j.watres.2015.04.002>
- Yang, T., Liu, X., Li, R., Li, B., Kai, X., 2019. Hydrothermal liquefaction of sewage sludge to produce bio-oil: Effect of co-pretreatment with subcritical water and mixed surfactants. *J. Supercrit. Fluids* 144, 28–38. <https://doi.org/10.1016/j.supflu.2018.10.005>
- Yin, F., Chen, H., Xu, G., Wang, G., Xu, Y., 2015. A detailed kinetic model for the hydrothermal decomposition process of sewage sludge. *Bioresour. Technol.* 198, 351–357. <https://doi.org/10.1016/j.biortech.2015.09.033>
- Yu, J., Guo, M., Xu, X., Guan, B., 2014. The role of temperature and CaCl₂ in activated sludge dewatering under hydrothermal treatment. *Water Res.* 50, 10–17. <https://doi.org/10.1016/j.watres.2013.11.034>
- Yu, J., Nickerson, A., Li, Y., Fang, Y., Strathmann, T.J., 2020. Fate of per- and polyfluoroalkyl substances (PFAS) during hydrothermal liquefaction of municipal wastewater treatment sludge. *Environ. Sci. Water Res. Technol.* 6, 1388–1399. <https://doi.org/10.1039/c9ew01139k>

- Yu, Y., Lei, Z., Yang, Xi, Yang, Xiaojing, Huang, W., Shimizu, K., Zhang, Z., 2018. Hydrothermal carbonization of anaerobic granular sludge: Effect of process temperature on nutrients availability and energy gain from produced hydrochar. *Appl. Energy* 229, 88–95. <https://doi.org/10.1016/j.apenergy.2018.07.088>
- Yu, Y., Yang, X., Lei, Z., Yu, R., Shimizu, K., Chen, N., Feng, C., Zhang, Z., 2019. Effects of three macroelement cations on P mobility and speciation in sewage sludge derived hydrochar by using hydrothermal treatment. *Bioresour. Technol. Reports* 7, 100231. <https://doi.org/10.1016/j.biteb.2019.100231>
- Yuan, S.J., Dai, X.H., 2014. Facile synthesis of sewage sludge-derived mesoporous material as an efficient and stable heterogeneous catalyst for photo-Fenton reaction. *Appl. Catal. B Environ.* 154–155, 252–258. <https://doi.org/10.1016/j.apcatb.2014.02.031>
- Yuan, X., Huang, H., Zeng, G., Li, H., Wang, J., Zhou, C., Zhu, H., Pei, X., Liu, Zhifeng, Liu, Zhantao, 2011. Total concentrations and chemical speciation of heavy metals in liquefaction residues of sewage sludge. *Bioresour. Technol.* 102, 4104–4110. <https://doi.org/10.1016/j.biortech.2010.12.055>
- Yuan, X., Leng, L., Huang, H., Chen, X., Wang, H., Xiao, Z., Zhai, Y., Chen, H., Zeng, G., 2015. Speciation and environmental risk assessment of heavy metal in bio-oil from liquefaction/pyrolysis of sewage sludge. *Chemosphere* 120, 645–652. <https://doi.org/10.1016/j.chemosphere.2014.10.010>
- Yue, Y., Yao, Y., Lin, Q., Li, G., Zhao, X., 2017. The change of heavy metals fractions during hydrochar decomposition in soils amended with different municipal sewage sludge hydrochars. *J. Soils Sediments* 17, 763–770. <https://doi.org/10.1007/s11368-015-1312-2>
- Zahari, S.M.S.N.S., Zulastry, N.A., Azman, H.H., 2020. A Preliminary Study of Catalytic Hydrothermal Conversion of Cellulose to Lactic Acid: Effects of Reaction Temperature and Metal Ion Catalyst, in: *Journal of Physics: Conference Series*. <https://doi.org/10.1088/1742-6596/1551/1/012014>
- Zhai, Y., Chen, H., Xu, B.B., Xiang, B., Chen, Z., Li, C., Zeng, G., 2014a. Influence of sewage sludge-based activated carbon and temperature on the liquefaction of sewage sludge: Yield and composition of bio-oil, immobilization and risk assessment of heavy metals. *Bioresour. Technol.* 159, 72–79. <https://doi.org/10.1016/j.biortech.2014.02.049>
- Zhai, Y., Liu, X., Zhu, Y., Peng, C., Wang, T., Zhu, L., Li, C., Zeng, G., 2016. Hydrothermal carbonization of sewage sludge: The effect of feed-water pH on fate and risk of heavy metals in hydrochars. *Bioresour. Technol.* 218, 183–188. <https://doi.org/10.1016/j.biortech.2016.06.085>
- Zhai, Y., Peng, C., Xu, B., Wang, T., Li, C., Zeng, G., Zhu, Y., 2017. Hydrothermal carbonisation of sewage sludge for char production with different waste biomass: Effects of reaction temperature and energy recycling. *Energy* 127, 167–174. <https://doi.org/10.1016/j.energy.2017.03.116>
- Zhai, Y., Wang, C., Chen, H., Li, C., Zeng, G., Pang, D., Lu, P., 2013. Digested sewage sludge gasification in supercritical water, in: *Waste Management and Research*. pp. 393–400. <https://doi.org/10.1177/0734242X12471097>
- Zhai, Y., Xiang, B., Chen, H., Xu, B., Zhu, L., Li, C., Zeng, G., 2014b. Recovery of phosphorus from sewage sludge in combination with the supercritical water process. *Water Sci. Technol.* 70, 1108–1114. <https://doi.org/10.2166/wst.2014.344>
- Zhang, C., Ma, X., Zheng, C., Huang, T., Lu, X., Tian, Y., 2020. Co-hydrothermal Carbonization of Water Hyacinth and Sewage Sludge: Effects of Aqueous Phase Recirculation on the Characteristics of Hydrochar. *Energy and Fuels* 34, 14147–14158. <https://doi.org/10.1021/acs.energyfuels.0c01991>
- Zhang, H., Hay, A.G., 2020. Magnetic biochar derived from biosolids via hydrothermal carbonization: Enzyme immobilization, immobilized-enzyme kinetics, environmental toxicity. *J. Hazard. Mater.* 384, 121272. <https://doi.org/10.1016/j.jhazmat.2019.121272>

- Zhang, H., Xue, G., Chen, H., Li, X., 2018. Magnetic biochar catalyst derived from biological sludge and ferric sludge using hydrothermal carbonization: Preparation, characterization and its circulation in Fenton process for dyeing wastewater treatment. *Chemosphere* 191, 64–71. <https://doi.org/10.1016/j.chemosphere.2017.10.026>
- Zhang, J. hong, Lin, Q. mei, Zhao, X. rong, 2014. The hydrochar characters of municipal sewage sludge under different hydrothermal temperatures and durations. *J. Integr. Agric.* 13, 471–482. [https://doi.org/10.1016/S2095-3119\(13\)60702-9](https://doi.org/10.1016/S2095-3119(13)60702-9)
- Zhang, L., Xu, C. (Charles), Champagne, P., 2010. Energy recovery from secondary pulp/paper-mill sludge and sewage sludge with supercritical water treatment. *Bioresour. Technol.* 101, 2713–2721. <https://doi.org/10.1016/j.biortech.2009.11.106>
- Zhang, X., Zhang, L., Li, A., 2017. Hydrothermal co-carbonization of sewage sludge and pinewood sawdust for nutrient-rich hydrochar production: Synergistic effects and products characterization. *J. Environ. Manage.* 201, 52–62. <https://doi.org/10.1016/j.jenvman.2017.06.018>
- Zhang, X.P., Zhang, C., Li, X., Yu, S.H., Tan, P., Fang, Q.Y., Chen, G., 2018. A two-step process for sewage sludge treatment: Hydrothermal treatment of sludge and catalytic hydrothermal gasification of its derived liquid. *Fuel Process. Technol.* 180, 67–74. <https://doi.org/10.1016/j.fuproc.2018.08.012>
- Zhao, P., Chen, H., Ge, S., Yoshikawa, K., 2013. Effect of the hydrothermal pretreatment for the reduction of no emission from sewage sludge combustion. *Appl. Energy* 111, 199–205. <https://doi.org/10.1016/j.apenergy.2013.05.029>
- Zhao, P., Shen, Y., Ge, S., Yoshikawa, K., 2014. Energy recycling from sewage sludge by producing solid biofuel with hydrothermal carbonization. *Energy Convers. Manag.* 78, 815–821. <https://doi.org/10.1016/j.enconman.2013.11.026>
- Zhen, G., Lu, X., Kato, H., Zhao, Y., Li, Y.Y., 2017. Overview of pretreatment strategies for enhancing sewage sludge disintegration and subsequent anaerobic digestion: Current advances, full-scale application and future perspectives. *Renew. Sustain. Energy Rev.* 69, 559–577. <https://doi.org/10.1016/j.rser.2016.11.187>
- Zheng, C., Ma, X., Yao, Z., Chen, X., 2019. The properties and combustion behaviors of hydrochars derived from co-hydrothermal carbonization of sewage sludge and food waste. *Bioresour. Technol.* 285, 121347. <https://doi.org/10.1016/j.biortech.2019.121347>
- Zheng, X., Chen, W., Ying, Z., Huang, J., Ji, S., Wang, B., 2019. Thermodynamic investigation on gasification performance of sewage sludge-derived hydrochar: Effect of hydrothermal carbonization. *Int. J. Hydrogen Energy* 44, 10374–10383. <https://doi.org/10.1016/j.ijhydene.2019.02.200>
- Zheng, X., Ye, Y., Jiang, Z., Ying, Z., Ji, S., Chen, W., Wang, B., Dou, B., 2020a. Enhanced transformation of phosphorus (P) in sewage sludge to hydroxyapatite via hydrothermal carbonization and calcium-based additive. *Sci. Total Environ.* 738, 139786. <https://doi.org/10.1016/j.scitotenv.2020.139786>
- Zheng, X., Zheng, X., Jiang, Z., Ying, Z., Ying, Z., Ye, Y., Chen, W., Wang, B., Wang, B., Dou, B., Dou, B., 2020b. Migration and Transformation of Phosphorus during Hydrothermal Carbonization of Sewage Sludge: Focusing on the Role of pH and Calcium Additive and the Transformation Mechanism. *ACS Sustain. Chem. Eng.* 8, 7806–7814. <https://doi.org/10.1021/acssuschemeng.0c00031>
- Zhou, G., Chen, Z., Fang, F., He, Y., Sun, H., Shi, H., 2015. Fenton-like degradation of Methylene Blue using paper mill sludge-derived magnetically separable heterogeneous catalyst: Characterization and mechanism. *J. Environ. Sci. (China)* 35, 20–26. <https://doi.org/10.1016/j.jes.2015.01.026>
- Zhu, W., Xu, Z.R., Li, L., He, C., 2011. The behavior of phosphorus in sub-and super-critical water

gasification of sewage sludge. *Chem. Eng. J.* 171, 190–196.
<https://doi.org/10.1016/j.cej.2011.03.090>

Zhuang, X., Huang, Y., Song, Y., Zhan, H., Yin, X., Wu, C., 2017. The transformation pathways of nitrogen in sewage sludge during hydrothermal treatment. *Bioresour. Technol.* 245, 463–470.
<https://doi.org/10.1016/j.biortech.2017.08.195>

Zhuang, X., Song, Y., Zhan, H., Bi, X.T., Yin, X., Wu, C., 2020a. Pyrolytic conversion of biowaste-derived hydrochar: Decomposition mechanism of specific components. *Fuel* 266.
<https://doi.org/10.1016/j.fuel.2020.117106>

Zhuang, X., Song, Y., Zhan, H., Yin, X., Wu, C., 2020b. Gasification performance of biowaste-derived hydrochar: The properties of products and the conversion processes. *Fuel* 260.
<https://doi.org/10.1016/j.fuel.2019.116320>

Zhuang, X., Song, Y., Zhan, H., Yin, X., Wu, C., 2020c. Influences of microstructural alternations and inorganic catalysis on the thermochemical conversion of biowaste-derived hydrochar. *Fuel Process. Technol.* 199, 106304. <https://doi.org/10.1016/j.fuproc.2019.106304>

Zhuang, X., Zhan, H., Huang, Y., Song, Y., Yin, X., Wu, C., 2018. Conversion of industrial biowastes to clean solid fuels via hydrothermal carbonization (HTC): Upgrading mechanism in relation to coalification process and combustion behavior. *Bioresour. Technol.* 267, 17–29.
<https://doi.org/10.1016/j.biortech.2018.07.002>

Zhuang, X., Zhan, H., Song, Y., Yin, X., Wu, C., 2019. Structure-reactivity relationships of biowaste-derived hydrochar on subsequent pyrolysis and gasification performance. *Energy Convers. Manag.* 199, 112014. <https://doi.org/10.1016/j.enconman.2019.112014>

Table 1 Typical treatment conditions of three types of hydrothermal treatment for municipal sludge and their products^a

HTP type	Temperature range (°C)	Pressure range (MPa)	Retention time (min)	Water state	Featured products and yield (%) ^b	Coproducts and yield (%) ^b
HTC	150–280	0.1–11	30–960	Sub-critical	Hydrochar (4–94)	Aqueous phase (12–63), biocrude (6–38) and gas (mainly CO ₂ , 1–19)
HTL	280–375	8–22	10–180	Sub- / near-critical	Biocrude (8–44)	Aqueous phase (8–62), hydrochar (5–80) and gas (mainly CO ₂ , 1–26)
HTG	> 375	> 22.1	0–60	Super-critical	Syngas (rich in H ₂ or CH ₄ , 7–52)	Aqueous phase (2–58), biocrude (2–46) and hydrochar (8–69)

^aHTP = hydrothermal processing; HTC = hydrothermal carbonization; HTL = hydrothermal liquefaction; HTG = hydrothermal gasification; references (Aida et al., 2016; Aragón-Briceño et al., 2017; Berge et al., 2011; Biller et al., 2018; Chen et al., 2014; Couto et al., 2018; Danso-Boateng et al., 2015; Escala et al., 2013; Fackaew et al., 2018; Fei et al., 2019a, 2019b; Feng et al., 2018; He et al., 2019, 2013; Huang et al., 2013, 2014; Huang et al., 2018; Huang and Tang, 2016; Inoue et al., 1997; Khoshbouy et al., 2019; Lee et al., 2019; Leng et al., 2018, 2015b; Li et al., 2010, 2012; M. Liu et al., 2017; Liu et al., 2018; Liu et al., 2019; Ma et al., 2019a, 2019b; Mishra and Mohanty, 2020; Molton et al., 1986; Nazari et al., 2017; Ovsyannikova et al., 2020; Paneque et al., 2017; Parmar and Ross, 2019; Peng et al., 2016; Qian et al., 2020; Ren et al., 2017; Saetea and Tippayawong, 2013a; Shah et al., 2020; Shao et al., 2015; Shi et al., 2019; Smith et al., 2016; Song et al., 2019; Su et al., 2019; L. Wang et al., 2017; Wang et al., 2016, 2019, 2013; Wang et al., 2020; Xu et al., 2019, 2018; Xu and Jiang, 2017; Yu et al., 2019, 2018; Zhai et al., 2017; Zhang et al., 2010; Zhang et al., 2018; Zhuang et al., 2020b, 2020a, 2018, 2017).

^bYield (%) = (mass of each product/mass of feedstock) × 100, dry basis.

Table 2 Characteristics of various municipal sludge reported in hydrothermal treatment^a

Parameters	Primary sludge	Waste activated sludge	Secondary sludge	Digested sludge	Others (mixed sludge or unspecified)
TS (% , db)	2.4–23.6	2.6–26.5	2.5–27	2.5–30	0.1–33.3
VM (% , db)	37.7–76.6	33.6–79.3	50.2–72.1	25.1–70.0	27.8–89.1
Ash (% , db)	7.5–56.6	13.7–65.9	15.2–63	15.4–65.9	10.9–70.1
FC (% , db)	3.5–10.6	0.4–14.1	6.7–17.4	0.1–16.4	0.7–21.9
Carbohydrate (% , db)	8–15	5–10	31.1–48.2	5.4–54	1.3–62.6
Lipids (% , db)	7–35	5.6–8.3	7.8–8.0	6.3–23.3	1.1–15
Protein (% , db)	20–30	15.2–19.6	37.8–43.2	15–34.1	8–34.4
Lignin (% , db)	26	0.14–4.4	–	1.8–10	11.6–18.0
Humic substances (% , db)	8–14	3.8–23.9	–	11–19	–
C (% , db)	19.4–47.8	7.6–44.4	13.1–45.4	17.1–46.1	11.2–47.0
H (% , db)	3.2–7.0	2.3–6.2	3.5–7.1	2.3–6.6	1.7–6.9
O (% , db)	14.2–37.9	16.7–37.3	13.7–29.6	11.9–38.3	4.2–42.66
N (% , db)	1.9–8.3	0.37–7.9	1.9–9.0	0.3–9.6	0.3–7.8
S (% , db)	0.37–1.68	0.69–2.85	0.2–3.43	0–6.78	0.1–5.62
P (% , db)	0.69–3.5	1.02–4.1	0.28–4.61	0.17–7.9	0.27–7.93
HHV (MJ/kg, db)	7.6–20.9	1.1–18.1	6.4–19.9	6.3–20.0	3.5–22.2
pH	5–7.4	5.8–8.1	5.6–8	6.4–8.5	5.7–7.9
Alkalinity (mg/L as CaCO ₃)	500–1500	580–1100	–	2500–3500	–
<i>Alkali Metals</i>					
K (% , db)	0.02–1.68	0.25–0.96	0.33–1.69	0.18–0.87	0.2–1.7
Na (% , db)	0.03–0.25	0.04–0.37	0.09–0.46	0.05–0.64	0.08–0.63
<i>Alkaline-earth metals</i>					
Ca (% , db)	0.49–4.02	0.33–2.96	0.9–4.12	0.2–14.8	0.33–4.89
Mg (% , db)	0.1–0.56	0.05–1.4	0.29–0.72	0.08–2.1	0.25–1.23
<i>Transition metals</i>					
Fe (% , db)	0.6–3.32	0.19–10.87	0.62–7.33	0.06–9.1	0.3–18
As (ppm, db)	3–19.3	1.6	737.3	5.6–18.2	1.5–47
Cd (ppm, db)	0.8–1.9	0.5–7	0.7–6.8	0.9–48.3	0.66–73
Cr (ppm, db)	1.93–82.3	22–739	16.1–551.9	19–150.7	26–1983.8
Co (ppm, db)	5	11.6	5.1	3.2–5.7	11–2700
Cu (ppm, db)	246–500	117–6329	133.5–590	130–1175	77–3324
Hg (ppm, db)	0.40	0.5–38	–	0.4–22.7	0.5–15.01
Mn (ppm, db)	53.4–150	500–1070	55.8–1336.9	200–811.5	58.7–566
Mo (ppm, db)	–	–	–	2.8–8.2	1.8–3.8
Ni (ppm, db)	0.02–32.11	28–119	7.4–313.9	16–2078	9–2100
Pb (ppm, db)	34–62.9	36–830	14.6–188.3	0–150.7	5–188.3
Zn (ppm, db)	303–1322	325–4306	51–1222	100–1258	392–2424
<i>Other metals</i>					
Al (% , db)	0.22–1.57	0.42–2.4	0.33–6.53	0.3–4.8	0.2–7.55
Se (ppm, db)	–	131	–	–	–

^adb = dry basis; TS = total solids of sludge feedstock; VM = volatile matter; FC = fixed carbon; HHV = higher heating value; references (Acelas et al., 2014; Afif et al., 2011; Ahn et al., 2020; Alatalo et al., 2013; Ali Shah et al., 2021; Amrullah and Matsumura, 2018; Anastasakis et al., 2018; Aragón-Briceño et al., 2017, 2020, 2021b; Becker et al., 2019; Berge et al., 2011; Bhatt et al., 2018; Biller et al., 2018; Breulmann et al., 2017; Brookman et al., 2018; Catallo and Comeaux, 2008; Chang et al., 2021; D. Chen et al., 2020; H. Chen et al., 2014; Chen et al., 2019, 2013b, 2013a; Chu et al., 2020; Conti et al., 2020; Couto et al., 2018;

Danso-Boateng et al., 2015; De la Rubia et al., 2018; Do et al., 2020; Ekpo et al., 2016; El-Deen and Zhang, 2012; Escala et al., 2013; Fakkaew et al., 2018; Fan et al., 2016; Fei et al., 2019b, 2019a; Feng et al., 2018; Ferrentino et al., 2020a; Fiori et al., 2012; Gai et al., 2016b, 2016a; Gao et al., 2019; Gaur et al., 2020; Gong et al., 2014b, 2016a, 2016b, 2018; Guo et al., 2010; He et al., 2013, 2014b, 2015b, 2016, 2019, 2020; Huang et al., 2011, 2013, 2014; R. Huang et al., 2018; Huang and Tang, 2015, 2016; Inoue et al., 1997; Itoh et al., 1994; Kapusta, 2018; Khoshbouy et al., 2019; Kim et al., 2014, 2017; Koottatep et al., 2016; Lai et al., 2018; Lee et al., 2019; Leng et al., 2014, 2015b, 2018; Li et al., 2017, 2010, 2012, 2018; Lishan et al., 2018; M. Liu et al., 2017; R. Liu et al., 2018; T. Liu et al., 2017a, 2017b, 2018b, 2018a; Liu et al., 2019, 2020; Ma et al., 2019a, 2019b; Malhotra and Garg, 2020; Malins et al., 2015; Marin-Batista et al., 2020; Marrone et al., 2018; Melo et al., 2018, 2019; Merzari et al., 2020; Mishra and Mohanty, 2020; Mittapalli et al., 2021; Molton et al., 1986; Mujahid et al., 2020; Munir et al., 2017; Nazari et al., 2017; Ovsyannikova et al., 2019, 2020; Paneque et al., 2017; Park et al., 2019; Parmar and Ross, 2019; Parshetti et al., 2013; Peng et al., 2016; Prajitno et al., 2018; Prestigiacomo et al., 2019, 2020; Qian et al., 2015, 2017, 2020; Ren et al., 2017; Saetea and Tippayawong, 2013; Sawai et al., 2014; Shah et al., 2020; Shan et al., 2020; Shao et al., 2015; Shi et al., 2013, 2014, 2019; Silva et al., 2020; Smith et al., 2016; Song et al., 2019; Su et al., 2019; Suzuki and Nakamura, 1989; Tasca et al., 2020; Tong et al., 2021; Usman et al., 2019b; Vardon et al., 2011; Villamil et al., 2020; vom Eyser et al., 2015; Waldmüller et al., 2021; C. Wang et al., 2017; Wang et al., 2019, 2019; C. Wang et al., 2021; H. Wang et al., 2020; Wang et al., 2016; L. Wang et al., 2017, 2019b, 2020; Wang et al., 2019; S. Wang et al., 2020; T. T. Wang et al., 2017; W. Wang et al., 2018; Wang et al., 2019, 2013; Z. Wang et al., 2020; Weijin et al., 2019; Wiedner et al., 2013; Wilk, 2016; Wilk et al., 2019; Wu et al., 2017; D. Xu et al., 2018, 2019; Xu et al., 1996; Xu and Antal, 1998; Xu and Jiang, 2017; Y. Xu et al., 2018; Xu et al., 2011, 2012, 2013; Z. X. Xu et al., 2019; Xu et al., 2020b; Xue et al., 2015; Yang et al., 2019; Yin et al., 2015; Yu et al., 2014, 2019; Yuan et al., 2011, 2015; Yue et al., 2017; Zhai et al., 2013, 2014a, 2014b, 2016, 2017; Zhang et al., 2010, 2017; X. P. Zhang et al., 2018; Zhao et al., 2013, 2014; C. Zheng et al., 2019; Zhu et al., 2011; Zhuang et al., 2017, 2018, 2019, 2020b, 2020a, 2020c)

Table 3 Summary of studies on co-hydrothermal processing of municipal sludge with other types of biomass^a

Feedstock mixture	MS in feedstock mixture (wt%)	HTP conditions	Reactor	Remarks	Reference
MS + rice straw, peanut shell, orange peel, or fallen leaves	25–75	220 °C, 12 h	100-mL batch	<ul style="list-style-type: none"> Hydrochar derived from MS with 75% of peanut shells showed the highest fuel ratio (0.79), carbon content (50%), and HHV (21.72 MJ/kg); 25% and 50% of peanut shells led to the most favorable aromatization and induced more –C=O and –OH than –COOH in hydrochar due to synergistic decarboxylation. 	(He et al., 2019)
DS + peat	25–75	200–250 °C, 1 h	1-L batch	<ul style="list-style-type: none"> Co-HTC of MS with peat enhanced the dehydration and decarboxylation reactions; Bonds of –C=O and –C=C were formed in hydrochar from co-HTC. 	(Kim et al., 2017)
FS + cassava pulp, leaves, pig manure, or rice husks	25–75	220 °C, 5 h	1-L batch	<ul style="list-style-type: none"> Co-HTC improved HHV of hydrochar compared to HTC of FS only. 	(Koottatep et al., 2016)
PS + <i>Chlorella</i> sp.	90	180–270 °C, 30 min	1-L batch	<ul style="list-style-type: none"> The H/C and O/C ratios of hydrochar from co-HTC decreased with the increasing temperature. 	(Lee et al., 2019)
MS + sawdust	25–75	220 °C, 1 h	Batch	<ul style="list-style-type: none"> Co-HTC showed higher HHV and yield of hydrochar than that from HTC of MS only; Enhanced aromatic degree was observed in hydrochar from co-HTC compared to that from HTC of MS only. 	(Ma et al., 2019a)
MS + sawdust	25–75	220 °C, 1 h	Batch	<ul style="list-style-type: none"> Co-HTC significantly improved the devolatilization performance of hydrochar, compared to HTC of MS only. 	(Ma et al., 2019b)
WAS + phenolic compounds	3.2–33.3 (daf)	140–260 °C, 2–10 h	250-mL batch	<ul style="list-style-type: none"> Phenolic compounds were incorporated in hydrochar from co-HTC; Adding phenolic compounds to MS during HTC increased yield, VM, FC, and HHV of hydrochar but decreased ash content. 	(Wang et al., 2020)
MS + cornstalk	50–80	190–280 °C, 1–8 h	1-L batch	<ul style="list-style-type: none"> Co-HTC showed synergistic effect on yield and energy recovery of hydrochar; Aromatic clusters and melanoidins could polymerize and form N-containing polyaromatic char. 	(R. Wang et al., 2021)

Feedstock mixture	MS in feedstock mixture (wt%)	HTP conditions	Reactor	Remarks	Reference
DS + cow dung biogas residue	25–75	200–280 °C, 1–5 h	50-mL batch	<ul style="list-style-type: none"> • Co-HTC promoted the hydrolysis of protein; • Dehydration was the main reaction during the co-HTC; • High temperature could enhance the degree of coalification of co-HTC. 	(Xu et al., 2019)
MS + sawdust, corncob, cornstalk, or rape straw	50	220–260 °C, 1 h	500-mL batch	<ul style="list-style-type: none"> • Hydrochar derived from MS with sawdust showed the greatest reduction in O/C ratio; • Energy recovery rate of hydrochar from co-HTC of MS with each waste biomass was following corncob > cornstalk > sawdust > rape straw. 	(Zhai et al., 2017)
MS + pinewood sawdust	25–75	220 °C	250-mL batch	<ul style="list-style-type: none"> • The addition of 50% pinewood showed the maximum hydrochar yield, C retention, and organics retaining; • Co-HTC improved nutrients such as N and P in hydrochar; • Co-HTC promoted the development of aromaticity and surface structure. 	(Zhang et al., 2017)
MS + water hyacinth	50	220 °C, 1 h	250-mL batch	<ul style="list-style-type: none"> • Co-HTC of MS with lignocellulosic biomass improved hydrochar yield and quality (higher HHV and power consumption index and lowered ash content); • Co-HTC promoted immobilization of Cd and Pb. 	(Zhang et al., 2020)
MS + food waste	30–70	180 °C, 1 h	Batch	<ul style="list-style-type: none"> • Co-HTC could significantly increase C content and HHV of hydrochar. 	(Zheng et al., 2019)
DS + swine manure	20/50/80	350 °C, 15 min	10-mL batch	<ul style="list-style-type: none"> • Co-HTL enhanced feedstock pumpability, energy recovery (58–68%) of biocrude, and hydrochar yield. 	(Ali Shah et al., 2021)
PS + lignocellulosic biomass	–	340 °C, 20 min	20-mL batch	<ul style="list-style-type: none"> • Energy recovery to bio-crude (75%) from co-HTL was increased compared to HTL of individual feedstock. 	(Biller et al., 2018)
MS + rice straw or wood sawdust	50	220–300 °C, 0–60 min (in ethanol)	300-mL batch	<ul style="list-style-type: none"> • Synergistic effects on biocrude yield and conversion rate were not observed during the co-HTL; • Introducing rice straw or wood sawdust to HTL of MS can decrease N and S contents but cause more phenolic compounds in biocrude; • Adding rice straw or wood 	(Huang et al., 2019)

Feedstock mixture	MS in feedstock mixture (wt%)	HTP conditions	Reactor	Remarks	Reference
MS + rice straw or wood sawdust	25–75	300 °C, 20 min (in ethanol)	500-mL batch	<p>sawdust to HTL did not affect the polarity but reduced the aromaticity of hydrochar.</p> <ul style="list-style-type: none"> • Synergistic effects with higher yield and better fuel properties of biocrude from co-HTL were observed; • No beneficial effects from co-HTL were observed on hydrochar yield. 	(Leng et al., 2018)
PS + <i>Monoraphidium</i> sp. (KMC4)	25–75	275–350 °C, 15–60 min	100-mL batch	<ul style="list-style-type: none"> • A maximum biocrude yield of 39 wt% (energy recovery of 77%) was obtained from co-HTL of PS with 75% KMC4 at 325 °C for 45 min; • Co-HTL dramatically promoted the production of low-boiling fractions in biocrude. 	(Mishra and Mohanty, 2020)
MS + microalgae (<i>Chlorella</i>)	25–75	340 °C, 30 min	4.9-mL batch	<ul style="list-style-type: none"> • Synergistic effects of higher biocrude yield and lower hydrochar yield from co-HTL were observed. 	(Xu et al., 2019)
DS + corn starch	40–50	340 °C, 74–113 min (2 g/min)	Tubular (6.22 mm ID × 1.016 m length)	<ul style="list-style-type: none"> • Results showed that WHSV between 1.5 and 3.1 hr⁻¹ had no noticeable effect on co-HTG; • Co-HTG of MS with corn starch had slightly more H₂ and less CH₄ in gas composition than HTG of corn starch only; • Co-HTG resulted in less TOC yield than HTG of corn starch only. 	(Xu and Antal, 1998)

^aDS = digested sludge; FS = fecal sludge; MS = municipal sludge; PS = primary sludge; WAS = waste activated sludge; daf = dry ash free basis; ID = inner diameter; HHV = higher heating value; HTC = hydrothermal carbonization; HTL = hydrothermal liquefaction; WHSV = weight hourly space velocity; HTG = hydrothermal gasification; TOC = total organic carbon.

Table 4 Summary of recent hydrothermal studies conducted with different municipal sludge and catalysts^a

MS Type	Catalyst	HTP conditions	Reactor	Remarks	Reference
DS	Nitric acid, pH = 4	190 / 220 °C, 2 h	220-mL batch	<ul style="list-style-type: none"> Adding nitric acid to HTC of MS increased N and O content but decreased ash in hydrochar; Addition of nitric acid enhanced ammonium and nitrate in aqueous phase from HTC. 	(Becker et al., 2019)
MS	FeSO ₄ ·7H ₂ O + Ca(ClO) ₂	150–210 °C, 1 h	2-L batch	<ul style="list-style-type: none"> Best sludge dewaterability was obtained at 180 °C, with 0.04 g Ca(ClO)₂ /g dry MS and FeSO₄·7H₂O/Ca(ClO)₂ molar ratio of 1.25; Combined catalyst in HTC helped break floc structure and remove the O-functional groups of extracellular polymeric substances. 	(Chen et al., 2020)
DS	1 wt% magnesium citrate and/or 1 wt% H ₂ SO ₄	260 °C, 1 h	–	<ul style="list-style-type: none"> More abundant carboxyl groups (C–N, C–O, and O=C–O) in hydrochar were produced with combined catalyst than magnesium citrate alone or non-catalyzed HTC. 	(Chu et al., 2020)
MS	2.5 g glucose + 1 g FeSO ₄ ·7H ₂ O	160–200 °C, 24–48 h	50-mL batch	<ul style="list-style-type: none"> Hydrochar nanocomposite was optimized using FeSO₄·7H₂O at 200 °C for 24 h; Optimized hydrochar showed an adsorption capacity of As(V) (2.1 mg/g). 	(El-Deen and Zhang, 2012)
DS	30 g citric acid	205 °C, 7 h	25-L batch	<ul style="list-style-type: none"> Citric acid had a negligible effect on ratios of H/C and O/C in hydrochar compared to non-catalyzed. 	(Escala et al., 2013)
WAS	10 wt% CaO	200 / 260 °C, 0.5 h	2-L batch	<ul style="list-style-type: none"> CaO addition at 260 °C had a lower VM content in hydrochar compared to that from 200 °C; CaO addition significantly promoted the transformation of NAIP to AP forms. 	(Feng et al., 2018)
MS	Na/Ca-acetate	160–250 °C	500-mL batch	<ul style="list-style-type: none"> Na-acetate slightly enhanced polypeptide-N in HTC aqueous by promoting protein hydrolysis; Ca-acetate reduced N content in hydrochar and increased ammonia in HTC aqueous by enhancing protein hydrolysis and deamination. 	(Huang et al., 2020)
FS	Acetic acid, lithium chloride, borax or zeolite	180–250 °C, 0.5–10 h	1-L batch	<ul style="list-style-type: none"> At 220 °C for 5 h, the highest hydrochar yield (77%) was generated with lithium chloride; Maximum hydrochar HHV of 28.5 MJ/kg was obtained with sludge/acetic acid/cassava pulp mixing mass ratio of 1/0.4/1 at 220 °C for 0.5 h. 	(Koottatep et al., 2016)
MS	Ca(OH) ₂ , pH=9–11	160 °C, 1 h	2-L batch	<ul style="list-style-type: none"> Raising initial pH increased ash but reduced VM, C, H, N, and O contents in hydrochar; 	(Li et al., 2017)

MS Type	Catalyst	HTP conditions	Reactor	Remarks	Reference
MS	Acetic acid / KOH, pH=2–12	270 °C, 2 h	500-mL batch	<ul style="list-style-type: none"> • Adding alkali enhanced the dewatering performance of hydrochar; • The increase of COD and NH₄⁺-N in the filtrate with increasing pH indicated promoted degradation of large organic molecules. • Ash content decreased with increasing pH and reached the lowest (66.12%) at pH=11; • pH of hydrochar was around neutral regardless of initial reaction pH; • Acidic environment favored the formation of fatty substance in hydrochar, while alkaline environment favored more N-containing organic compounds and ketone organics; • Hydrochar produced at pH=5 had the best combustion performance. 	(Liu et al., 2020)
WAS	0–12.3 mmol HCl/g dry MS	170 °C, 30 min	250-mL batch	<ul style="list-style-type: none"> • P was noticeably transferred from hydrochar to aqueous phase when the HCl content was above 1.28 mmol/g dry sludge; • HCl addition improved the bioavailability of residual P in the hydrochar. 	(Shi et al., 2019)
DS	Acetic acid / NaOH (pH=3–11)	200–260 °C, 2 h	500-mL batch	<ul style="list-style-type: none"> • Disregarding the initial reaction pH, the pH of hydrochar and liquid phase tended to be neutral; • P content in hydrochar raised with increasing pH; • An acidic environment promoted the transformation of AP to NAIP and OP to IP, while an alkaline condition led to the opposite. 	(Wang et al., 2017)
WAS	FeCl ₃ /Al(OH) ₃	180 °C, 1 h	500-mL batch	<ul style="list-style-type: none"> • Addition of FeCl₃ and Al(OH)₃ promoted the decomposition and hydrolysis of organics; • Adding FeCl₃ or Al(OH)₃ significantly increased the exchangeable fractions of heavy metals (Zn, Pb, Cr, and Cd) in hydrochar. 	(Xu and Jiang, 2017)
WAS	HNO ₃ /NaOH (pH=4–11); 0.1–10 g CaO	260 °C, 4 h	100-mL batch	<ul style="list-style-type: none"> • Total P in hydrochar increased with increasing alkalinity due to the promoted P precipitation; • The addition of CaO caused more metal accumulation in hydrochar and enhanced the transformation of NAIP to AP. 	(Xu et al., 2018)
MS	0.1 wt% NaCl or (NH ₄) ₂ SO ₄	180–260 °C, 1 h	50-mL batch	<ul style="list-style-type: none"> • Both salts can be absorbed on hydrochar surface and catalyze hydrolysis and carbonization; • NaCl could decrease the thermal decomposition temperature of hydrochar. 	(Xu et al., 2020a)
WAS	2–12 wt% CaCl ₂	100–200 °C, 6 h	100-mL batch	<ul style="list-style-type: none"> • Adding CaCl₂ significantly enhanced the dewaterability of hydrochar but the 	(Yu et al., 2014)

MS Type	Catalyst	HTP conditions	Reactor	Remarks	Reference
		h		improvement became neglected at over 180 °C;	
PS	5 or 10 mmol FeCl ₃ , CaCl ₂ or AlCl ₃	200 °C, 1 h	200-mL batch	<ul style="list-style-type: none"> A continuous enhancement of dewaterability was observed till the dose of CaCl₂ reached 6 wt% All added metal cations promoted P immobilization during HTC; Both Al³⁺ and Fe³⁺ addition enhanced the formation of NAIP and decreased AP in hydrochar; Adding Ca²⁺ significantly improved AP content in hydrochar. 	(Yu et al., 2019)
SS	Acetic acid or KOH (pH=2–12)	270 °C, 2 h	500-mL batch	<ul style="list-style-type: none"> Generally, alkaline environment immobilized heavy metals (Pb, Ni, Cd, and Zn) in hydrochar; Cu and Cr were mobilized with increasing feedwater pH (except for pH=12). 	(Zhai et al., 2016)
MS	2–8 wt% CaO	160–280 °C, 2 h	500-mL batch	<ul style="list-style-type: none"> Increased HTC temperature enriched P and formed more AP in hydrochar; Adding 2–4% CaO during HTC significantly improved P-bioavailability in hydrochar. 	(Zheng et al., 2020a)
MS	0.1–1.6 wt% CaCl ₂	280 °C, 2 h	500-mL batch	<ul style="list-style-type: none"> Over 80% P was enriched in hydrochar regardless of initial MS pH (3–11); Adding 0.8–1.6 wt% CaCl₂ favored complete transformation of NAIP into AP (mainly Ca₃(PO₄)₂ and CaHPO₄). 	(Zheng et al., 2020b)
MS	0.5 g NaOH	320 °C	1-L batch	<ul style="list-style-type: none"> Adding NaOH greatly reduced leachable Cu, Cd, and Zn in hydrochar compared to non-catalyzed; Adding NaOH lowered the overall ecological risk index of heavy metals in hydrochar. 	(Huang et al., 2011)
MS	5 wt% NaOH, Na ₂ CO ₃ , Ca(OH) ₂ or FeSO ₄	220 °C, 30 min (in ethanol-water)	300-mL batch	<ul style="list-style-type: none"> The addition of NaOH and Na₂CO₃ improved the biocrude yield from HTP; Adding Na₂CO₃ reduced HHV and energy conversion rate of biocrude. 	(Lai et al., 2018)
SS	Inorganic (HCl, HNO ₃ , and H ₂ SO ₄) and organic (formic, acetic and oxalic) acids for prewash	300 °C, 40 min	1-L batch	<ul style="list-style-type: none"> Compared to no pretreatment, hydrochar yields decreased from MS prewashed by inorganic acids but increased from organic acid prewashing, which was consistent with the change of ash content in feedstock; HCl pre-treatment obtained the highest yield (26.75%), HHV (36 MJ/kg), and energy recovery (45%) of biocrude and promoted the formation of light oil. 	(Liu et al., 2018)
MS	5 wt% Na ₂ CO ₃ , Raney-nickel, FeSO ₄ , or MoS ₂	200–350 °C, 10–100 min	1-L batch	<ul style="list-style-type: none"> Catalysis enhanced the HHV and energy recovery of biocrude compared to without catalyst; Using FeSO₄ as a catalyst achieved the highest yield of biocrude (45.58%), energy recovery (67.63%), and total 	(Malins et al., 2015)

MS Type	Catalyst	HTP conditions	Reactor	Remarks	Reference
				conversion (68.21%).	
MS	10 wt% NiMo-Al ₂ O ₃ , CoMo-Al ₂ O ₃ or activated carbon felt	325 °C, 30 min,	16-mL batch	<ul style="list-style-type: none"> Compared to non-catalyzed HTL, catalysis removed O in biocrude; Biocrude obtained with activated carbon felt had the highest HHV (38.19 MJ/kg); Energy recovery rates were reduced by catalysts due to the decreased biocrude yields. 	(Prestigiacomo et al., 2019)
SS	2% K ₂ CO ₃	350 / 400 °C, 15 min	10-mL batch	<ul style="list-style-type: none"> The addition of K₂CO₃ improved biocrude yield but decreased hydrochar yield under both subcritical and supercritical conditions; The highest energy recovery (74.60%) of biocrude was obtained under 350 °C with catalyst. 	(Shah et al., 2020)
DS, WAS, MPS	0–20% Na ₂ CO ₃	300 °C, 0 min	300-mL batch	<ul style="list-style-type: none"> Adding catalyst had no significant effects on biocrude quality; Without catalyst addition, HTL of MS can achieve satisfactory results. 	(Suzuki et al., 1988)
MPS	5% Na ₂ CO ₃	250–300 °C, 0 / 60 min	300-mL batch	<ul style="list-style-type: none"> Adding catalyst had no significant effects on biocrude yield; Adding Na₂CO₃ significantly increased BOD and COD in aqueous phase at almost all conditions; At severer HTP conditions, the aqueous phase was more biodegradable. 	(Suzuki and Nakamura, 1989)
MPS	0–10 wt% Na ₂ CO ₃	350–450 °C, 0–30 min	2-L batch	<ul style="list-style-type: none"> Catalyst amount had no significant effects on biocrude yield. 	(Wang et al., 2013)
SS	6 g CuSO ₄ , ZnSO ₄ , CoSO ₄ , or FeSO ₄	270 °C, 30 min	600-mL batch	<ul style="list-style-type: none"> Adding CuSO₄ achieved the maximum biocrude yield (47.45%) and conversion rate (97.74%); S and N contents in biocrude obtained with CuSO₄ were reduced by 55.0% and 14.6%, respectively, compared to non-catalysis. 	(Wang et al., 2018)
MS	3.4 g sludge-based activated carbon (SAC)	350 / 400 °C, 30 min	500-mL batch	<ul style="list-style-type: none"> SAC obtained from pyrolysis with longer retention time had a better effect on the increase of HHV and yield of biocrude from HTP; Adding SAC to HTP, the risk of Cu, Zn, and Pb was reduced at 350 °C, whereas the risk of Cd, Cu, and Zn was decreased at 400 °C. 	(Zhai et al., 2014a)
WAS	0–1.8 g Raney nickel / g dry MS	380 °C, 15 min	50-mL batch	<ul style="list-style-type: none"> Carbon gasification ratios increased with increasing catalyst addition and achieved 69% at 1.8 g catalyst/g dry MS; With increased catalyst loading, methane yields linearly increased while hydrogen yield reached a maximum at 1.5 g catalyst/g dry MS. 	(Afif et al., 2011)
MS	0.1–0.9 wt%	540 °C,	Fluidized	<ul style="list-style-type: none"> Among the tested catalysts, K₂CO₃ had a 	(Chen et al.,

MS Type	Catalyst	HTP conditions	Reactor	Remarks	Reference
	KOH, K ₂ CO ₃ , NaOH, or Na ₂ CO ₃	25 g/min	bed (915 mm length × 30 mm ID)	<ul style="list-style-type: none"> better enhancement on gasification efficiency; Catalytic improvement on hydrogen production followed the order: KOH > K₂CO₃ > NaOH > Na₂CO₃. 	2013a)
MS	0–6 wt% formic acid	400 °C, 30 min	Batch	<ul style="list-style-type: none"> Increasing load of formic acid significantly improved hydrogen yield from 0.16 to 10.07 mol/kg organic matter. 	(Fan et al., 2016)
MS	0–5 wt% NaOH/Ni	400 °C, 10 min	100-mL batch	<ul style="list-style-type: none"> The addition of 3.33 wt% Ni and 1.67 wt% NaOH reached the maximum yield of hydrogen (4.8 mol/kg organic matter), which was almost 5 times higher than that from non-catalytic HTG. 	(Gong et al., 2014b)
MS	H ₂ O ₂ (O ₂ /COD = 0–0.5) / 1 wt% activated carbon	360–425 °C, 30–120 min	572-mL batch	<ul style="list-style-type: none"> Adding activated carbon effectively enhanced the H₂ production at low H₂O₂ concentration; More H₂O₂ addition enhanced COD removal in aqueous phase but resulted in increased CO₂ yield and decreased combustible gas products. 	(Guo et al., 2010)
DS	CaO (Ca/C = 0.05–0.2)	380 °C, 20 min	1-L batch	<ul style="list-style-type: none"> Adding CaO to HTG increased ash content and decreased HHV of hydrochar; With Ca/C molar ratio of 2, H₂ yield increased nearly 6 times compared to non-catalyzed HTG. 	(He et al., 2015a)
MS	CaO (Ca/C = 0.05–0.2)	380 °C, 20 min	1-L batch	<ul style="list-style-type: none"> The addition of CaO led to the lowest N/C (0.029) and aromaticity (27.8%) in hydrochar 	(He et al., 2016)
MS	H ₂ O ₂ (O ₂ /COD = 0–4)	400–600 °C, 20 min	–	<ul style="list-style-type: none"> Increasing load of oxidants improved carbon gasification efficiency from 17% to 90%, but dramatically decreased the yield of combustible gases (H₂, CO, and CH₄) from 3.6 mol/kg to 0. 	(Qian et al., 2015)
WAS	10–200% Ni on silica-alumina or 10% K ₂ CO ₃	600 °C, 60 min	3-L batch	<ul style="list-style-type: none"> Ni catalyst could improve gasification; The deposition of salts and char could degrade the catalytic performance. 	(Sawai et al., 2014)
MS	0–8 wt% Na ₂ CO ₃ /K ₂ CO ₃	400 °C, 30 min	100-mL batch	<ul style="list-style-type: none"> With the addition of 2–8 wt% alkaline catalysts, the migration of P from hydrochar to aqueous phase was enhanced from 41.0 to 2214.5 mg/L. 	(Wang et al., 2019)
MS	0–10 wt% Ni/H ₂ O ₂	400 °C, 60 min	100-mL batch	<ul style="list-style-type: none"> The combined catalysts of H₂O₂ and Ni had better enhancement on H₂ production and inhibiting the formation of PAHs than individual catalyst; The growth of Ni/H₂O₂ ratio increased PAHs with 4–6 rings from 13% to 44% in total PAHs. 	(Wang et al., 2017)
MS	5 wt% NaOH, Ni or H ₂ O ₂	400 °C, 30 min	100-mL batch	<ul style="list-style-type: none"> Adding NaOH and H₂O₂ catalysts inhibited the formation of char and tar; Ni catalyst promoted gas production through steam-reforming reactions. 	(Wang et al., 2019)
MS	0–8 wt%	450 °C,	100-mL	<ul style="list-style-type: none"> Adding alkali salts, except for Ca(OH)₂, 	(Xu et al.,

MS Type	Catalyst	HTP conditions	Reactor	Remarks	Reference
	K ₂ CO ₃ , KOH, Ca(OH) ₂ , Na ₂ CO ₃ or NaOH	30 min	batch	enhanced H ₂ yield and suppressed char formation by alkaline catalyzed hydrolysis; <ul style="list-style-type: none"> Alkali salts had no significant effects on organic matter or total phenol contents in aqueous phase. 	2013)
MS	Coconut shell activated carbon	650 °C, WHSV 0.5 h ⁻¹	Tubular (4.75 mm ID×0.41 m length)	<ul style="list-style-type: none"> High gasification efficiency (98%) was observed with the carbon catalyst, but no control comparison. 	(Xu et al., 1996)
DS	2.6 g K ₂ CO ₃	400 °C, 30 min	500-mL batch	<ul style="list-style-type: none"> The addition of K₂CO₃ achieved 4 times higher carbon gasification efficiency (20.02%) compared to non-catalysis; Adding K₂CO₃ greatly increased the yield of CO₂ and CH₄. 	(Zhai et al., 2013)

^aDS = digested sludge; FS = fecal sludge; MS = municipal sludge; MPS = mixed primary and secondary sludge; PS = primary sludge; SS = secondary sludge; WAS = waste activated sludge; HTP = hydrothermal processing; HTC = hydrothermal carbonization; VM = volatile matter; NAIP = non-apatite inorganic phosphorus; AP = apatite phosphorus; HHV = higher heating value; COD = chemical oxygen demand; OP = organic phosphorus; IP = inorganic phosphorus; HTG = hydrothermal gasification; HTL = hydrothermal liquefaction; BOD = biochemical oxygen demand; PAHs = polycyclic aromatic hydrocarbons; WHSV = weight hourly space velocity.

Table 5 Summary of hydrothermal studies using different sludge with organic solvents^a

MS type	Solvent/co-solvent	HTP conditions	Reactor	Remarks	Reference
MS	Ethanol	300/350 °C, 30 min	500-mL batch	<ul style="list-style-type: none">• Heavy metals were effectively immobilized in hydrochar from supercritical ethanol;• Supercritical ethanol process etched the reactor wall.	(Chen et al., 2014)
MS	Ethanol or ethanol-water	300 °C, 10 min	500-mL batch	<ul style="list-style-type: none">• Higher yield of biocrude was obtained from HTL in ethanol-water co-solvent (15.1 wt%) than pure ethanol (10.9 wt%);• HTL with pure ethanol had higher content of esters and abundant dibutyl phthalate (54.77%) in biocrude;• Hexadecanoic acid and ethyl ester (42.88%) are dominant in biocrude produced from HTL with co-solvent.	(Huang et al., 2019)
SS	Methanol, ethanol, and acetone	260–380 °C, 20 min	500-mL batch	<ul style="list-style-type: none">• The highest conversion rates for methanol, ethanol, and acetone treatments were obtained at 320 °C, which were 54.6%, 53.7%, and 51.4%, respectively;• The biocrude yields for ethanol and acetone treatments increased with increasing temperature and achieved 43.82% and 45.65%, respectively, at 380 °C;• The biocrude yield for methanol treatment reached the maximum of 32.78% at 280 °C but reduced with further increased temperature;• Higher HHV values of biocrude were obtained in methanol (37.69 MJ/kg) and ethanol (38.42 MJ/kg) treatments than that from acetone (26.74 MJ/kg) treatment at 360 °C.	(Huang et al., 2014)
MS	Ethanol	350 °C, 20 min	500-mL batch	<ul style="list-style-type: none">• In supercritical ethanol, the yield and HHV of biocrude from MS reached up to 39.5% with an HHV of 36.14 MJ/kg, which were higher than those from rice straw and <i>Spirulina</i> sp.	(Huang et al., 2013)
MS	Ethanol-water (0–100% v/v)	220 °C, 30 min	300-mL batch	<ul style="list-style-type: none">• Synergistic effects were present in ethanol-water co-solvents;• Maximum biocrude yield (36%) was reached at an ethanol-water ratio of 75% (v/v);• Higher energy recovery of biocrude (75.5%) was achieved at an ethanol-water ratio of 50% (v/v) than pure ethanol (62.4%) or water (56.4%);• Pure ethanol led to the lowest yield of biocrude (26%) but the highest yield of hydrochar (66%).	(Lai et al., 2018)
MS	Ethanol	300 °C, 20 min	500-mL batch	<ul style="list-style-type: none">• Synergistic effects of co-processing of MS with other biomass were present in supercritical ethanol.	(Leng et al., 2018)
WAS	Methanol, ethanol, or acetone	280–380 °C, 20 min	500-mL batch	<ul style="list-style-type: none">• O content and O/C ratio in biocrude from acetone treatment were relatively higher than those from methanol and ethanol treatments;• Ketones (6.8–9.9%) and esters (20.5–30.0%) were the main compounds in biocrude from acetone treatment;• Biocrude from methanol and ethanol treatments	(Leng et al., 2015a)

MS type	Solvent/co-solvent	HTP conditions	Reactor	Remarks	Reference
				was mainly composed of esters, with 70.4–74.9% of methyl esters and 60.1–73.5% of ethyl esters, respectively.	
MS	Ethanol or acetone	280–360 °C, 20 min	500-mL batch	<ul style="list-style-type: none"> Higher biocrude yield and hydrochar yield were obtained in acetone than those in ethanol under each treatment temperature. 	(Leng et al., 2014)
SS	Methanol, ethanol, or acetone	260–380 °C, 20 min	500-mL batch	<ul style="list-style-type: none"> Hydrochar yields in acetone (48.65–53.12%) were relatively higher than those in ethanol (46.29–50.41%) and methanol (45.38–51.22%); Hydrochar produced from different solvents showed an adsorption performance on cationic dyes following the order: acetone > ethanol > methanol; Lower temperatures favored the adsorption performance of hydrochar due to abundant surface functional groups, although the surface areas and pore volumes were low. 	(Leng et al., 2015b)
SS	50% v/v methanol-water or n-hexane-water	300–360 °C, 0–60 min	500-mL batch	<ul style="list-style-type: none"> HHV values of biocrude obtained in co-solvents (34.1–36.5 MJ/kg) were much higher than that from pure water (28.5 MJ/kg) due to the significant reduction of O contents; Decreased HHV and increased ash contents of hydrochar were found from HTP with co-solvents compared to pure water; Ester content in biocrude was enhanced in methanol-water treatment due to the esterification; Aliphatic compounds in biocrude increased in n-hexane-water treatment due to the high solubility of n-hexane. 	(Li et al., 2018)
MS	Ethanol-water (0–100% v/v)	260–400 °C, 20 min	1-L batch	<ul style="list-style-type: none"> Increased ethanol-water ratios enhanced the yield but reduced O contents of biocrude; In pure ethanol, biocrude yield increased while hydrochar yield first decreased and then raised with the increase of reaction temperature. 	(Li et al., 2010)
MS	Water, methanol, ethanol, or mixture	300–400 °C, 10–120 min	140-mL batch	<ul style="list-style-type: none"> Alcohol solvents were consumed and reacted with the reaction intermediates during HTL; Three fractions (light, medium, and heavy) of biocrude were extracted from the HTL products, and over 100% energy recovery was achieved; Light biocrude was mainly comprised of methylated short-chain esters when using methanol, while ketones and alcohols were the primary compounds when using ethanol; In terms of gas temperature distribution and radiative heat flu, mixing MS-derived biocrude with heavy fuel oil showed comparable performance to pure heavy fuel oil. 	(Prajitno et al., 2018)
MS	Methanol	300 °C, 30 min	500-mL batch	<ul style="list-style-type: none"> Environmental toxicity/risk of Cu, Cr, and Zn in MS could be reduced through supercritical methanol liquefaction. 	(Shao et al., 2015)
SS	Ethanol-water	210–330 °C, 0–8 h	600-mL batch	<ul style="list-style-type: none"> The maximum biocrude yield (47.45%) and liquefaction conversion (97.74%) were achieved at 270 °C for 30 min, in ethanol-water (50%, v/v) and with CuSO₄ as the catalyst; 	(Wang et al., 2018)

MS type	Solvent/co-solvent	HTP conditions	Reactor	Remarks	Reference
MS	N-hexane-water	150–340 °C, 90 min	1-L batch	<ul style="list-style-type: none"> • Biocrude yield and liquefaction conversion increased with increasing volume ratios of ethanol/water and reached maximum values at 50% v/v. • Direct n-hexane extraction obtained biocrude yields of 22.8–24.2% with a low O content (3.5–6.0%); • Many solvent-soluble organics (asphaltenes and preasphaltenes) were still present in hydrochar from HTP at 260–340 °C. 	(Wu et al., 2017)
WAS	Methanol-water	Pre-treatment with 5–20% surfactant at 160–200 °C + 340 °C for 40 min	500-mL batch	<ul style="list-style-type: none"> • The cetyl trimethyl ammonium bromide pre-treatment significantly enhanced the alcohol content in biocrude; • The fatty alcohol polyoxyethylene ether pre-treatment remarkably increased the portion of hydrocarbons and their derivatives in biocrude; • Pre-treatment with mixed surfactants doubled the yield of biocrude and reduced its acid content by 95%. 	(Yang et al., 2019)
MS	Acetone/ethanol	360 °C, 20 min	500-mL batch	<ul style="list-style-type: none"> • The exchangeable fraction of heavy metals was consistently higher in biocrude from HTL with ethanol and especially for Zn (72.32%), compared to biocrude from HTL with acetone (28.28%). 	(Yuan et al., 2015)
MS	Acetone	320 °C	1-L batch	<ul style="list-style-type: none"> • The mobility and availability of heavy metals are significantly reduced under supercritical acetone conditions. 	(Yuan et al., 2011)

^aMS = municipal sludge; SS = secondary sludge; WAS = waste activated sludge; HTP = hydrothermal processing; HTL = hydrothermal liquefaction; HHV = higher heating value; v/v = volume ratio.

Table 6 Physicochemical properties of municipal sludge-derived hydrochar obtained under various hydrothermal conditions from selected studies^a

MS feed ^b	T	t	Reactor	Yield	pH	C	H	O	N	S	Ash	VM	FC	HHV	Reference																
9.5% WAS	180	60	500-mL batch	68.3	6.2	38.0	4.7	16.0	4.5	0.9	36.0	38.3	22.3	16.5	(Alipour et al., 2021)																
9.5% SS	180	60		62.3	6.4	45.8	4.6	8.8	5.1	1.1	34.5	35.1	27.1	19.9	(Aragón-Briceño et al., 2017)																
4.5% DS	160	30	500-mL batch	68.8	–	35.5	4.2	15.5	5.1	1.1	38.6	49.7	9.2	14.96	(Aragón-Briceño et al., 2020)																
	220	30		73.4	–	33.2	3.9	14.7	2.0	1.1	45.1	43.8	9.1	13.81																	
	250	30		56.8	–	38.0	4.9	14.8	4.2	1.2	36.9	51.1	9.2	16.79																	
2.5–30% DS	250	30	500-mL batch	68–76	–	32.1–	4.2–	8.7–	1.9–	0.8	48.8–	41.1–	5.0–	14.1–	(Aragón-Briceño et al., 2020)																
						34.4	4.4	10.5	2.8	–	52.2	42.8	8.7	15.3																	
2.5% PS	160	30	500-mL batch	–	–	40.3	6.3	22.5	2.1	0.1	–	–	–	18.5	(Aragón-Briceño et al., 2021b)																
	250	30		–	–	37.4	5.3	15.6	1.0	0.1	–	–	–	16.8																	
2.5% SS	160	30	500-mL batch	–	–	33.1	5.3	21.7	3.3	0.7	–	–	–	14.8	(Aragón-Briceño et al., 2021b)																
	250	30		–	–	36.1	4.6	11.6	1.9	0.5	–	–	–	15.9																	
2.5% MPS	160	30	500-mL batch	–	–	37.5	6.0	21.6	2.6	0.5	–	–	–	17.3	(Aragón-Briceño et al., 2021b)																
	250	30		–	–	35.8	5.2	15.2	1.1	0.3	–	–	–	16.2																	
2.5% DS	160	30	500-mL batch	–	–	28.9	4.5	19.8	2.1	0.5	–	–	–	12.4	(Aragón-Briceño et al., 2021b)																
	250	30		–	–	27.3	3.8	11.4	1.1	0.3	–	–	–	11.7																	
3% DS	250	120	160-mL tubular	47.1	–	27.8	3.9	7.8	2.0	0.8	55.8	34.5	6.4	12.4	(Berge et al., 2011)																
20% DS	180	30	1-L batch	78.0	–	42.3	5.3	15.2	4.1	1.1	32.1	54.2	13.7	18.8	(Bhatt et al., 2018)																
	200	15		91.0	–	43.1	5.5	13.8	3.7	1.0	32.8	54.5	12.7	19.4																	
	200	30		63.0	–	42.2	5.3	13.7	4.0	1.1	33.9	53.6	12.6	18.9																	
	200	60		63.0	–	44.0	5.6	12.0	4.2	1.1	33.1	53.4	13.5	20.0																	
4.3% PS	220	30	250-mL batch	63.0	–	43.9	5.4	11.8	3.8	1.1	33.9	52.7	13.4	19.8	(Danson-Boateng et al., 2015)																
	140	240		74.6	–	28.6	4.1	40.8	3.5	–	22.9	76.0	1.1	10.1																	
	160	240		67.1	–	25.0	3.6	34.7	2.4	–	34.4	64.3	1.3	8.6																	
	180	240		61.9	–	23.3	3.2	32.7	1.7	–	39.2	57.4	3.5	7.6																	
20.1–23.9% DS	205	420	25-L batch	60.0	–	41.1	5.8	26.8	2.5	0.4	–	–	–	18.4	(Escalera et al., 2013)																
																20% FS	250	300	1-L batch	70–73	–	38.8	4.1	9.13	1.9	1.2	42.9	39.8	12.6	19.3–	(Fakkaew et al., 2018)
																						–39.7	–4.5	–9.56	–2.0	–	–44.8	–43.7	–14.6	19.9	
																						20%	150	120	Batch	92.8	5.3	12.6	2.4	12.6	
200	120	84.2	–	11.7	2.1	9.6	0.8	–	75.9	20.3	3.8	3.9																			
250	120	82.6	6.3	11.0	1.9	8.7	0.7	–	77.8	17.6	4.5	3.5																			
20% MS	300	120	500-mL batch	79.7	–	11.4	1.9	5.6	0.8	–	80.4	16.0	3.6	3.9	(Fei et al., 2019a)																
	150	120		92.8	–	12.4	2.4	10.8	1.4	–	–	–	–	6.0																	
	200	120		84.2	–	11.5	2.1	7.6	0.8	–	–	–	–	5.6																	
12% DS	250	120	2-L batch	82.6	–	9.9	1.8	7.8	0.6	–	–	–	–	4.8	(Ferreirantino et al., 2020a)																
	190–250	180		62.9–	–	26.9–	4.0–	8.1–	1.8–	–	44.5–	52.4–	–	11.6–																	
10% DS	200–300	30–120	500-mL batch	48.9–72.9	–	38.4–42.4	5.1–5.6	4.4–12	1.9–2.7	–	–	–	–	17.4–19.9	(Gaur et al., 2020a)																

MS feed ^b	T	t	Reactor	Yield	pH	C	H	O	N	S	Ash	VM	FC	HHV	Reference
14.3 % DS	200	240	125-mL batch	53.9	–	33.3	4.4	18.5	2.1	3.8	43.9	50.6	5.5	14.3	(He et al., 2020)
	200	360		58.7	–	33.2	4.3	17.8	2.1	3.8	44.4	50.3	5.4	14.2	(He et al., 2013)
	200	480		59.8	–	32.6	4.2	17.6	2.2	3.8	44.7	48.8	6.6	13.9	
	200	600		60.2	–	32.5	4.1	17.4	2.2	3.8	46.6	45.4	8.0	13.7	
MS	200	720		60.4	–	32.5	4.1	16.9	2.2	3.9	46.7	45.0	8.3	13.8	
	220	720	100-mL batch	67.7	–	16.5	2.4	7.8	1.1	0.4	71.8	23.1	5.1	6.3	(He et al., 2019)
11.1 % SS	170	60	400-mL batch	89.2	–	46.2	6.0	23.6	8.3	–	15.9	71.5	12.6	20.3	(Khosbhoy et al., 2019)
	200	60		35.3	–	49.7	5.6	16.0	6.2	–	22.5	61.6	15.9	21.9	
	230	60		32.7	–	52.0	5.5	12.1	4.8	–	25.7	57.1	17.3	22.7	
	260	60		31.1	–	53.9	5.2	9.7	4.7	–	26.6	18.0	55.4	23.3	
3.8% DS	180	30	1-L batch	93.9	–	28.2	4.2	33.0	5.1	0.2	29.4	62.3	8.4	10.7	(Kim et al., 2014)
	200	30		92.6	–	28.4	4.1	32.8	5.0	0.1	29.6	61.1	9.3	10.7	
	220	30		88.7	–	27.7	3.6	31.1	4.1	0.1	33.3	57.2	9.5	10.0	
	250	30		83.4	–	27.6	2.9	26.7	3.8	0.1	38.9	50.4	10.7	9.5	
	280	30		80.4	–	29.1	2.5	25.5	3.0	0.0	40.0	47.3	12.7	9.5	
PS	180	30	1-L batch	93.1	–	42.4	6.4	26.8	5.5	0.6	18.8	70.5	11.4	19.2	(Lee et al., 2019)
	210	30		85.8	–	45.0	5.9	24.2	5.2	0.5	19.3	68.4	12.3	19.7	
	240	30		67.9	–	43.6	5.0	22.2	5.5	0.4	23.2	63.3	13.5	18.3	
	270	30		40.8	–	39.8	4.5	17.5	4.2	0.4	33.5	52.4	14.1	16.7	
DS	300	60	1-L batch	63.8	–	26.0	3.4	5.7	2.0	0.7	62.1	30.6	7.3	11.3	(Liu et al., 2017)
16.7 % MS	160	600	100-mL batch	70.8	–	29.0	4.7	17.5	2.6	1.1	45.1	49.5	5.5	13.0	(Liu et al., 2019)
	180	600		67.2	–	29.2	4.6	15.1	2.3	1.1	47.7	46.8	5.5	13.2	
	200	600		65.1	–	30.0	4.4	13.2	2.0	1.2	49.2	44.9	5.9	13.4	
	220	600		61.7	–	28.8	4.3	13.4	1.9	1.2	50.5	43.2	6.3	12.7	
	240	600		59.9	–	30.7	4.2	7.7	2.2	1.1	54.2	39.5	6.4	13.9	
8.4% MPS	200	60–480	700-mL batch	47.9–55.2	–	32.5–33	3.7–4.4	14.3–17.4	3.1–4.8	–	40.5–45.4	47.3–46.6	2.9–4.0	13.2–14.0	(Malhotra and Garg, 2020)
16.5 % DS	180–240	60	4-L batch	51.8–74.2	–	30.8–32.6	4.1–4.3	10.0–16.8	4.1–4.2	1.0–1.1	42.9–48.1	44.0–50.9	6.2–7.9	13.2–14.2	(Marin - Batista et al., 2020)
9.1% AGS	250	120	50-mL batch	80.2	–	38.3	4.3	29.6	1.1	0.3	26.7	53.6	19.7	19.0	(Mittapalli et al., 2021)
2.9% MPS	190–250	30–60	50-mL batch	49.4–77.2	5.3–6.1	41.2–46.1	5.0–6.5	21.6–28.5	1.9–2.2	0.3–0.5	24.4–37.2	56.7–71.0	4.3–6.1	17.3–20.5	(Merzari et al., 2020)
2.9% DS				64.6–82.8	6.2–7.3	10.2–19.2	1.4–2.6	7.2–18.9	0.7–1.6	0.1–0.2	57.2–77	21.7–41.1	–	1.8–6.7	
PS	200	30	1-L batch	87.0	6.5	22.4	3.0	10.8	1.6	–	61.1	–	–	8.9	(Panneque et al., 2017)
	200	180		87.0	6.5	21.4	2.7	11.0	1.4	–	62.5	–	–	8.2	
	260	30		82.0	6.4	21.3	2.6	8.2	1.1	–	65.6	–	–	8.3	
	260	180		82.0	6.6	22.1	2.7	7.2	1.2	–	65.7	–	–	8.8	
WAS	260	30		83.0	6.7	23.3	3.0	12.8	2.5	–	57.0	–	–	9.1	
	200	180		79.0	6.2	23.3	2.7	8.9	2.4	–	61.2	–	–	9.1	
	260	30		76.0	6.3	22.5	2.6	6.9	2.0	–	64.5	–	–	8.8	
	260	180		73.0	6.4	22.4	2.5	5.7	1.9	–	66.1	–	–	8.8	
16.7 % DS	150	60	600-mL batch	87.0	–	29.7	3.0	12.2	1.9	0.0	53.1	37.6	9.3	11.5	(Parmar and Ross, 2019)
	200	60		76.0	–	32.2	3.3	13.3	1.6	0.3	49.4	41.7	9.0	12.7	
	250	60		68.0	–	27.8	2.7	9.0	1.4	0.1	59.0	31.7	9.2	10.7	
10% MS	180	30	500-mL batch	66.2	–	21.2	3.5	4.3	1.6	0.7	68.5	22.2	9.3	9.7	(Peng et al., 2016)
	220	30		60.6	–	19.6	3.2	3.3	1.3	0.6	72.0	18.8	9.2	8.8	
	260	30		56.2	–	24.3	3.9	7.3	1.6	0.5	62.5	27.3	10.3	11.1	
	300	30		53.0	–	21.9	3.4	2.1	1.1	0.5	71.0	16.8	12.2	9.9	
	260	60		58.5	–	24.5	3.7	4.5	1.6	0.6	65.2	23.1	11.7	11.11	
	260	90		59.4	–	24.1	3.7	8.0	1.5	0.6	62.0	24.8	13.2	10.7	

MS feed ^b	T	t	Reactor	Yield	pH	C	H	O	N	S	Ash	VM	FC	HHV	Reference	
	260	360		63.3	–	19.9	3.2	5.4	1.2	0.5	69.7	22.6	7.7	8.8		
	260	480		66.2	–	24.1	3.7	10.5	1.5	0.7	59.5	34.3	6.1	10.5		
10% WAS	220	60	500-mL batch	68.0	6.6	–	–	–	–	–	86.0	13.9	0.1	–	(Ren et al., 2017)	
	220	120		67.0	6.7	–	–	–	–	–	86.4	13.6	0.1	–		
	220	180		66.0	6.7	–	–	–	–	–	86.5	13.4	0.1	–		
	250	60		67.7	6.2	–	–	–	–	–	86.2	13.2	0.6	–		
	250	120		66.3	6.6	–	–	–	–	–	86.3	13.1	0.7	–		
	250	180		65.7	6.4	–	–	–	–	–	86.8	13.1	0.1	–		
	280	60		66.8	6.6	–	–	–	–	–	87.4	12.5	0.1	–		
	280	120		65.3	6.7	–	–	–	–	–	87.2	12.1	0.7	–		
	280	180		65.0	6.7	–	–	–	–	–	87.3	12.2	0.5	–		
25% DS	200	120	1-L batch	80.7	–	28.2	3.4	15.6	1.9	0.5	49.7	37.9	12.2	11.2	(Saetea and Tippayawong, 2013)	
	200	240		78.1	–	29.8	3.3	15.5	2.2	0.6	48.7	37.4	13.9	11.7		
	200	360		74.2	–	29.5	3.5	15.3	2.3	0.5	48.4	37.2	14.2	11.8		
9.9% WAS	200–260	60	50-mL batch	63.9–78.5	–	15.5–15.9	3.1–3.5	10.5–14.0	1.4–1.9	0.4–0.5	–	–	–	6.5–6.9	(Shan et al., 2020)	
	18.7%	170	30	250-mL batch	75.2	–	40.0	5.6	17.3	5.0	1.7	30.5	–	–	18.2	(Shi et al., 2019)
	200	30		68.4	–	41.6	5.5	14.9	4.5	1.5	32.0	–	–	18.9		
	230	30		71.0	–	40.6	5.2	11.2	4.2	1.2	37.6	–	–	18.5		
	260	30		59.4	–	41.8	5.2	8.6	4.1	1.3	39.0	–	–	19.1		
	320	30		51.3	–	40.3	4.5	5.0	3.7	1.0	45.6	–	–	17.9		
33.3% MS	100–200	0–60	200-mL batch	73.7–89.0	–	32.4–37.2	4.1–5.0	18.4–31.7	3.2–4.5	1.6–1.8	24.2–38.8	49.4–60.5	9.0–15.3	13.1–16.2	(Silva et al., 2020)	
9.8% SS	200	60	600-mL batch	73.6	–	13.2	1.8	5.2	1.1	0.1	78.7	–	–	4.5	(Smith et al., 2016)	
	250	60		64.5	–	11.6	1.3	4.6	0.9	0.1	81.5	–	–	3.4		
9.8% DS	200	60		63.1	–	14.0	1.4	9.3	0.5	0.1	74.8	–	–	4.0		
	250	60		52.9	–	22.5	1.8	7.1	0.7	0.0	72.2	–	–	7.7		
MS	200	60	3-L batch	65.8	–	45.3	6.1	16.9	4.7	0.6	27.6	59.8	12.5	20.7	(Song et al., 2019)	
5–14.4% WAS	180–230	32–293	300-mL batch	55.3–68.1	–	20.1–24.2	3.3–3.9	8.8–14.7	2.0–3.5	0.5–0.9	55.4–62.3	33.7–40.7	3.2–5.7	8.5–10.4	(Tasca et al., 2020)	
16.7% MS	200	120	Batch	–	–	19	3	7.4	2.1	0.6	68	29.3	2.7	18.7	(Tong et al., 2021)	
15% WAS	208	60	4-L batch	–	–	43.1	5.8	26.5	4.6	0.2	19.7	65.4	14.9	18.7	(Villa mil et al., 2020)	
19.4% DS	230	150	Batch	–	–	27.9	3.8	4.3	2.2	0.9	61	–	–	12.5	(Wald müller et al., 2021)	
14.4% WAS	120	60	280-mL tubular	96.4	–	–	–	–	–	–	31.4	58.9	8.8	–	(Wang et al., 2016)	
	150	60		58.4	–	–	–	–	4.9	–	39.5	52.4	8.2	–		
	180	60		50.4	–	–	–	–	3.4	–	47.3	44.6	8.1	–		
	210	60		46.2	–	–	–	–	2.8	–	51.3	39.7	9.0	–		
14.4% WAS	180	60	280-mL tubular	50.4	–	30.2	4.1	13.0	3.4	–	47.3	44.6	8.1	13.0	(Wang et al., 2017)	
20% MS	170	60	1-L batch	88.4	–	16.4	2.0	21.6	1.3	1.0	57.6	39.1	3.3	4.8	(Wang et al., 2019)	
	200	60		87.1	–	15.8	1.8	19.6	1.2	1.1	60.5	31.0	8.5	4.5		
	230	60		86.7	–	15.5	1.7	19.4	1.0	1.0	61.5	29.5	9.0	4.2		
	260	60		81.7	–	15.7	1.7	16.8	0.9	1.0	63.9	26.9	9.2	4.4		
	290	60		79.7	–	15.3	1.6	16.0	0.8	1.1	65.3	24.7	10.0	4.3		
	320	60		77.2	–	14.4	1.5	15.8	0.6	1.1	66.6	23.6	9.8	3.9		
	350	60		73.4	–	13.2	1.4	15.2	0.5	0.9	68.9	22.7	8.5	3.3		
SS	180	30	500-mL batch	82.4	–	47.0	6.1	5.8	0.9	3.0	40.3	59.3	0.4	22.4	(Wang et al., 2020)	
	200	30		85.1	–	46.4	6.5	8.0	1.0	3.0	38.0	59.7	2.3	22.5		
	220	30		84.8	–	47.7	6.2	4.4	0.9	2.9	40.9	57.3	1.8	22.9		
	240	30		84.9	–	47.5	5.0	6.6	0.7	2.5	40.3	56.8	3.0	21.1		
	260	30		80.8	–	45.4	5.6	7.0	0.8	3.0	41.2	54.8	4.1	21.2		

MS feed ^b	T	t	Reactor	Yield	pH	C	H	O	N	S	Ash	VM	FC	HHV	Reference
6.8% MS	280	30	1-L batch	72.9	–	47.3	5.8	3.1	0.9	3.0	42.9	54.8	2.3	22.4	(H. Wang et al., 2020)
	300	30		69.3	–	44.4	6.1	8.1	0.9	3.5	40.5	55.1	4.4	21.3	
	180–240	60–600		61.8–75.0	–	15.5–19.6	2.8–3.7	13.6–22.0	1.3–2.0	–	52.6–66.7	–	–	5.9–7.8	
20% MS	250	300	100-mL batch	41.3	–	16.8	2.5	9.1	1.9	0.3	69.4	–	–	6.4	(C. Wang et al., 2021)
	450	30		15.4	–	9.6	1.8	3.2	1.2	0.0	84.1	–	–	3.4	
MS	200	240	1-L batch	64.0	–	26.2	3.1	11.1	2.3	1.4	55.8	34.0	9.0	10.6	(Wilk et al., 2019)
3.4% PS	200	60	200-mL batch	73.1	–	45.1	6.7	–	1.3	–	–	–	–	–	(Yu et al., 2019)
10% MS	220	60	500-mL batch	57.7	–	22.3	3.3	11.4	2.2	0.5	60.3	30.3	9.4	9.3	(Zhai et al., 2017)
	240	60		53.0	–	22.7	2.9	6.6	1.7	0.5	65.6	24.7	9.7	9.3	
	260	60		48.2	–	23.2	2.3	2.3	1.2	0.4	70.6	19.4	10.0	9.1	(Zhang et al., 2017)
11.8% MS	220	–	250-mL batch	39.8	–	40.4	4.7	11.9	3.9	–	38.6	47.3	14.1	17.5	
9.1% PS	120	30	300-mL batch	90.3	–	18.5	3.4	13.4	2.6	0.5	61.6	34.7	3.8	7.8	(Zhuan g et al., 2020a)
	180	30		75.3	–	13.9	2.3	12.9	1.9	0.4	68.6	28.0	3.4	4.8	
	240	30		69.7	–	9.7	1.8	10.1	1.2	0.3	77.0	19.5	3.5	2.9	
9.1% MS	300	30	250-mL batch	67.2	–	8.8	1.6	7.8	0.9	0.3	80.6	16.1	3.2	2.5	(Zhuan g et al., 2020b)
	150	30		79.5	–	17.4	2.9	11.6	2.2	–	65.4	31.6	3.1	6.9	
	180	30		75.0	–	15.7	2.3	7.5	1.7	–	72.5	24.7	2.8	5.8	
	210	30		72.0	–	14.7	2.1	3.7	1.3	–	77.9	19.7	2.4	5.5	
9.1% MS	240	30	250-mL batch	68.0	–	13.6	1.9	2.1	1.1	–	81.0	16.8	2.2	5.0	(Zhuan g et al., 2018)
	120	30		88.9	–	18.5	3.4	12.8	2.6	0.5	62.2	34.1	3.5	7.8	
	180	30		77.1	–	13.9	2.3	9.0	1.9	0.4	72.5	24.7	2.8	5.1	
	240	30		70.2	–	9.7	1.8	6.0	1.2	0.3	81.0	16.8	2.2	3.2	
	300	30		66.4	–	8.8	1.6	3.5	0.9	0.3	84.9	14.3	0.8	2.8	
	300	60		65.8	–	7.6	1.5	3.0	0.8	0.3	86.8	12.2	1.0	2.3	
	300	120		65.1	–	7.5	1.4	2.6	0.8	0.2	87.5	11.6	0.9	2.2	
3.6% MS	225	15	150-mL tube bomb reactor	75.0	–	33.0	–	–	1.1	–	–	–	–	–	(Aida et al., 2016)
	225	30		67.0	–	30.8	–	–	–	0.8	–	–	–	–	
	225	45		63.0	–	29.5	–	–	–	0.7	–	–	–	–	
	225	60		63.0	–	29.1	–	–	–	0.7	–	–	–	–	
	250	15		69.0	–	30.8	–	–	–	0.9	–	–	–	–	
	250	30		56.0	–	27.0	–	–	–	0.7	–	–	–	–	
	250	45		50.0	–	24.8	–	–	–	0.8	–	–	–	–	
	250	60		48.0	–	24.0	–	–	–	0.8	–	–	–	–	
	275	15		52.0	–	26.1	–	–	–	0.7	–	–	–	–	
	275	30		38.0	–	20.1	–	–	–	0.9	–	–	–	–	
	275	45		33.0	–	19.3	–	–	–	0.9	–	–	–	–	
	275	60		34.0	–	19.7	–	–	–	1.0	–	–	–	–	
1% MS	220	30		300-mL batch	55.0	6.0	11.6	1.7	6.4	1.7	1.0	77.6	20.7	1.7	
10% MS	240–360	30	250-mL batch	–	–	4.7–8.6	0.3–1.3	6.5–10.2	0.6–0.9	–	80.3–88.2	7.2–16.1	2.6–4.5	–	(Chan g et al., 2021)
2.5% SS	350	15	10-mL batch	28.1	–	13.7	0.7	13.6	1.5	–	70.5	–	–	2.6	(Conti et al., 2020)
	400	15		27.3	–	9.5	0.3	3.7	1.2	–	85.3	–	–	1.5	
17% SS	340	20	500-mL batch	16.7 ^c	–	26.3	2.6	–	1.2	1.1	70.0	24.8	5.1	–	(Li et al., 2018)
11.9% PS	318–353	18	300-mL plug flow	5.0	–	28.4	3.0	16.2	1.8	0.5	64.4	–	–	10.4	(Marro ne, 2016; Marro ne et al., 2018)
9.7% SS	276–358	19		12.0	–	26.9	3.2	20.5	1.5	0.7	64.5	–	–	9.8	
16% DS	332–358	30	300-mL plug flow	16.0	–	20.3	2.5	15.4	1.1	1.7	73.3	–	–	7.1	

MS feed ^b	T	t	Reactor	Yield	pH	C	H	O	N	S	Ash	VM	FC	HHV	Reference
4% PS	350	20	20-L continuous pilot	~10	–	–	–	–	0.9	0.2	79.6	–	–	–	(Ovsyannikova et al., 2020)
10% MS	325	30	16-mL batch	27.0 ^c	–	–	–	–	–	–	–	–	–	–	(Prestigiacomo et al., 2020)
	350	30		16.0 ^c	–	24.2	1.5	8.4	1.2	1.0	63.7	36.0	–	8.1	
	350	30		22.0 ^c	–	27.6	2.6	15.0	1.5	0.8	52.4	48.0	–	10.1	
	400	0		12.0 ^c	–	20.3	1.2	10.3	0.9	1.1	66.2	33.0	–	6.1	
	400	0		18.0 ^c	–	30.1	1.5	17.5	1.7	1.1	48.1	51.0	–	9.6	
27% SS	350	15	10-mL batch	12.5 ^c	–	15.8	0.7	4.3	1.5	–	77.6	–	–	4.3	(Shah et al., 2020)
	400	15		11.5 ^c	–	10.3	0.0	2.0	1.0	–	86.8	–	–	1.6	
24.2% DS	350	15	10-mL batch	9	–	11.7	1.3	9.2	1.4	–	76.3	–	–	3.1	(Ali Shah et al., 2021)
9.1% MS	375	30	1-L batch	65.7	6.7	–	–	–	–	–	–	12.2	–	–	(Li et al., 2012)
	375	60		64.5	6.6	–	–	–	–	–	–	11.8	–	–	
	400	30		68.2	6.9	–	–	–	–	–	–	8.5	–	–	
	400	60		69.4	6.9	–	–	–	–	–	–	8.6	–	–	
2.4% PS	150	30	500-mL batch	72.2	–	14.2	2.4	10.1	2.0	0.5	70.9	25.3	3.8	5.2	(Zhang et al., 2018)
	200	30		63.5	–	11.3	1.9	7.1	1.1	0.4	78.1	18.4	3.4	3.9	
	250	30		60.5	–	9.5	1.6	4.7	0.9	0.4	83.0	14.2	2.8	3.0	
	300	30		54.2	–	7.8	1.4	4.2	0.8	0.4	85.5	12.4	2.2	2.1	
	350	30		54.5	–	6.6	1.2	3.7	0.7	0.3	87.5	10.9	1.6	1.5	

^aT = reaction temperature (°C); t = residence time (min); VM = volatile matter; FC = fixed carbon; HHV = higher heating value (MJ/kg, dry basis); AGS = anaerobic granular sludge; FS = fecal sludge; MPS = mixed primary and secondary sludge; MS = municipal sludge (unspecified in original reference); PS = primary sludge; SS = secondary sludge; WAS = waste activated sludge; units are all %, dry basis, unless otherwise specified.

^bFeedstock with solids content on a dry basis.

^cYield in %, dry ash free basis.

Table 7 Total concentrations of heavy metal (ppm, dry basis) in municipal sludge-derived hydrochar from different countries versus land application criteria in Canada, the European Union (EU), and the United States (US)

Heavy metals	Measured values in:					Limits for land application in:		
	Canada	China	Japan	EU	US	Canada	EU	US
As	<50	10.44–31.53	–	0.9–1.8	–	75	Not limited	75
Cd	<50	1.5–8.7	–	0.2–2.4	–	20	20–40	85
Cr	309–1070	79–1240	–	23.3–303.5	–	1060	Not limited	Not limited
Co	<50	–	–	0.5–13	–	150	Not limited	Not limited
Cu	2130–2340	152–11550	301–879	249–1098	200–330	2200	1000–1750	4300
Hg	–	41–64	–	0.1–33.2	–	15	16–25	57
Mo	<50	–	–	0.8–4	–	20	Not limited	75
Ni	749–8570	41–400	–	12.9–530	–	180	300–400	420
Pb	<50	39–125	8.7–11.3	30–108.3	–	500	750–1200	840
Se	–	–	–	–	–	14	Not limited	100
Zn	2950–3500	400–4848	2113–3801	552–3380	450–720	1850	2500–4000	7500
Reference	(Marrone et al., 2018)	(Fei et al., 2019b; Leng et al., 2015b; Li et al., 2012; Ma et al., 2019a; Ren et al., 2017; Shi et al., 2019; Wang et al., 2016; Yue et al., 2017; Zhang et al., 2018)	(Yu et al., 2018)	(Conti et al., 2020; Escala et al., 2013; Ferrentino et al., 2020a; Merzari et al., 2020; Shah et al., 2020; Tasca et al., 2020)	(Huang et al., 2018)	B.C. Reg. 18/2002 (Class B biosolids)	Directive 86/278/EEC	40 CFR Part 503 (Ceiling limits)

Table 8 Band assignments of FTIR spectra for hydrochar reported in hydrothermal studies (Chen et al., 2013b; Gai et al., 2016a; He et al., 2016; Kim et al., 2017; Leng et al., 2015b; Parshetti et al., 2013; Peng et al., 2016; Zhang et al., 2014; Zhao et al., 2013).

Group	Wavenumber (cm ⁻¹)	Vibration	Functional group or component
Organics	3600–3200	–OH stretching	Hydroxyl or carboxyl group
	3280	–N–H stretching	Amino group compounds
	2930–2920	Asymmetric –C–H stretching	Aliphatic compounds
	2860–2850	Symmetric –C–H stretching	Aliphatic compounds
	2300–2350, 1460–1396	–C–O stretching	Hydroxyl, carboxylates or ether
	2090	–C=N stretching	Isonitrile
		–C≡N stretching	Nitrile
	1728	–C=O stretching	Ester carbonyl groups
	1700, 1632, 1620, 1550, 1531, 1460–1400	–C=C stretching	Aromatic substances
	1681, 1651, 1126	–C–N stretching	Amide
	1660–1645	–C=O stretching	Amide I
		–COO stretching	Carboxylates
	1622	–C=N stretching	Amides
	1600	–C=C stretching	Aromatic substances
		–C=O stretching	Aldehydes, ketones, lactones, carboxylic compounds
	1575–1525	–N–H in-plane bending	Amide II and secondary amines
	1543	–C=O stretching	Carboxylic acids
	1240–1230	–C–N stretching	Amide III
		–C–O–C stretching	Esters
	1120–1050	–C–O stretching	Alcohols or phenolics
	1080	–C–O–C stretching	Aliphatic ethers
	1035–1030	–C–O–C stretching	Aliphatic ethers
		–C–O stretching	Alcohols or phenolics
	1000	–C–O stretching	Alcohols or phenolics
		–C–C stretching	Alkanes
	800–785	Out of plane –N–H wagging	Amides
		–C–H bending	Aromatic substances
776	–C=C– stretching	Alkenes or aromatic substances	
Inorganics	3600–3700	–OH stretching	Minerals
	1443	–C–O stretching	Carbonate
	1404	–N–O stretching	Nitrite
	1400	–N–O stretching	Nitrate
	1110	–S–O stretching	Sulfate
	1030	–Si–O stretching	Clay materials
		–Si–O–Si stretching	Silica
	875	–C–O out of plane bending	Carbonate
	713	–C–O in-plane bending	Carbonate
	560	–M–X stretching	Organic and inorganic halogens compounds (M = metal, X = halogen)

Table 9 Applications of municipal sludge-derived hydrochar in energy production^a

Sludge type	HTP conditions	Application	Remarks	Reference
MS	200 °C, 4–12 h	Combustion	<ul style="list-style-type: none"> Two stages of combustion (150–350 °C and 350–590 °C) were identified for hydrochar (HHV of 14.4–15.1 MJ/kg); The first order was best fitted to combustion reaction; Hydrochar can provide a more stable flame and longer combustion process than MS. 	(He et al., 2013)
WAS	200 °C, 30 min	Combustion	<ul style="list-style-type: none"> With improved devolatilization properties, hydrochar during separated combustion and air-staging combustion had a NO emission reduction of 50.7% and 56.4%, respectively, compared to MS. 	(Zhao et al., 2013)
SS	250 °C, 15 min	Combustion	<ul style="list-style-type: none"> Co-combustion of hydrochar (HHV of 15.82 MJ/kg) with low-rank coal produced less emission gas (CO₂, CO, and CH₄), compared to combustion of low-rank coal only. 	(Parshetti et al., 2013)
MS	180–300 °C, 0.5–8 h	Combustion	<ul style="list-style-type: none"> The first-order reaction was the best fitting model for hydrochar combustion; Hydrochar produced at 260 °C for 1 h showed the optimal fuel properties with an HHV 12.06 MJ/kg and stable combustion. 	(Peng et al., 2016)
SS	200 and 250 °C, 1 h	Combustion	<ul style="list-style-type: none"> Due to the high alkali index (0.88–1.67), MS-derived hydrochar would probably show slagging and fouling during combustion; NO_x formation at 800–1100 °C can be prevented due to the enhanced thermal efficiency by the high deformation (1220–1240 °C) and flow (1440–1470 °C) temperatures of hydrochar ash. 	(Smith et al., 2016)
MS	120–300 °C, 30 min	Combustion	<ul style="list-style-type: none"> In terms of combustion performance, 120–240 °C could be a suitable HTC temperature for upgrading biowastes to fuel. 	(Zhuang et al., 2018)
MS	180, 230 and 280 °C, 1 h	Combustion	<ul style="list-style-type: none"> Co-HTC of MS with food waste produced hydrochar with better combustion performance compared to HTC of MS only under identical conditions: Highest HHV (22.87 MJ/kg), reduced ignition temperature and burnout temperature, and enhanced comprehensive combustion characteristic index. 	(Zheng et al., 2019)
MS	200 °C, 1 h	Combustion	<ul style="list-style-type: none"> Hydrochar needed 50% lower activation energies than MS. 	(Wilk et al., 2019)
MS	160–240 °C, 10 h	Combustion	<ul style="list-style-type: none"> Compared to MS combustion, hydrochar achieved lower activation energy and mitigated slagging and fouling. 	(Liu et al., 2019)
MS	220 °C, 1 h	Combustion	<ul style="list-style-type: none"> Average activation energy for hydrochar was reduced about 50% to 221 kJ/mol compared to MS combustion 	(Ma et al., 2019b)
MS	170–350 °C, 1 h	Combustion	<ul style="list-style-type: none"> Emissions of SO₂ and NO_x from hydrochar combustion reduced with the increase of corresponding HTP reaction temperature; 	(Wang et al., 2019)
PS	180–270 °C, 30 min	Combustion	<ul style="list-style-type: none"> Three stages of combustion were identified: dehydration (<130 °C), devolatilization and combustion (130–480 °C) and char combustion (>480 °C) 	(Lee et al., 2019)
MS	220 °C, 12 h	Combustion	<ul style="list-style-type: none"> By co-HTC of MS with fruit and agricultural wastes, hydrochar reached an HHV of 21.72 MJ/kg and showed balanced activation energies in 	(He et al., 2019)

Sludge type	HTP conditions	Application	Remarks	Reference
MS	270 °C, 2 h (pH=2–12)	Combustion	<ul style="list-style-type: none"> devolatilization/combustion and char combustion stages. Based on the comprehensive combustibility index, hydrochar produced at initial pH=5 showed the best combustion performance. 	(Liu et al., 2020)
MS	200 °C, 30 min	Combustion	<ul style="list-style-type: none"> Hydrochar showed comparable HHV (19.73 MJ/kg) with Indonesian subbituminous coal (23.32 MJ/kg) and wood pellet (19.59 MJ/kg); High NO_x and SO₂ emission of hydrochar combustion can be mitigated by co-combustion with coal and wood pellet; Fly ash from hydrochar combustion was mainly composed of Al (4.7%), Ca (5.0%), Fe (3.4%), P (7.8%), and Si (5.2%). 	(Ahn et al., 2020)
DS	220–380 °C, 20 min	Combustion	<ul style="list-style-type: none"> Hydrochar obtained at 320 °C (called HC-320) had the highest HHV of 20.35 MJ/kg; Blend HC-320 with coals reduced the activation energy; Regarding the combustion performance and burnout efficiency, HC-320 showed positive synergistic effects when co-combustion with moderate-rank coal, but negative synergistic effects with low/high-rank coals. 	(He et al., 2014b)
MS	200 °C, 1 h	Pyrolysis	<ul style="list-style-type: none"> Gas product was mainly composed of CO₂ (41–58 Nm³/ton sample), CO (20–48 Nm³/ton sample), and H₂ (12–39 Nm³/ton sample) from pyrolysis (450–650 °C) of hydrochar. 	(Wang et al., 2020)
MS	180 °C, 1 h	Steam gasification	<ul style="list-style-type: none"> Hydrochar showed higher energy density (1.65–3.73 MJ/MJ) and gasification efficiency (41–91%) through direct steam gasification, compared to SS at identical conditions. 	(Gai et al., 2016b)
MS	220 °C, 1 h	Steam gasification	<ul style="list-style-type: none"> Hydrochar showed a better H₂ yield (30–77 g H₂/kg hydrochar) and gasification efficiency (50–88%) with lower total energy consumption through direct steam gasification, compared to pyrochar at identical conditions. 	(Gai et al., 2016a)
MS	180–240 °C, 15–45 min	Steam gasification	<ul style="list-style-type: none"> Hydrochar produced at 200 °C for 30 min had the optimum carbon conversion rate (93.9%) and cold gas efficiency (64.4%). 	(Zheng et al., 2019)
MS	220 °C, 1 h	Steam gasification	<ul style="list-style-type: none"> Compared MS-derived hydrochar, co-HTC of MS with sawdust enhanced the gasification performance Under optimal conditions, a gasification efficiency of 77.73% and LHV (8.15 MJ/Nm³) of the syngas were reached. 	(Ma et al., 2019a)
MS	150–240 °C, 30 min	Steam gasification	<ul style="list-style-type: none"> Compared to MS gasification, hydrochar produced syngas with better qualities (maximum LHV of 9.6 MJ/Nm³) and significantly increased H₂ contents (maximum of 56%); Only half tar was produced from hydrochar gasification compared to MS; High contents of PAHs (maximum of 61.5%) were found in tar after hydrochar gasification. 	(Zhuang et al., 2020b)
MS	120–300 °C, 30 min	Steam gasification	<ul style="list-style-type: none"> The catalytic effect of specific AAEMs on gasification conversion rate were identified in the order: Na > K > Mg > Ca > Fe; 	(Zhuang et al., 2020c)

Sludge type	HTP conditions	Application	Remarks	Reference
			<ul style="list-style-type: none"> Na and K mainly contributed to CO₂ generation during the gasification of hydrochar. 	

^aDS = digested sludge; MS = municipal sludge; PS = primary sludge; SS = secondary sludge, WAS = waste activated sludge; HHV = higher heating value; HTC = hydrothermal carbonization; LHV = lower heating value; PAHs = polycyclic aromatic hydrocarbons; AAEMs = alkali and alkaline earth metals.

Table 10 Adsorption models used for examining the performance of hydrochar-based adsorbents (Alatalo et al., 2013; Aragón-Briceño et al., 2021a; El-Deen and Zhang, 2012; Khoshbouy et al., 2019; Leng et al., 2015b)

Adsorption model	Equation	Parameters
Langmuir isotherm	$q = q_m \frac{K_L C}{1 + K_L C}$	q : Equilibrium adsorption capacity, mg/g q_m : Maximum adsorption capacity, mg/g C : Equilibrium adsorbate concentration, mg/L K_L : Langmuir affinity constant of binding sites, L/mg
Freundlich isotherm	$q = K_F C^{(1/n_F)}$	K_F : Freundlich constant related to adsorption capacity, mg/g (L/mg) ^{1/n_F} n_F : Freundlich constant related to adsorption intensity
Sips isotherm (Langmuir–Freundlich)	$q = q_m \frac{(K_S C)^{n_S}}{1 + (K_S C)^{n_S}}$	K_S : Sips affinity constant, L/mg n_S : Sips surface heterogeneity
Temkin isotherm	$q = B_T \ln(K_T C)$ $B_T = RT/b$	K_T : Temkin equilibrium binding constant, L/g B_T : Temkin constant R : Universal gas constant, 8.314 J/mol K T : Absolute temperature, K b : Temkin constant related to the heat of adsorption, J/mol
Pseudo-first-order model	$q_t = q (1 - e^{-k_1 t})$	q_t : Adsorption capacity at time t (min), mg/g q : Adsorption capacity at equilibrium, mg/g k_1 : Pseudo-first-order rate constant, min ⁻¹
Pseudo-second-order model	$q_t = \frac{q^2 k_2 t}{1 + q k_2 t}$	k_2 : Pseudo-second-order rate constant, g/(mg min)
Intraparticle-diffusion model	$q_t = k_{ID} t^{0.5} + C$	k_{ID} : Rate constant of intraparticle diffusion, mg/(g min ^{0.5}) C : Thickness of the boundary layer, mg/g

Table 11 Comparison of the physicochemical properties and adsorption performance of hydrochar-based adsorbents^a

MS type	Hydrothermal conditions			Catalyst	Activation	Point of zero charge	S _{BET} (m ² /g)	Pore volume (cm ³ /g)	Pore diameter (nm)	OFG (mmol/g)	Effective adsorbate (pH)	q _m	K _L	K _F	n _F	k ₁	k ₂	Reference
	T (°C)	t (h)	Solvent															
DS	200	24	Water	No	No	3.2	18	0.09	–	–	Pb(II) (5)	11.3–13	0.11	–	–	0.38	0.05	(Alatalo et al., 2013)
WA	120	24	Water	Al/Mg salts	No	–	–	–	–	–	Pb(II) (4.3)	62.4	2.48	33.5	0.19	0.01–0.05	0.02–0.08	(Luo et al., 2020)
MS	200	24	Water	Glucose + FeSO ₄ ·7H ₂ O	Ethanol washing	–	–	–	–	–	As(V) (5)	2.2	0.61	0.68	2.0	0.03	1.6	(El-Deen and Zhang, 2012)
SS	260	1	Water	No	No	–	6	0.015	2.98	2.08	Methylene blue (8.1–8.6)	63.3	0.35	24.1	4.3	0.03	0.01	(Khoshbouy et al., 2019)
					Thermal (900 °C) with CO ₂	–	262	0.195	3.08	1.12		122.4	0.14	9.7	58.3	0.04	0.03	
					Thermochemical (KOH + 700 °C) + chemical (HCl)	–	1614	0.877	2.01	1.6		588.2	1.89	8.7	340.9	0.24	0.02	
DS	190	3	Water	No	No	–	31	–	–	–	Methylene blue (6.2–6.6)	70.5	0.05	5.8	5.8	0.01	0.004	(Ferrentino et al., 2020a)
						–	8.8	–	–	–		54.3	0.38	9.7	2.4	0.005	0.001	
						–	11.9	–	–	–		37.6	0.14	5.8	2.5	0.002	0.0003	
					Chemical (2M KOH for 1h)	–	0.3	–	–	–	–	–	3.6	1.2	–	–0.01		
						–	2.7	–	–	–	–	140.1	0.06	10.7	1.5	0.07	0.02	
						–	13.4	–	–	–	–	–	–	13.9	1.2	0.03	0.003	
MS/ coconut shell (1:1, db)	180	4	Water	No	Chemical (2M KOH for 30 min) + thermal (700 °C for 50 min)	–	874	0.57	2.51	–	Methylene blue (7 at 20–40 °C)	588–652	10.7	559–621	52–102	0.13	0.007	(Tu et al., 2021)
											Congo Red (7 at 30–40 °C)	248–295	0.34	86–136	4.2–3.3	0.19	0.011	
MS	280	0.3	Acetone	No	No	6.9	12	0.058	18.7	3.61	Malachite green (7)	49.3	41	5.37	8.8	–	0.14	(Leng et al., 2015b)
						6.7	17	0.081	18.1	2.71		34.2	48	8.78	5.4	–	0.15	
						7.2	16	0.082	20.1	2.66		27.3	42	4.63	4.6	–	0.21	
MS	220	1	Water	No	Chemical (ZnCl ₂) + thermal (650 °C) + chemical (HCl)	4.3	417	0.38	3.7	0.56	Acid orange 7 (6.2–6.6)	–	–	–	–	–	–	(Liu et al., 2017b)
					Chemical (ZnCl ₂) + thermal (650 °C) + chemical (HCl) + HF	6.4	519	0.59	4.8	0.49		440.5	1.5	240	7.7	0.15	0.01	

^aDS = digested sludge; WAS = waste activated sludge; MS = municipal sludge; SS = secondary sludge; T = hydrothermal temperature; t = residence time; S_{BET} = Brunauer-Emmett-Teller (BET) surface area; OFG = oxygen-containing functional groups; q_m = maximum adsorption capacity (mg/g); K_L = Langmuir affinity constant of binding sites, L/mg; K_F = Freundlich constant related to adsorption capacity, mg/g (L/mg)^{1/n_F}; n_F = Freundlich constant related to adsorption intensity; k_1 = pseudo-first-order rate constant (min⁻¹); k_2 = pseudo-second-order rate constant, g/(mg min).

Table 12 Comparisons of various nutrient recovery methods for municipal sludge-derived hydrochar^a

MS type	HTP condition	P content in hydrochar	Recovery category	Recovery procedures	Recovered nutrient	Total recovery rate (MS based)	Reference
MS	400–600 °C, 15–60 min	–	Wet-chemical	Acidic leaching: Hydrochar + oxalic or sulfuric acid, pH=2.	P-rich leachate	P: 80–95%	(Acelas et al., 2014)
DS	190 °C, 2 h, pH=4 190 °C, 2 h, pH=8.5 220 °C, 2 h, pH=4 220 °C, 2 h, pH=8.5	4.2% 4.2% 4.2% 4.5%	Wet-chemical	i. Acidic leaching: Hydrochar + citric acid, pH=2; ii. Precipitation: Hydrochar leachate + N-rich HTC aqueous + Mg ²⁺ (Mg:N:P = 1.3:1:1), pH=9.	Struvite (N, P)	– P: 82.5% – –	(Becker et al., 2019)
MPS	180 °C, 1 h	–	Wet-chemical	i. Acidic leaching: Mixed sample (slurry) + concentrated HCl; ii. Precipitation: Acidified liquid + Mg ²⁺ , pH=9.	Struvite (N, P)	Struvite: 9.5 kg/100 m ³ sludge	(Munir et al., 2017)
PS	350 °C, 60 L/h	9.9%	Wet-chemical	i. Acidic leaching: Hydrochar + H ₂ SO ₄ , pH=2; ii. Precipitation: Hydrochar leachate + N-rich HTL aqueous + Mg ²⁺ (Mg:N:P = 2.6:1.1:1), pH=9.	Struvite (N, P)	N: 6.8%, 4.6 g/h; P: 23.7%, 11.6 g/h; K: 2%, 0.1 g/h	(Ovsyannikov et al., 2020)
MS	170 °C, 30 min, HCl addition	–	Wet-chemical	i. HTC coupled acidification: 6.13–12.3 mmol/g of HCl + MS; ii. Precipitation: HTC aqueous + NH ₄ ⁺ + Mg ²⁺ , pH=7.5.	Struvite (N, P)	P: 98%	(Shiet al., 2019)
MS	350 °C, 22 MPa, 30 min 400 °C, 31 MPa, 30 min	2.68% 2.79%	Wet-chemical	i. Acidic leaching: Hydrochar + HCl (1 M); ii. P adsorption: Hydrochar leachate + HTL aqueous + activated alumina (Al ₂ O ₃); iii. P release: (ii) solid residue + NaOH solution (0.1 M); v. Precipitation: (iii) extract + Ca(OH) ₂ , pH=9.	Calcium phosphate	– P: > 85%	(Zhai et al., 2014b)
SS	200 °C, 4 h 200 °C, 4 h, FeCl ₃ addition	– –	Wet-chemical	i. Alkaline leaching: Hydrochar + KOH (pH = 12); ii. Chelating interfering metals: Hydrochar leachate + 20.8 mM EDTA; iii. Precipitation: (ii) solution + MgCl ₂ (Mg/P = 2.5), pH = 11.	K-struvite (K, P)	P: > 92%	(Liet al., 2020)
SS	Control (no HTC) 200 °C, 30 min	– 1.4%	Thermo-chemical	i. Steam gasification: hydrochar + 900 °C; ii. Gasified ash collection.	P-rich ash	P: 55% P: 22%	(Feng et al., 2018)

MS type	HTP condition	P content in hydrochar	Recovery category	Recovery procedures	Recovered nutrient	Total recovery rate (MS based)	Reference
	220 °C, 30 min	1.6%				P: 56%)
	240 °C, 30 min	1.6%				P: 55%	
	260 °C, 30 min	1.6%				P: 35%	
MPS	225–275 °C, 15–60 min	–	Integrated biological	i. Acidic saccharification: hydrochar + sulfuric acid; ii. Algae cultivation: saccharified liquid (neutralized) + HTC aqueous + algae.	Recycled N, P (microalgae)	–	(Aida et al., 2016)

^aDS = digested sludge; MPS = mixed primary and secondary sludge; MS = municipal sludge; PS = primary sludge; SS = secondary sludge; HTP = hydrothermal processing; HTC = hydrothermal carbonization; HTL = hydrothermal liquefaction.

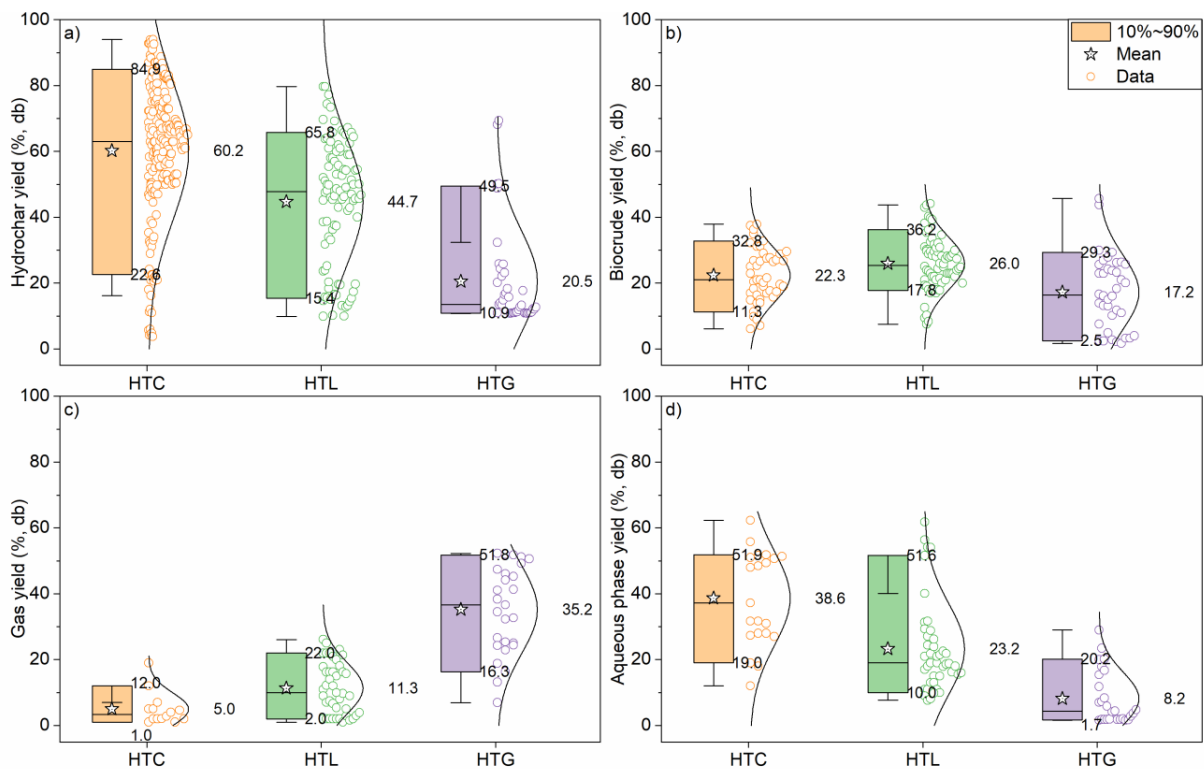


Fig. 1 Bar normal distributions depicting yields of (a) hydrochar, (b) biocrude, (c) gas, and (d) aqueous phase from various hydrothermal processes. Data collected from references in Table 1. HTC = hydrothermal carbonization; HTL = hydrothermal liquefaction; HTG = hydrothermal gasification; db = dry basis.

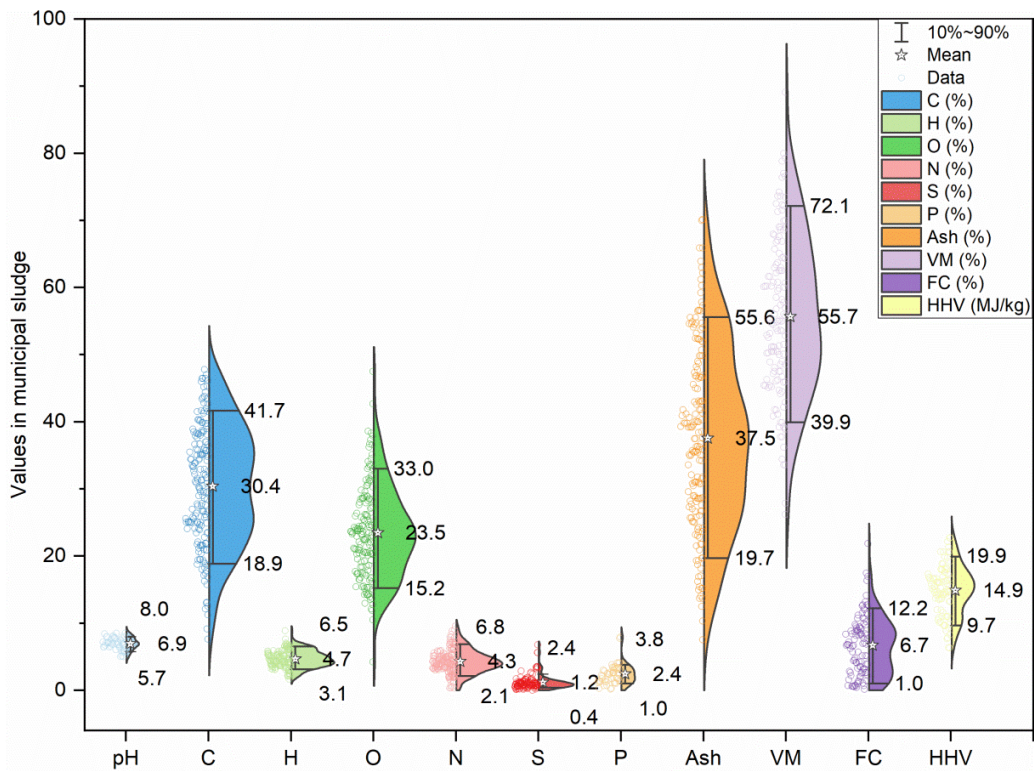


Fig. 2 Violin distribution plot of various properties (data in dry basis except for pH) of municipal sludge reported in hydrothermal studies. Data collected from references in [Table 2](#). VM = volatile matter; FC = fixed carbon; HHV = higher heating value.

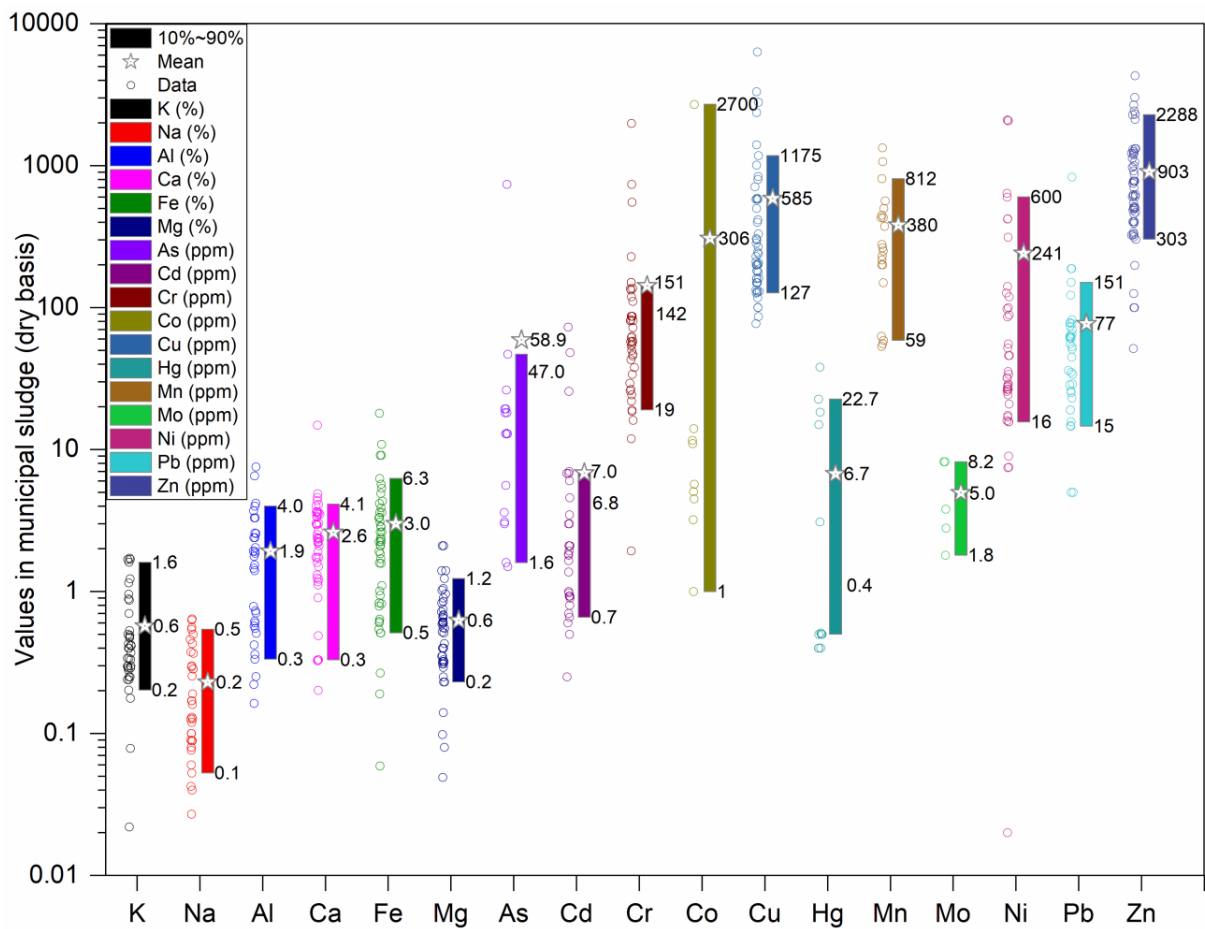


Fig. 3 Distribution plot of metals in municipal sludge reported from hydrothermal studies. Data collected from references in [Table 2](#).

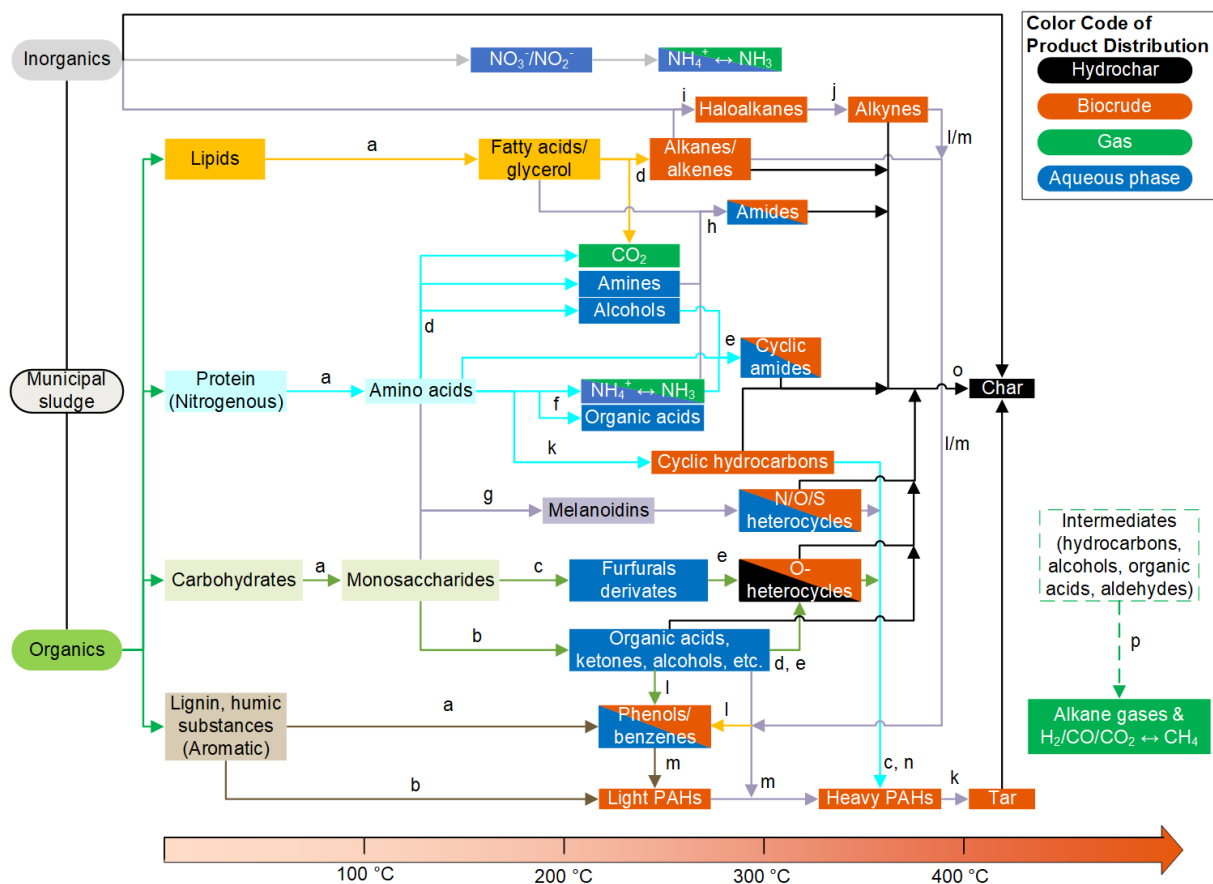


Fig. 4 Possible reaction pathways and corresponding products distribution for the hydrothermal processing of municipal sludge: (a) hydrolysis; (b) decomposition; (c) dehydration; (d) decarboxylation; (e) cyclization; (f) deamination; (g) Maillard reaction; (h) aminolysis; (i) halogenation; (j) dehydrohalogenation; (k) condensation; (l) Diels-Alder reaction; (m) hydrogen abstraction acetylene addition reaction; (n) aromatization; (o) polymerization; (p) free radical reactions or metal-catalyzed C-C/C-O cleavage (Azadi et al., 2013; Chen et al., 2014; Gong et al., 2018, 2017, 2016b; He et al., 2015b, 2014a; Inoue et al., 1997; Liu et al., 2017a; Paneque et al., 2017; Sevilla and Fuertes, 2009; Su et al., 2019; Usman et al., 2019a; Wang et al., 2019a; Wang et al., 2018; Wang et al., 2012; Watson et al., 2020; Zhuang et al., 2017). PAHs = polycyclic aromatic hydrocarbons. Note: Metal ions have a potential catalytic or inhibitory role on reactions a–c.

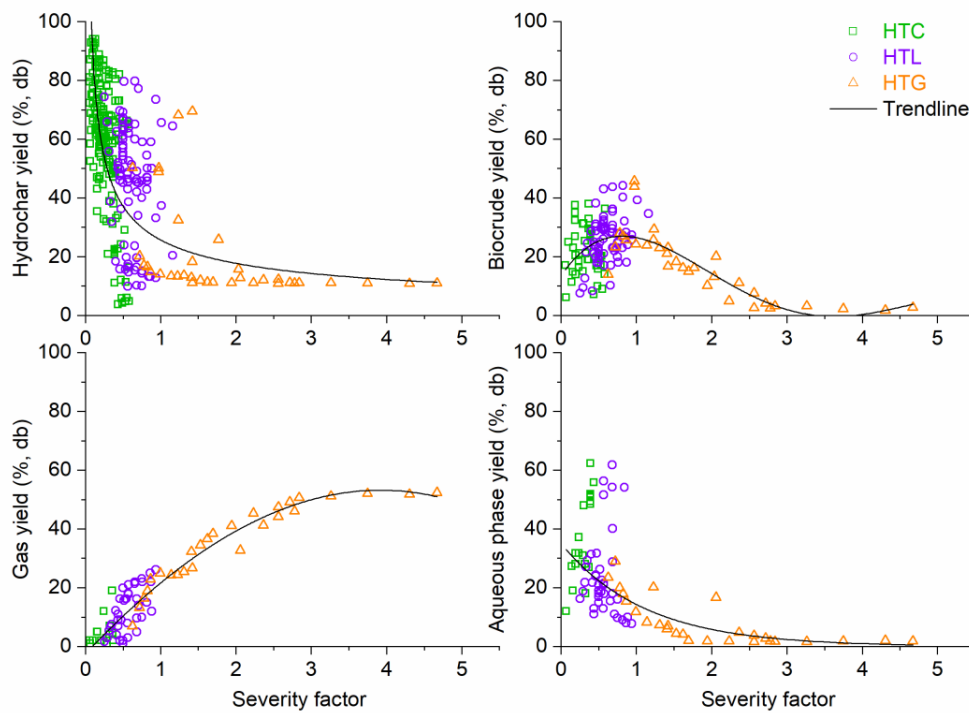
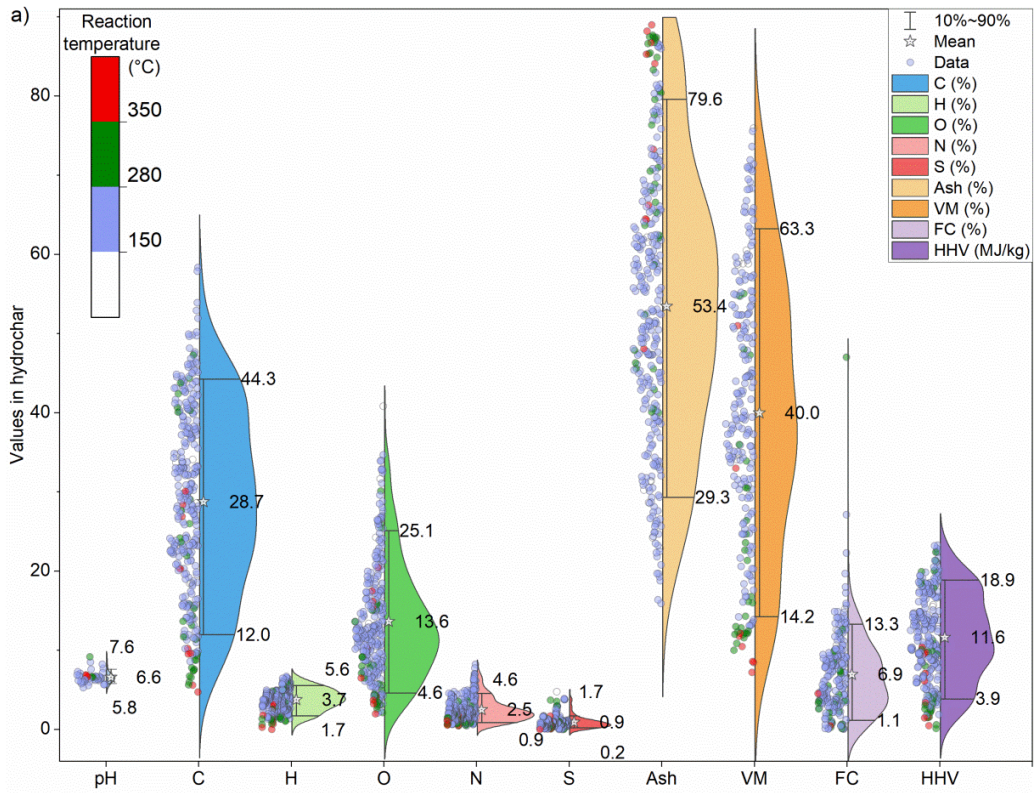
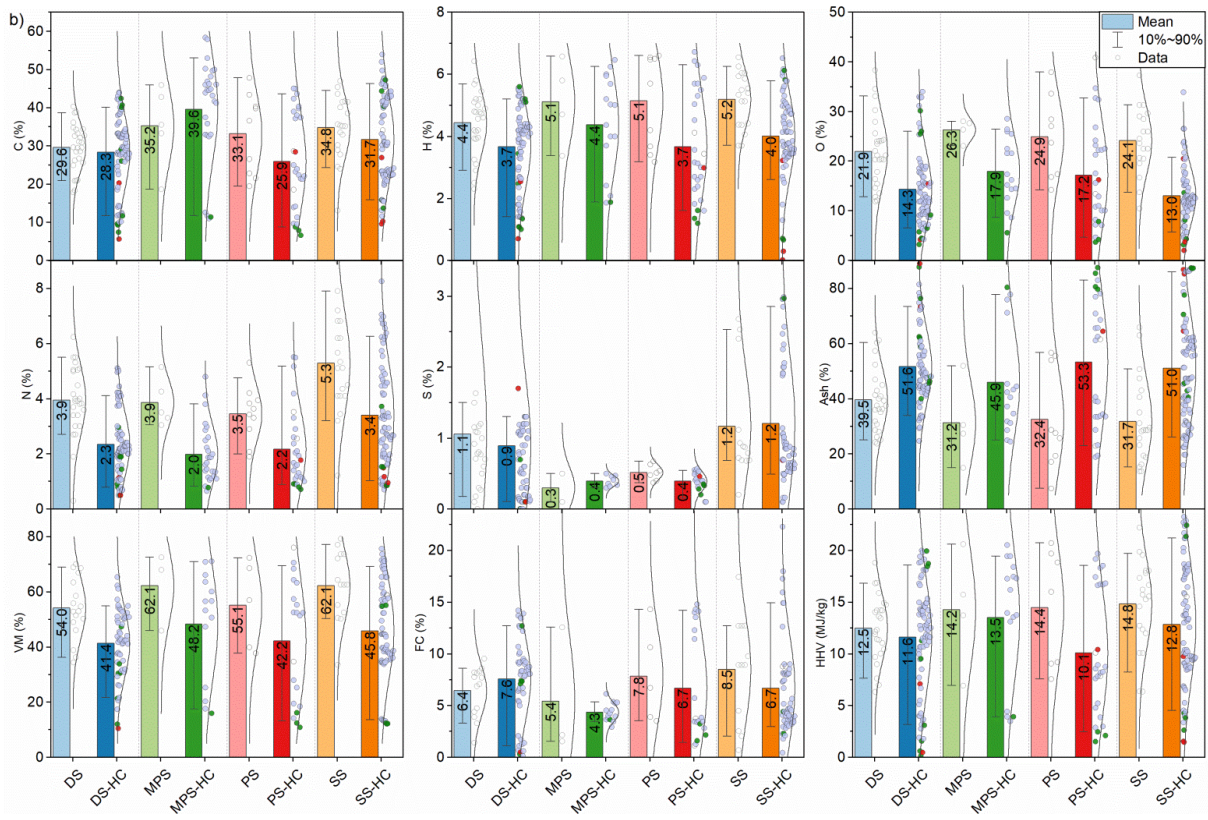


Fig. 5 Influence of the reaction severity on the product yields from the hydrothermal processing of municipal sludge. Data collected from references in [Table 1](#). HTC = hydrothermal carbonization; HTL = hydrothermal liquefaction; HTG = hydrothermal gasification; db = dry basis.





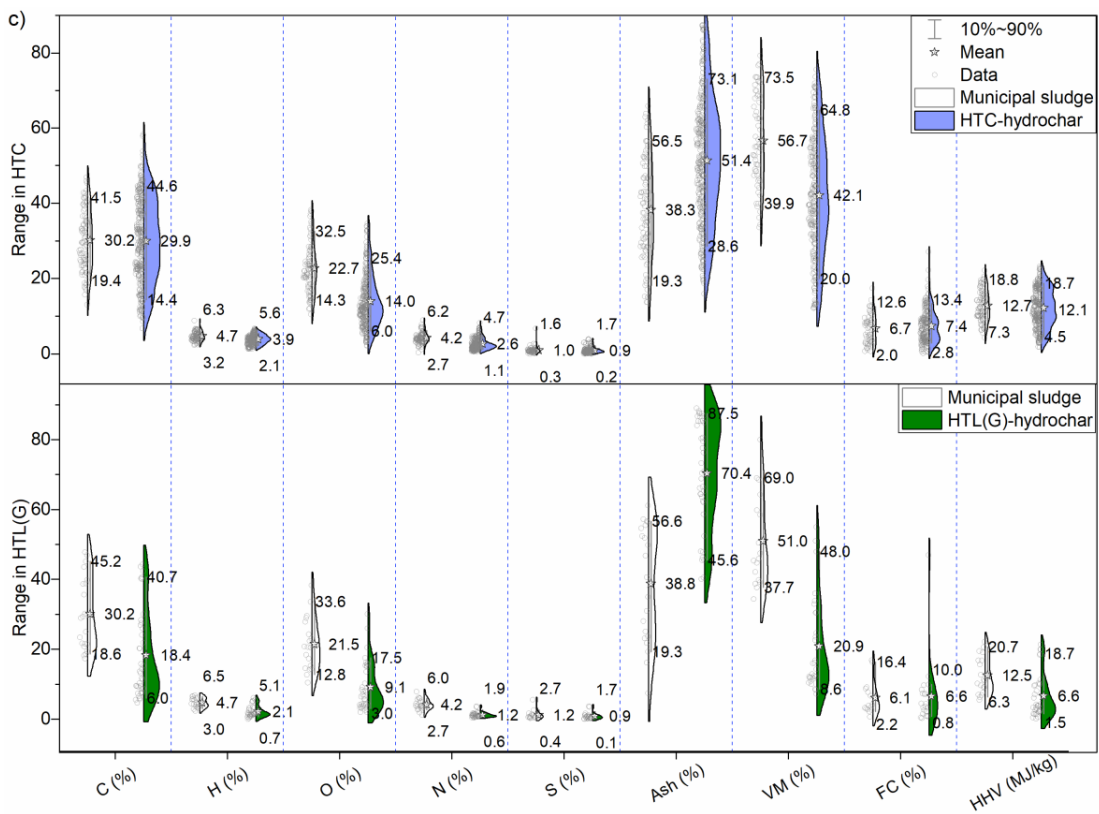


Fig. 6 (a) Violin distribution plot of various properties of hydrochar and comparisons of sludge to its derived hydrochar (b) based on feedstock sludge type and (c) hydrothermal processes (all values on the dry basis except for pH, data from [Table 6](#)). VM = volatile matter; FC = fixed carbon; HHV = higher heating value; DS = digested sludge; MPS = mixed primary and secondary sludge; PS = primary sludge; SS = secondary sludge (including waste activated sludge); HTC = hydrothermal carbonization; HTL(G) = hydrothermal liquefaction/gasification.

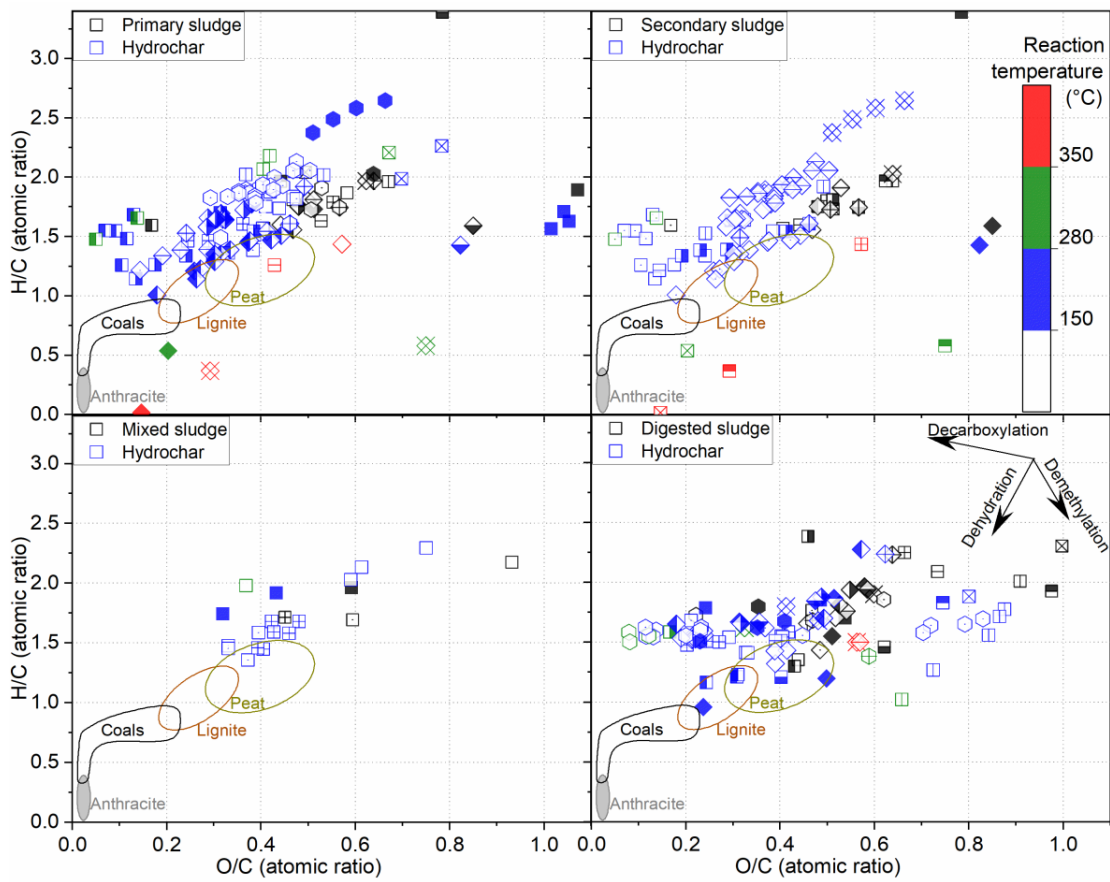


Fig. 7 van Krevelen diagram of municipal sludge (in black color) and the corresponding hydrochar (in other colors depending on reaction temperature) (data from Table 6). Same data shape donates from the same study.

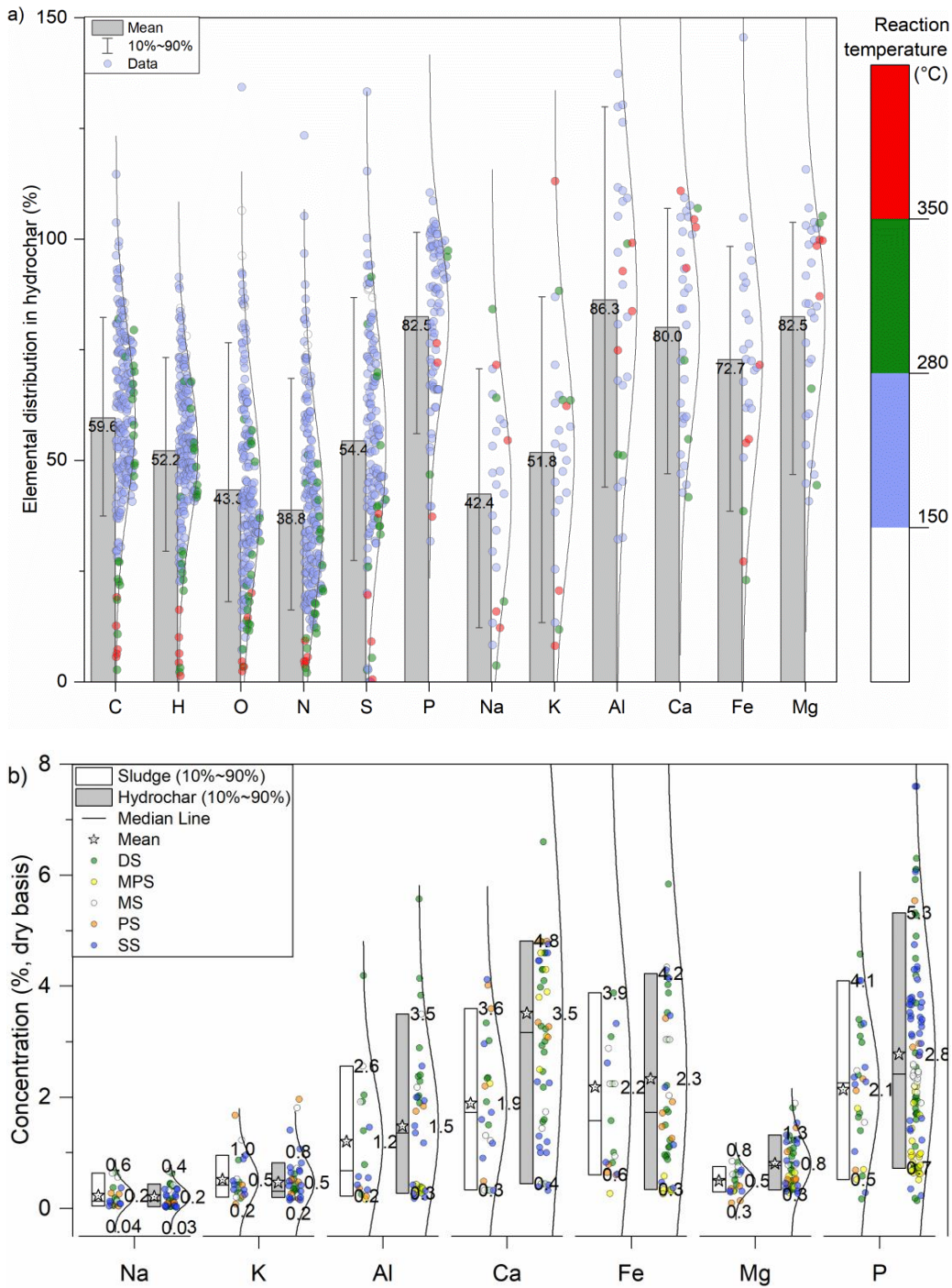


Fig. 8 (a) Bar normal distribution of macro elements in hydrochar and (b) concentrations of macronutrients in various sludge and its derived hydrochar (data from references in Table 6). Elemental distribution = elemental mass in hydrochar/elemental mass in sludge feedstock \times 100%; DS = digested sludge; MS = municipal sludge (non-specified); PS = primary sludge; SS = secondary sludge (including waste activated sludge); MPS = mixed PS and SS.

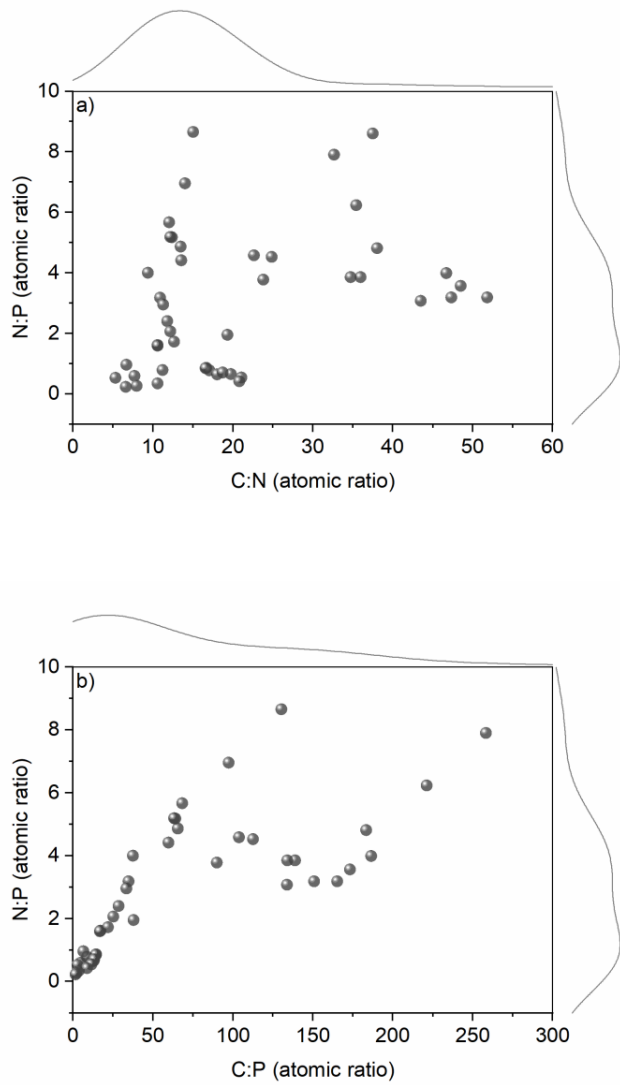
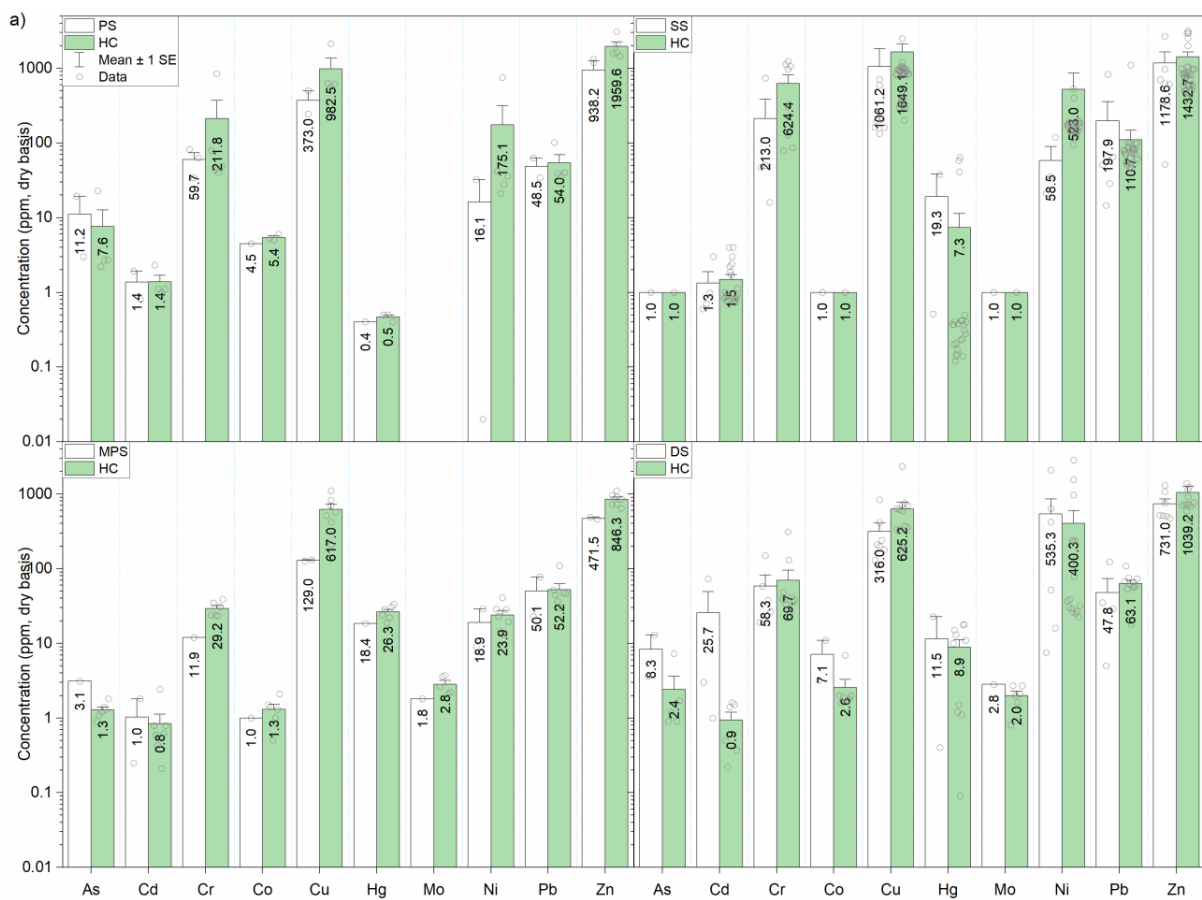


Fig. 9 Atomic ratios of (a) N:P versus C:N and (b) N:P versus C:P in municipal sludge-derived hydrochar with Kernel smooth distribution (data from references in [Table 6](#)).



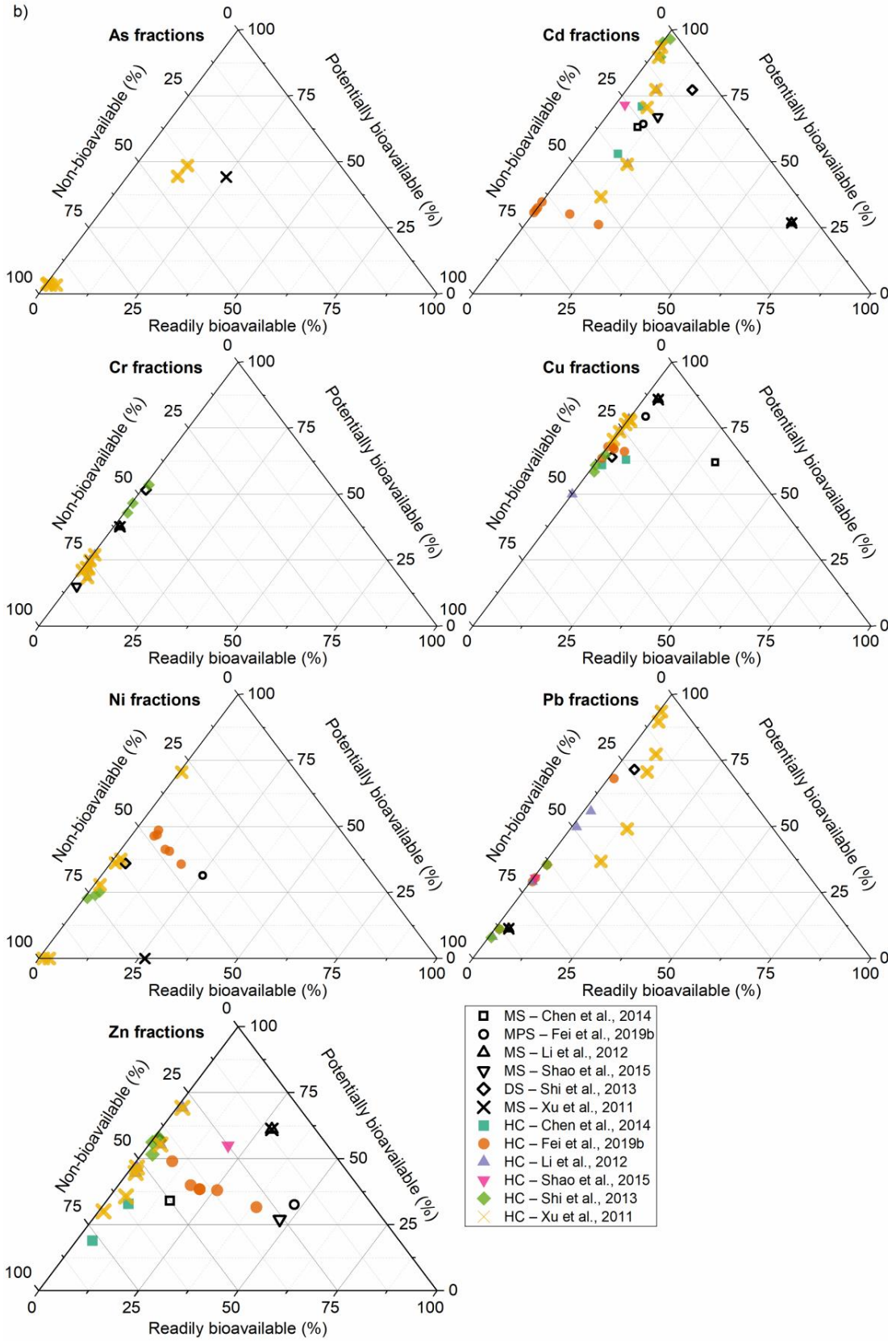


Fig. 10 (a) Total concentrations (data from **Table 7**) and (b) fractional distribution of heavy metals in various municipal sludge (MS) and the corresponding hydrochar (HC). DS = digested sludge; PS = primary sludge; SS = secondary sludge (including waste activated sludge); MPS = mixed PS and SS.

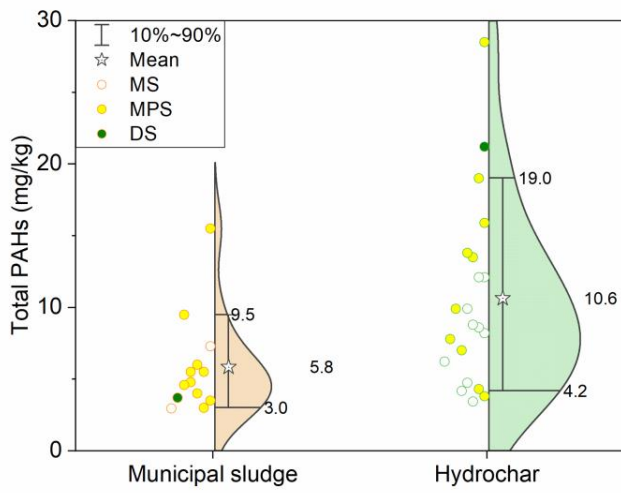


Fig. 11 Violin distribution of total polycyclic aromatic hydrocarbons (PAHs) in municipal sludge and the corresponding hydrochar (Gong et al., 2016b, 2018; T. Liu et al., 2021; Melo et al., 2019; Wiedner et al., 2013).

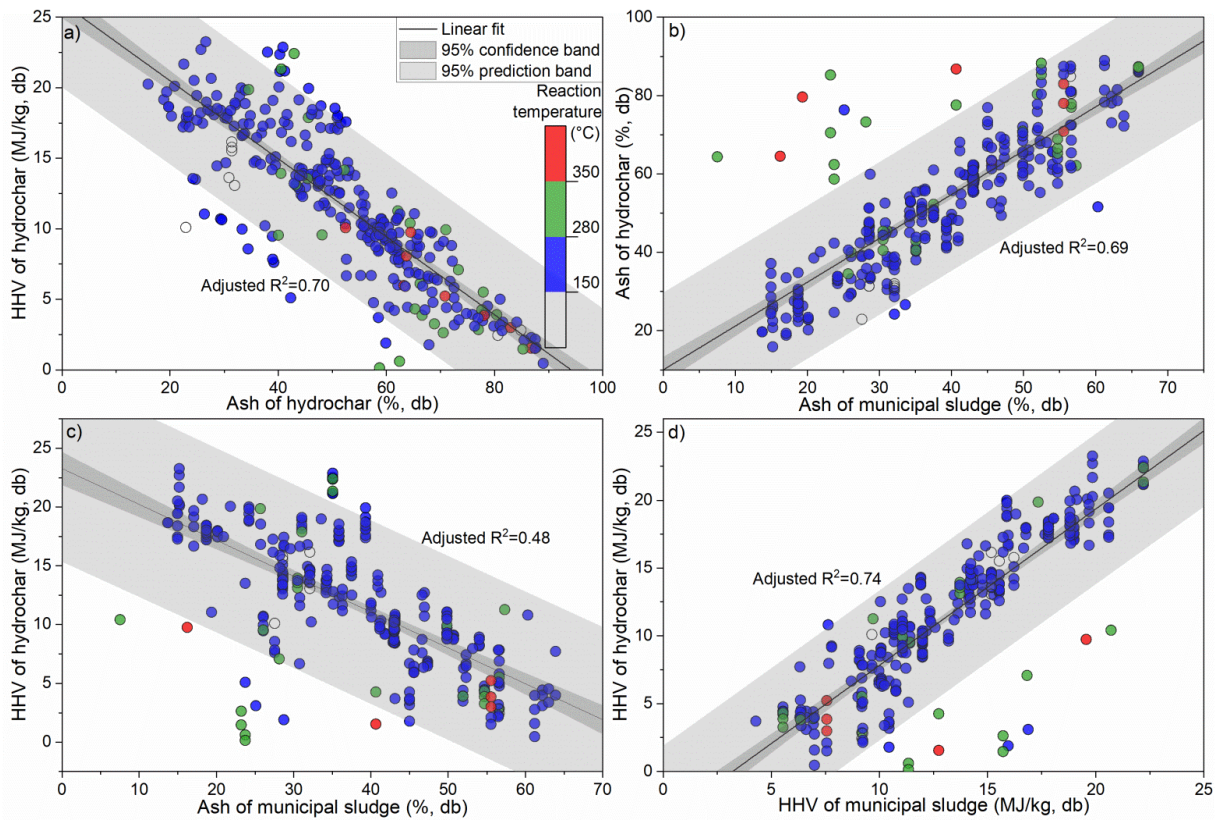
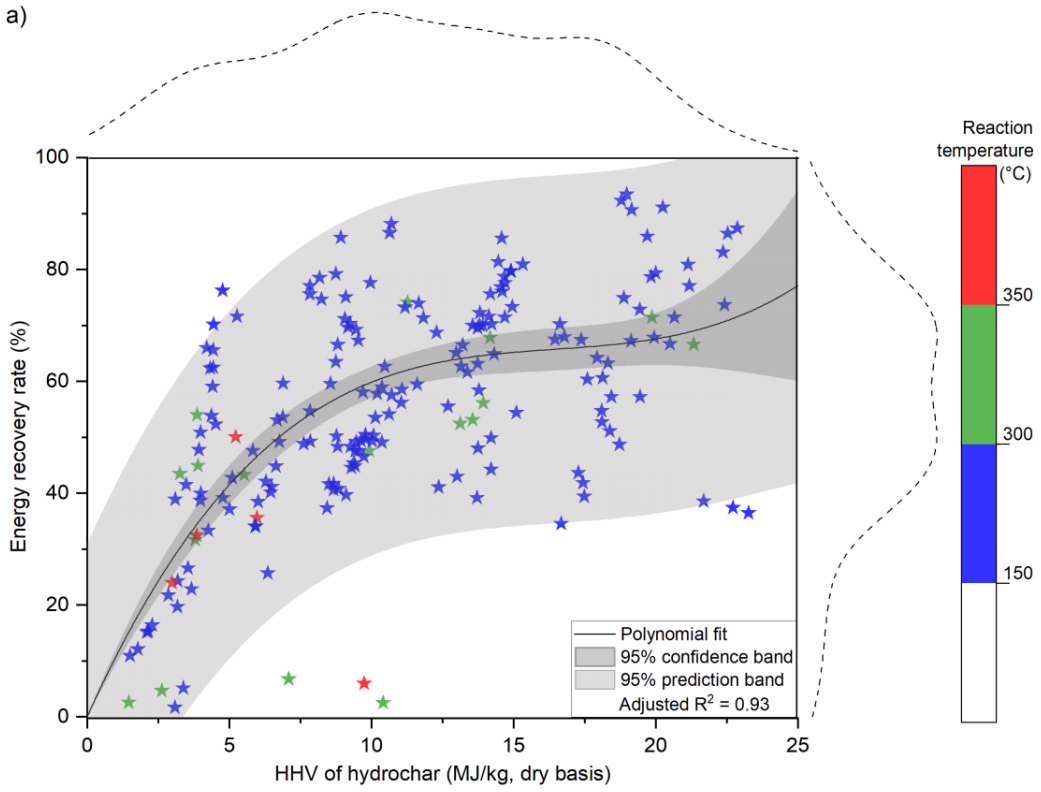


Fig. 12 Correlations among properties of hydrochar and municipal sludge (data obtained from **Table 6**). HHV = higher heating value; db = dry basis.

a)



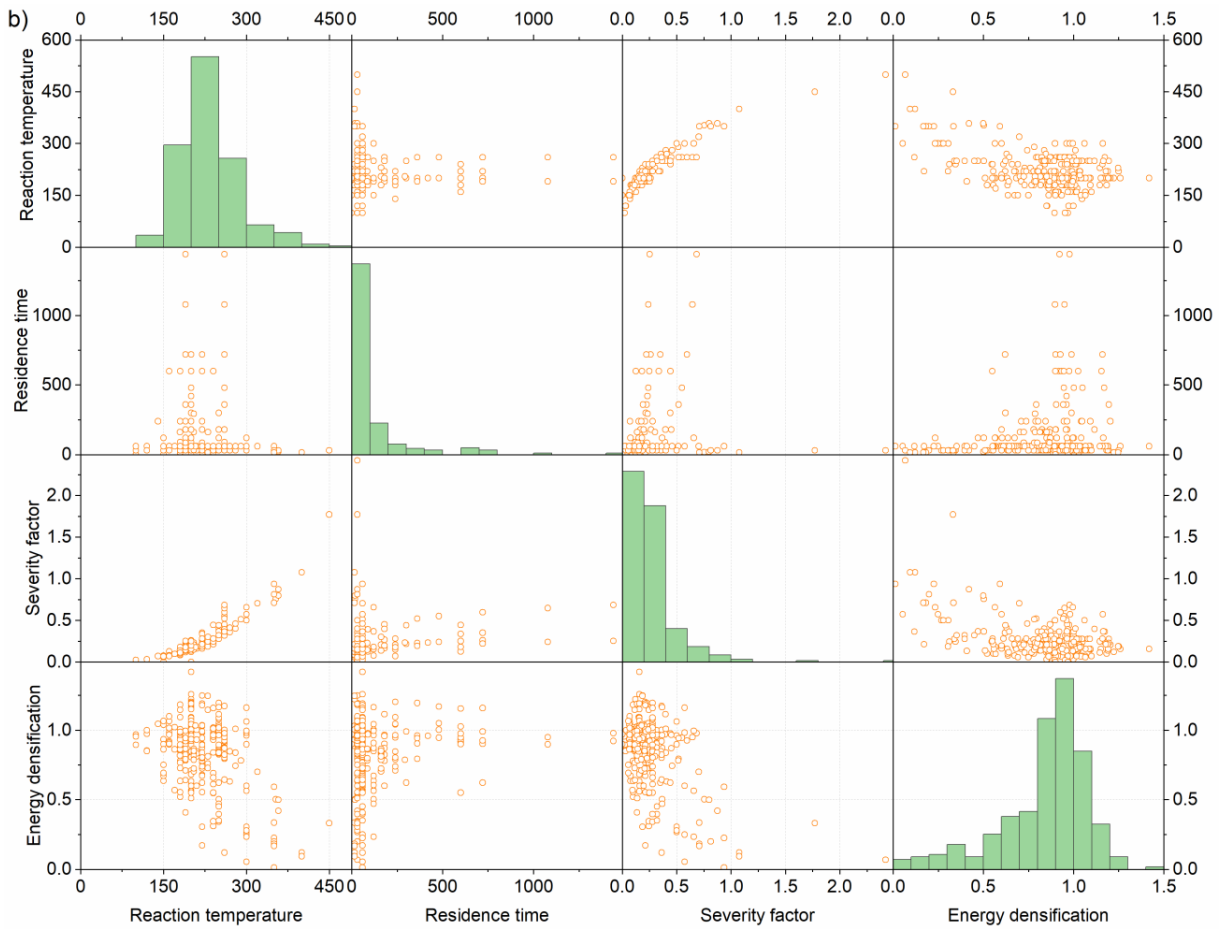


Fig. 13 (a) Plot of energy recovery rate versus higher heating value (HHV) of hydrochar with Kernel distribution and (b) scatter matrix of energy densification and hydrothermal conditions (data obtained from **Table 6**). Energy recovery rate (%) = hydrochar HHV/sludge HHV \times hydrochar yield (%); energy densification = hydrochar HHV/sludge HHV.

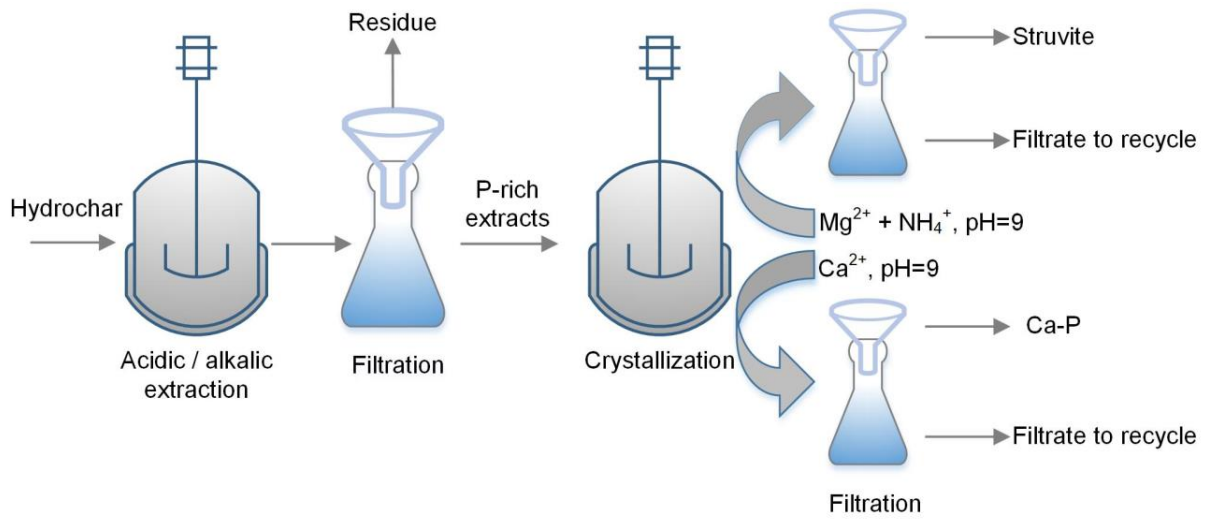


Fig. 14 Typical nutrient recovery process from sludge-derived hydrochar through wet chemical extraction and crystallization



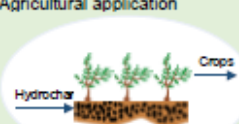
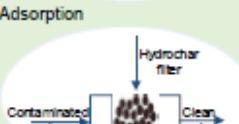
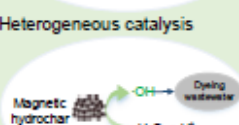
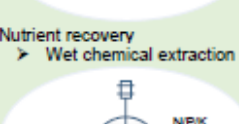
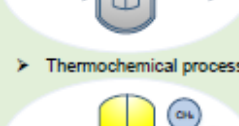

Approaches	Advantages	Challenges
Energy production > Combustion 	<ul style="list-style-type: none"> o Direct and easy application o Low investment o No chemicals required o No concern of organic pollutants 	<ul style="list-style-type: none"> • Feedstock selective • Potential ash slagging and fouling • Secondary contamination • Nutrient loss
> Gasification 	<ul style="list-style-type: none"> o Low requirement on feedstock o Energy gas produced o High conversion rate o Coupled P recovery 	<ul style="list-style-type: none"> • High investment • High requirement on reactors • Concentrated pollutants in residue • Lack of economic analysis
Agricultural application 	<ul style="list-style-type: none"> o Direct and easy application o Low investment o Alternative cheap fertilizer o Win-win benefits 	<ul style="list-style-type: none"> • Environmental and human health risks • Potential side effects on crops • Lack of long-term field trials • Farmer's perception and concerns
Adsorption 	<ul style="list-style-type: none"> o Possible direct application o Alternative cheap adsorbent o Excellent performance after activation 	<ul style="list-style-type: none"> • Limited capacity for direct application • Expensive activation • Limited results • No field application • Concern of pre-existing contaminants
Heterogeneous catalysis 	<ul style="list-style-type: none"> o Promising catalytic effects o Cost-effective process o High stability and reusability o No additional reactor required 	<ul style="list-style-type: none"> • Potential toxicity • Limited results • Low efficiency in real application • Lack of validation
Nutrient recovery > Wet chemical extraction 	<ul style="list-style-type: none"> o Simple and easy operation o High recovery rate o Profitable in batch scale 	<ul style="list-style-type: none"> • Additional chemicals and equipment required • Lack of comprehensive economic analysis • Low efficiency for continuous system • Concern of contaminants in recovered products • Utilization or disposal of by-products
> Thermochemical process 	<ul style="list-style-type: none"> o Low risk of problematic metals in recovered product o Coupled with energy gas generation 	<ul style="list-style-type: none"> • High investment • High requirement on reactors • Low efficiency without additives • Lack of validation
> Integrated biotechnology 	<ul style="list-style-type: none"> o Emerging technique o Green and sustainable o Dual benefits: Nutrient recycling and biocrude production 	<ul style="list-style-type: none"> • Additional chemicals and equipment required • Efforts and care required for algal cultivation • Concern of inhibitors in algal growth • Lack of validation • No economic analysis

Fig. 15 Evaluations of the state of different sludge-derived hydrochar valorization approaches.

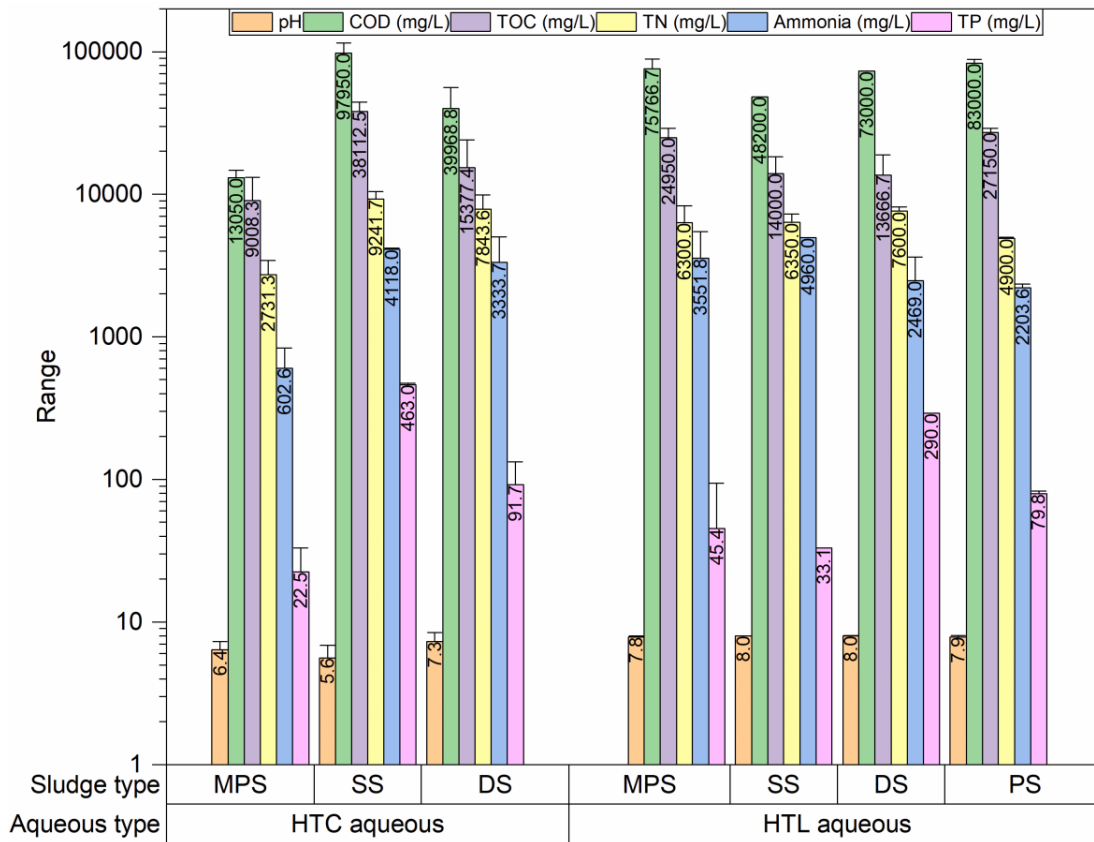


Fig. 16 Characteristics of aqueous phase from hydrothermal carbonization (HTC) and liquefaction (HTL) of various sludge (Ahmed et al., 2021a; Aragón-Briceño et al., 2017, 2020; Belete et al., 2019; Chen et al., 2019; Ferrentino et al., 2020b; Gaur et al., 2020; Lu et al., 2017; Maddi et al., 2017; Marin-Batista et al., 2020; Marrone et al., 2018; Merzari et al., 2020; Ovsyannikova et al., 2020; Snowden-Swan et al., 2017; Villamil et al., 2019, 2020; Xu et al., 2020a, 2020b). PS = primary sludge; SS = secondary sludge; MPS = mixed PS and SS; DS = digested sludge; COD = chemical oxygen demand; TOC = total organic carbon; TN = total nitrogen; TP = total phosphorus.

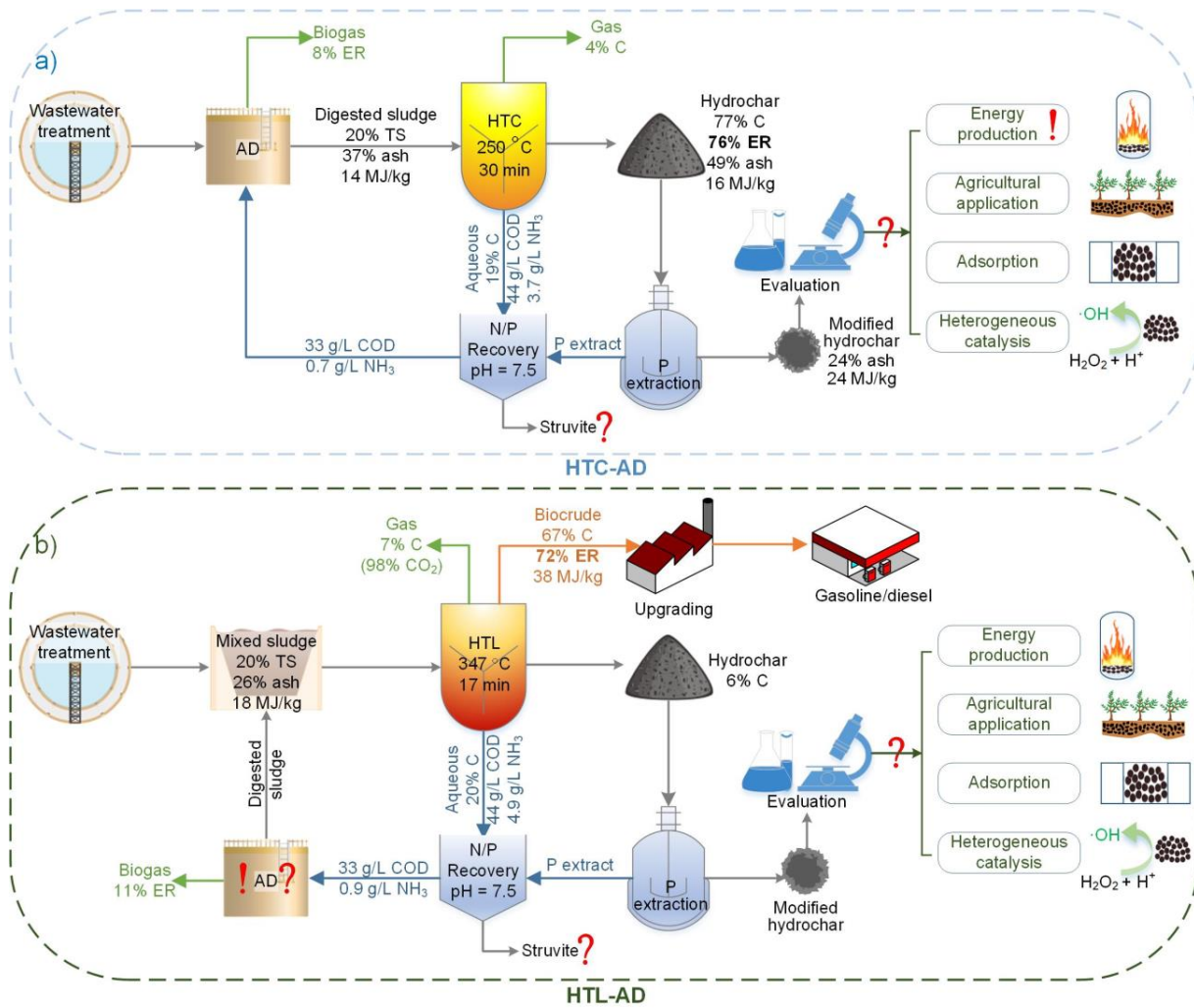


Fig. 17 Concepts of developing a sustainable waste treatment system for municipal sludge. Data adapted from (Aragón-Briceño et al., 2020; Li et al., 2021; Posmanik et al., 2017a; Snowden-Swan et al., 2017). Distribution of C and energy recovery (ER) is based on the feedstock (sludge). Assumptions: Struvite precipitation removed 82% ammonia and 25% COD (P. Wang et al., 2021); acid washing during P extraction removed 50% ash (Marin-Batista et al., 2020). AD = anaerobic digestion; COD = chemical oxygen demand; HTC = hydrothermal carbonization; HTL = hydrothermal liquefaction.